Distribution Agreement

Signature:

_______________________________________ ___________

Jier Huang Date

Charge Separation Dynamics between Semiconductor Nanoparticles and Molecular Adsorbates

By

Jier Huang
Doctor of Philosophy

Chemistry

Dr. Tianquan Lian, Advisor

Dr. Michael C. Heaven, Committee Member

Dr. Joel M. Bowman, Committee Member

Accepted:

Dean of the Graduate School
Lisa A. Tedesco. Ph.D.

Date

Charge Separation Dynamics between Semiconductor Nanoparticles and Molecular Adsorbates

By

Jier Huang

B.S. Lanzhou University, P.R. China, 2001
M.S. Lanzhou University, P.R. China, 2004

Advisor: Tianquan Lian, Ph.D.

An abstract of
A dissertation submitted to the Faculty of the
James T. Laney School of Graduate Studies of Emory University
in partial fulfillment of the requirements for the degree of
Doctor of Philosophy
in Chemistry
2010

Abstract

Charge Separation Dynamics between Semiconductor Nanoparticles and Molecular Adsorbates

By Jier Huang

The understanding of the interfacial charge transfer dynamics between semiconductor nanoparticles and molecular adsorbates is essential to their potential applications in solar cells. In this dissertation, we investigated two types of semiconductor nanoparticle – molecular adsorbate systems: (1) quantum dots (QD)-adsorbate complexes and (2) dye sensitized semiconductor films, by using transient absorption spectroscopy and time resolved fluorescence spectroscopy.

For the first system, we conducted a series of studies on exciton dissociation dynamics in QDs through charge transfer to the adsorbed molecules. We investigated single exciton dissociation dynamics in CdSe QDs through electron transfer (ET) to a Re-bipyridyl complex, methylene blue (MB^+) molecules, and Flavin mononucleotide by monitoring the spectral features of both the QDs and molecular adsorbates. It was found that the ET rate depends on the number of adsorbatess per QD as well as the QD particle size. The fastest observed ET rates were on the sub-ps time scale, which is much faster than the exciton-exciton annihilation process, indicating the possibility to dissociate multiple excitons through ET from QDs to molecular adsorbates. Additionally, we have investigated exciton dissociation dynamics in CdSe QDs through hole transfer to phenothiazine molecules (PTZ). It was shown that the hole transfer time was ～ 2.5 ns in 1:1 CdSe-PTZ complexes and reached ～ 300 ps in samples with an average of ～ 6 PTZ per QD. Furthermore, we demonstrated the capability to dissociate multiple excitons in CdSe-MB^+ complex. It was shown that ～ 3 excitons in CdSe QDs can be dissociated through ET to MB^+.

For the second system, we examined the ET dynamics from Rhodamine (Rh) dyes to different semiconductor films. Electron injection kinetics from RhB to In_2O_3, SnO_2, and ZnO films were compared to examine the effect of the semiconductor nature on the ET dynamics. It was found that ET rate follows the order of $In_2O_3 \approx SnO_2 > ZnO$. Additionally, we also explored the impact of dye energetics on ET dynamics by comparing the injection kinetics from RhB, Rh101, and Rh6G to the same semiconductor. The results showed that the ET rate decreases with a decrease in the excited state oxidation potential.

. **Charge Separation Dynamics between Semiconductor Nanoparticles and Molecular Adsorbates**

By

Jier Huang

B.S. Lanzhou University, P.R. China, 2001
M.S. Lanzhou University, P.R. China, 2004

Advisor: Tianquan Lian, Ph.D.

A dissertation submitted to the Faculty of the
James T. Laney School of Graduate Studies of Emory University
in partial fulfillment of the requirements for the degree of
Doctor of Philosophy
in Chemistry
2010

ACKNOWLEDGEMENT

First, I would like to express my sincere gratitude to my advisor, Professor Tianquan Lian, for his inspirational guidance and general support throughout my graduate career. His wide knowledge and logical way of thinking have been of great value to me. Without his supervision, I would not have achieved the necessary skills in experimental design and scientific reasoning, and would not have established the confidence to be a scientist. I also wish to extend sincere thanks to my graduate committee members, Dr. Michael C. Heaven and Dr. Joel M. Bowman, for their insightful comments, hard questions and valuable time.

I would like to show my gratitude to my lab fellows for their support and friendship. Dr. Jianchang Guo and Dr. Chunxing She provided guidance in my earlier graduate career. Dr. David Stockwell, from whom I learned laser skills, offered the most valuable support and friendship. Shengye Jin provided the fluorescence measurements in this thesis. Zhuangqun Huang has provided me with quantum dots for this thesis with consistent quality. Chantelle Anfuso has made herself available to offer help and suggestions whenever I need her. Ye Yang offered special help in experiments and by challenging my ideas. I am also grateful for the help from my other group members, Haimin Zhu, Nianhui Song, Dr. Abey Issac, Dr. Baohua Wu, Zhe Zhang, and David Wu.

Last but not least, I would like to thank my entire family. My parents and in-laws have given me encouragement and support when I had difficult times and gave special help in taking care of my two sons. My husband, Zhihui Zhang, has given me unlimited love and support by encouraging me at every step of the way. My two lovely sons, Ethan and Andrew, have provided me with happiness and understanding.

Table of Contents

List of Figures

Chapter 1

Chapter 2

Chapter 3

Chapter 4

Chapter 5

Chapter 6

Chapter 7

List of Tables

Chapter 3

Chapter 5

Chapter 6

Chapter 7

Chapter 1. Introduction

The increasing demand for clean and efficient energy makes photovoltaic solar cells an ideal energy device. Conventional solar cells, made from bulk silicon consisting of a single p-n junction, were first commercialized in the 1960s.[1,2] Since then, cell efficiency has been dramatically improved while production costs have decreased. However, these cells are still not efficient enough (current commercially available cells are ~15% efficient) and are too expensive to manufacture for large scale electricity generation. Over the years, considerable efforts have been made to develop a solar cell that is efficient in terms of energy and potentially less expensive to produce. In an effort to achieve these two objectives, quantum dot (QD) based solar cells and dye sensitized solar cells (DSSC) have emerged as the two potential alternatives to the conventional silicon solar cells.

1.1. Ultrafast Exciton Dissociation in CdSe Quantum Dots through Charge Transfer to Molecular Adsorbates

1.1.1 Introduction

Quantum dot based solar cells have drawn intense attention during the past few years because they may be the most promising alternative to the conventional solar cell, primarily due to their potential to boost the energy conversion efficiency beyond the traditional Shockley and Queisser limit of 31% in silicon solar cells.[3] Shown in Figure 1.1a is the configuration of a QD solar cell, in which QDs are dispersed in a blend of electron- and hole- conducting polymers.[4] Upon excitation, electrons in the valence band of the QDs are promoted to the conduction band and thus leave the holes behind. The electrons and holes are then separated by charge transfer to an electron conducting polymer (electron acceptor) and a hole conducting polymer (hole acceptor), respectively. There are specific advantages of employing QDs as light sensitizers in solar cells. First, QDs are semiconductor nanoparticles that exhibit tunable band gaps,[5] offering the possibility to harvest more light in the solar spectrum through the design of rainbow solar cells. Second, QDs can create multiple carriers by absorbing a single high energy photon, a process known as multi-exciton generation (MEG). This phenomenon does not readily occur in bulk semiconductors where the extra energy simply dissipates away as heat before it can cause another electron-hole pair to form. However, in QDs, the probability of forming multi-excitons is significantly enhanced due to quantum-confinement effects, which reduce the phonon-mediated relaxation channel as well as increase the Coulomb interactions between hot carriers.[4,6] This MEG process allows for over 100% quantum efficiency in generating electron-hole pairs, providing the potential capability to improve the solar-to-electric power conversion efficiency in QD-based solar cells.[4]

Recently, considerable efforts have been made to characterize MEG in QDs. Very efficient MEG has been reported in a series of semiconductor QDs such as PbS, PbSe, PbTe, Si, CdSe and InAs, as well as in carbon nanotubes.[6-18] However, there is a key challenge that must be overcome before the MEG process can be exploited for practical applications: extracting the photogenerated multiple excitons before the ultrafast exciton-exciton aninihilation process, which occurs on a timescale of 10s to 100s of picoseconds (ps) for many QDs.[19,20] One approach to achieving this goal is to dissociate the excitons through ultrafast charge transfer. In the presence of electron acceptors or donors, the excitons in QDs can dissociate by transferring the electrons to the acceptors or holes to the donors.[21-25] Charge transfer from QDs to molecular adsorbates and oxide nanoparticles have been studied since the early 1980s.[22,26-41] Some of these studies revealed that the rates of charge transfer to molecular acceptors are on the 10s of picoseconds and faster timescale. This is similar to or shorter than the lifetime of the multiple excitons, thus illuminating the possibility of separating multiple excitons by ultrafast charge transfer before the exciton-exciton quenching process.

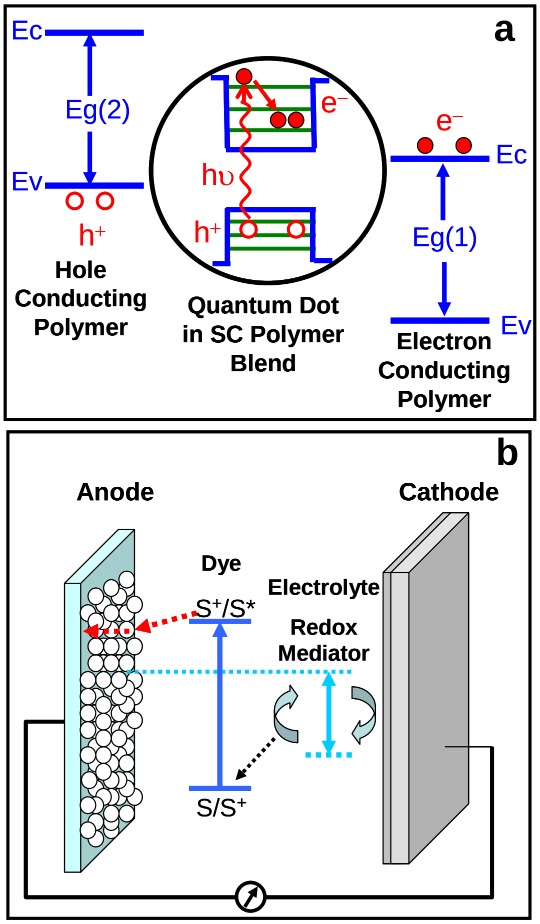

Figure 1.1 Schematic diagram showing the configurations of (a) quantum dot solar cell with QDs dispersed in a blend of electron- and hole- conducting polymers and (b) dye sensitized solar cell.

Unfortunately, despite decades of extensive attempts, few QD/molecular acceptor systems have been found in which the multi-excitons in QDs can be ultimately dissociated through ultrafast charge separation. Matylitsky et al. first reported the dissociation of multiple excitons in CdSe QDs through electron transfer to adsorbed Methylviologen (MV^{2+}).[42] The ET rate for the dissociation of the single exciton state was observed to be 70 fs, and up to 4 excitons were reported to have been dissociated in this system. While this study successfully demonstrated the capability to extract multiple excitons from QDs through electron transfer to molecular adsorbates, a large fraction of the photogenerated excitons were quenched through exciton-exciton annihilation instead of being extracted. This quenching fundamentally limits the potential to improve the efficiency of solar-to-electric conversion. To obtain a proper perspective for how to achieve the dissociation of all of the photogenerated excitons in QDs, one needs to be aware of both the theoretical and experimental information on the dynamics of exciton dissociation in QD-adsorbate systems. The main focal point of the research in this work is to experimentally determine the factors that affect these dynamics. The research presented in Chapters 3, 4 and 5 focuses on a series of studies on single exciton dissociation dynamics in QDs through charge transfer to different molecular adsorbates. The factors that control the exciton dissociation pathways and affect the dissociation rates will also be discussed. The capability of dissociating multiple excitons through ultrafast charge transfer will be demonstrated in Chapter 6.

1.1.2 Single Exciton Dissociation

Before attempting to achieve multi-exciton dissociation in QDs through charge transfer to molecular acceptors, it is highly desirable to understand the dissociation dynamics from a single exciton state in QDs. Understanding the single exciton dissociation dynamics can provide important insight for achieving multiexciton dissociation in future studies.

Excitons in QDs can be dissociated through charge transfer to molecular adsorbates by two different pathways. As shown in Figure 1.2, when the conduction band edge of a QD is higher than the lowest unoccupied orbital (LUMO) of the molecular adsorbate, the exciton may dissociate by transferring an electron to the molecular acceptor, thus forming a reduced adsorbate. Alternatively, if the valence band edge of a QD is lower than the highest occupied orbital (HOMO) of the adsorbate, then the exciton may dissociate by transferring the hole to the adsorbate, producing an oxidized molecule.

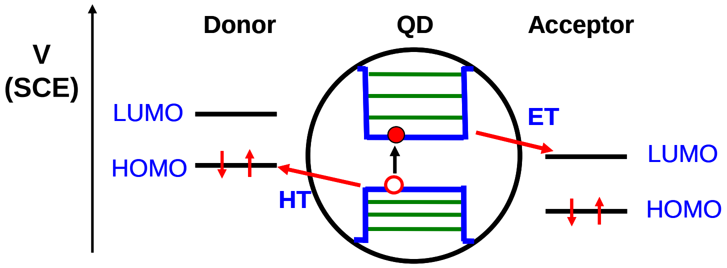

Figure 1.2. Schematic diagram of the exciton dissociation process in a QD-adsorbate complex.

1.1.2.1 Exciton Dissociation through ET

Photoinduced charge separation through electron transfer has for many decades been the preferred method used in the investigation of exciton dynamics in QDs, due to its ultrafast transfer time scale as well as the well-known spectral features associated with this process. Various combinations of semiconductor nanoparticles/molecular adsorbates have been explored to separate the charges in the nanoparticles through ET. The first of these studies involved photoexcitation of colloidal CdS crystallites which then reduced adsorbed methylviologen (MV^{2+}) thirty years ago.[27-29,31,33,43] The focuses of these reports are on the elucidation of the ET processes by employing fluorescence, laser flash photolysis, resonance Raman spectroscopy, and microwave absorption techniques. It was shown that the band gap emission of CdS can be efficiently quenched with the addition of MV^{2+}. Experiments using laser flash photolysis, which monitored the transient bleaching in colloidal CdS after bandgap excitation, have shown that the ET is essentially complete within 30 ps[26,33] In addition to monitoring the spectral features of CdS colloidal particles, Brus et al examined ET from CdS to MV^{2+} by recording the resonance Raman spectrum of reduced MV^{2+} (MV^{+}) after a fixed time delay following the bandgap photoexcitation of CdS.[28,29] They claimed that the reduction of MV^{2+} on the surface of the nanoparticles occurs on a time scale of less than ～ 20 ps, which is in good agreement with the value determined from picosecond transient absorption studies. In addition to MV^{2+}, several other organic dyes have also been used as electron acceptors to investigate the reduction reaction between semiconductor nanoparticles and dye molecules. For example, Kamat and his co-workers have used Methylene blue (MB^{+}) ($MB^{+}/MB^{\cdot}$, -0.231 V vs SCE) as an electron scavenger of CdS colloidal particles.[30] They observed efficient emission quenching of CdS, the absorption of the reduced semimethylene blue radical anion at 420 nm, and the depletion of MB^{+} absorption at 650 nm, all of which confirmed the one electron transfer process from CdS to MB^{+}.

Despite the fact that these early studies successfully showed evidence of ET from CdS to the adsorbed dyes with a time scale in the ps or ns regime, these ET times can be misleading. These measurements were conducted with ps or even ns laser pulses, thus limiting the time resolution of these experiments. One of the most important contributions to the study of exciton dynamics in semiconductor nanoparticles is the advent of the femtosecond (fs) laser pulse. As a result of this innovation, later work has used femtosecond transient absorption spectroscopy to explore exciton carrier dynamics from various QDs to molecular acceptors. Both transient visible and transient IR pump-probe experiments have been conducted to time resolve the ET process.[39-41,44-46] Some of these studies have shown that photoexcitation of QDs led to the bleach of the lowest excitonic transition with a time scale of less than 100 fs, which is attributed to a band filling mechanism similar to that observed in the early studies on colloidal semiconductor nanoparticles. This bleach feature resulting from the presence of electrons in the conduction band of QDs has been well characterized and used to directly study the dynamics of ET from QDs to electron acceptors. For the CdS/MV^{2+} complex, El-Sayed and co-workers have found that the addition of MV^{2+} to CdS accelerated the bleach recovery from ～ 30 ps to 7.5 ps.[35] A similar increased bleach recovery rate was observed in CdS QDs with benzyl viologen as the electron acceptor, which has a higher reduction potential than MV^{2+} by 0.1 V. However, the factors that control the pathways and rates of electron transfer remain poorly understood.

In this work, the exciton dissociation dynamics of CdSe QDs with two molecular adsorbates, Re(CO)3Cl(dcbpy) (dcbpy = 4,4’-dicarboxy-2,2’-bipyridine) (ReC0A) and Methylene Blue (MB), have been investigated, and are presented in Chapters 3 and 5, respectively. By monitoring the spectral features of both the QDs and molecular adsorbates, we show that the excitons in CdSe dissociate by ET to these molecules. The effect of QD particle size and the number of adsorbates per QD on the ET rate is also presented. Additionally, the preliminary results on charge separation in CdS QDs through ET to Flavin mononucleotide (FMN) are presented in Chapter 4.

1.1.2.2. Exciton Dissociation through Hole Transfer

In addition to ultrafast electron transfer, separation of multiexcitons also requires ultrafast transfer of holes to acceptors. Compared to the research on exciton dissociation in QDs through the ET pathway, few examples have been reported of the HT process. A possible reason for this is the lack of clear spectral signatures of holes in QDs. Some studies have shown that the presence of holes results in a featureless and relatively weak broad absorption in the near IR, although the exact nature of this transition has not been determined.[47-49] Klimov et al. have shown that the dynamics in the spectral range up to 2 μm is mainly due to the relaxation of the hole.[47] Burda and co-workers have also investigated the relaxation dynamics of CdSe in the spectral range from 450 nm to 5 μm.[49] They assigned the NIR signal to a hole transition by adsorbing a hole quencher to the photoexcited nanoparticles.

Most of the current knowledge on the HT process in QDs was inferred from fluorescence quenching of excited QDs by hole transfer. One of the initial studies involved monitoring both the fluorescence decay and picosecond bleach recovery in a CdSe QD-n-Butylamine system.[50] The authors observed that the addition of butylamine to CdSe QDs led to a decrease in fluorescence intensity, but with no effect on the picosecond exciton bleach recovery or the fluorescence lifetime. They proposed that the decrease in CdSe fluorescence can be attributed to the elimination of the fluorescence site though the binding of the hole acceptor to the hole trapping emitting sites. Very recently, Sykora and co-workers reported their studies on charge carrier dynamics in CdSe-Ru polypyridine complexes, which they investigated using transient PL up-conversion and femtosecond transient absorption experiments.[38] Specifically, they used the dynamics of the exciton bleach recovery to determine the depopulation rate of the electron 1S state, while using the PL quenching dynamics to calculate the product of the electron and hole population numbers. They found that the electron dynamics based on the transient absorption experiment remained almost unchanged, while hole dynamics based on the fluorescence signal developed a ～ 5 ps decay component for the CdSe-Ru complex compared to that of CdSe. They attributed this to the hole transfer process.

In addition to fluorescence emission quenching, laser photolysis and transient absorption experiments have also been used to investigate hole transfer from semiconductor QDs to hole acceptors by monitoring the formation of the oxidation product of the adsorbate. Gratzel et al. reported the observation of the one-electron oxidation product of N-methyl-2(carboxymethyl)phenothiazine (reduction potential 0.448 V vs SCE) when this molecule was employed as an electron donor to a colloidal CdS particle.[26] They claimed that the HT time essentially followed the time profile of the laser pulse, the width of which was 15 μs. Recently, Kamat and co-workers observed the formation of the cation of the adsorbate p-phenylenediamine through transient absorption measurements and reported the hole transfer time scale to be ～ 10 ns in this system.[37]

In this work, we report on the dynamics of exciton dissociation in CdSe QDs through hole transfer to phenothiazine monitored by both transient absorption spectroscopy and time-resolved fluorescence spectroscopy. The hole transfer rate was determined to be 2.5 ns in a 1:1 CdSe-PTZ complex, and ~300 ps in a CdSe-PTZ sample in which there were an average of 6.2 adsorbed PTZ molecules per QD. These results will be discussed in Chapter 5.

1.1.3. Multiple Exciton Dissociation

Our results on single exciton dissociation dynamics through both ET and HT to molecular adsorbates have shown that exciton dissociation through ET in some QD-adsorbate systems can reach the sub-picosecond time scale, indicating the possibility of achieving multi-exciton dissociation. This possibility was first demonstrated in a CdSe-MV^{2+} complex by Matylitsky and co-workers, who reported that up to 4 excitons were dissociated through ET to MV^{2+}. In their experiment, multiple excitons were generated through the absorption of multiple photons by one QD, which was achieved by using femtosecond laser excitation under high photon flux. As reported by Matylitsky and co-workers, the average number of photons absorbed per QD ($\langle N_0 \rangle$) was determined by the following equation: $\langle N_0 \rangle = J(0)\dfrac{1-\exp(-OD\ln 10)}{cL}$, where J(0) is the photon flux at the cuvette's entrance, OD is the optical density at the excitation wavelength, c is the concentration of the QDs and L is the optical path length within the cuvette. The calculated $\langle N_0 \rangle$ is the average number of excitons per QD for the sample. However, it is important to note that the quantification of the photon flux J(0), which is determined by the beam focus, mode, beam sizes et al., is subject to large errors. Additionally, they also determined the number of excitons dissociated by the absorption of $MV^{+\cdot}$ at ～ 400 nm, though it overlapped with the much stronger QD absorption in this region.

In order to establish an accurate relationship between the average number of excitons per QD and the excitation power, as well as to overcome the problem of spectral overlap, we investigated the multiple exciton dissociation dynamics in a CdSe-MB^+ complex by examining the exciton bleach amplitude as a function of excitation power, followed by a simulation of the data. These results are presented in Chapter 6.

1.2. ET Dynamics from Molecular Adsorbates to Semiconductor Nanocrystalline Thin Films

Another alternative to conventional solar cells are DSSC,[51,52] which can be produced for a much lower price, although their efficiency still needs to be enhanced to make them practically viable. Figure 1.1b shows the schematic operating principle of a DSSC, which basically consists of a wide band-gap semiconductor electrode adsorbed with a monolayer of dye molecules, a platinum electrode, and a redox electrolyte sandwiched between them.[1,53] Upon illumination, the dye molecules are excited and can inject electrons into the conduction band of the semiconductor. The oxidized dyes are then regenerated by an electron donor present in the electrolyte. The electrons in the conduction band are collected and flow through the external circuit to arrive at the counter electrode, where they cause the reverse reaction of the redox mediator. Among these processes, electron injection by the excited molecular dye into the semiconductor plays the key role in determining the efficiency of the DSSC. Fast electron transfer from the excited dye to the semiconductor and slow recombination of the electron in the conduction band with the oxidized dye are desired to achieve high efficiency.

For this reason, interfacial electron transfer dynamics between semiconductor nanoparticles and molecular adsorbates have been a subject of intense interest recently.[22,54,55] The ET dynamics for different combinations of sensitizers and semiconductors have been reported by many groups. ET dynamics for $Ru(dcbpy)_2(NCS)_2$ [dcbpy=(4,4'-dicarboxy-2,2'-bipyridine)] (RuN3) sensitized TiO_2 semiconductor films have been the most extensively studied systems due to their highest light-to-electric energy conversion efficiency in DSSC, which was reported to be ～10% with an incident-photon-to-current conversion efficiency (IPCE) near unity at peak absorption wavelengths.[56-66] This high IPCE has been attributed to ultrafast electron injection from the RuN3 excited states to TiO_2,[57-64,67-75] and a much slower charge recombination from TiO_2 to the oxidized dye molecules and redox electrolytes.[65,66,76-82] In contrast, it has been reported that the cells based on other semiconductors, such as SnO_2, ZnO, Nb_2O_5, WO_3, Ta_2O_5 and In_2O_3 et al., show lower efficiency.[56,83-90] However, the reasons resulting in this lower efficiency have not been well understood. The investigation of the impact of the properties of the semiconductors and sensitizers on ET dynamics may provide a better understanding of the ET mechanism and hence the possibility to improve the efficiencies of these cells.

The ET dynamics from RuN3 dyes to several different semiconductor films, such as TiO_2, SnO_2, ZnO and In_2O_3, have been reported by many groups.[56,58-66,69,91-95] Electron injection dynamics on these films are all biphasic, consisting of a < 100 fs ultrafast component and one or more slower components on the picosecond or longer time scales.

However, the amplitude of the fast component and the rate of the slow components vary widely with semiconductor, as reported recently by our group.[93-95] Injection dynamics to TiO_2 are dominated by ultrafast injection, while those to SnO_2, In_2O_3 and ZnO are dominated by slower components. The fast component, which reflects the injection rate from ^{1}MLCT of RuN3 to the semiconductor, was found to follow the order of $TiO_2 > SnO_2 \approx In_2O_3 >$ ZnO, which has been attributed to the difference in their electron accepting density of states.

The dependence of ET dynamics on sensitizer energetics has also been investigated by comparing the electron injection kinetics to the same semiconductor from adsorbates with varying excited state potentials. The comparisons of electron injection from RuN3, Ru505, and Ru470 to TiO_2,[51] SnO_2,[96] In_2O_3,[93] and Nb_2O_5[97] have been reported. These studies showed that the injection rates from these dyes to each above semiconductor follow the order of RuN3 > Ru505 > Ru470, decreasing as the excited state oxidation potential lowers, which is consistent with the reduction of the semiconductor accepting states. These comparisons of injection rates among different semiconductors and different sensitizers suggest that the ET dynamics heavily depend on the electron accepting state density in the semiconductor. This work continues to focus on the examination of this dependence by using organic dyes as sensitizers. The effects of the nature of the semiconductor as well as the sensitizer energetics on ET dynamics are discussed.

1.3. Summary

In summary, we have conducted a series of studies on the interfacial charge separation dynamics in quantum dots adsorbed with molecular adsorbates and dye sensitized semiconductor film systems by using both transient absorption spectroscopy and time-resolved fluorescence spectroscopy. For the QD-molecular adsorbate system, exciton dissociation dynamics in CdSe QDs through both electron and hole transfer to electron and hole acceptors, respectively, have been systematically investigated. Multiple exciton dissociation in QDs has also been achieved by choosing the proper QD-adsorbate complex. For the dye sensitized semiconductor film system, ET dynamics for different combinations of organic dyes and semiconductor nanocrystalline thin films have been compared to explore the dependence of the ET rate on the nature of both the semiconductors and dye sensitizers.

The rest of this work is organized as follows: Chapter 2 summarizes the experimental procedures, including the preparation of quantum dots, semiconductor nanoparticles, and semiconductor films, as well as the experimental techniques. Chapter 3 introduces the exciton dissociation dynamics in CdSe QDs through ET to ReC0A. Chapter 4 presents the preliminary results of charge separation in CdS QDs through ET to FMN. Chapter 5 examines the exciton dissociation dynamics in CdSe QDs through hole transfer to Phenothiazine. hapter 6 demonstrates the multiple exciton dissociation dynamics in CdSe QDs through ET to Methylene Blue. Finally, Chapter 7 presents the investigation of ET dynamics from Rhodamine dyes to semiconductor nanocrystalline films. The dependence of ET dynamics on semiconductor as well as sensitizer energetics will also be discussed in this chapter.

References

(1) Gregg, B. A. *J. Phys. Chem. B.* **2003**, *107*, 4688.

(2) Fahrenbruch, A. L. B., R. H. *Academic Press: New York,* **1983**.

(3) Shockley W.; Queisser, H. J. *J. Appl. Phys.* **1961**, *32*, 510.

(4) Nozik, A. J. *Physica E: Low-Dimensional Systems & Nanostructures (Amsterdam, Netherlands)* **2002**, *14*, 115.

(5) Yu, W. W.; Qu, L.; Guo, W.; Peng, X. *Chem. Mater.* **2003**, *15*, 2854.

(6) Schaller, R. D.; Klimov, V. I. *Phys. Rev. Lett.* **2004**, *92*, 186601.

(7) Ellingson, R. J.; Beard, M. C.; Johnson, J. C.; Yu, P.; Micic, O. I.; Nozik, A. J.; Shabaev, A.; Efros, A. L. *Nano Letters* **2005**, *5*, 865.

(8) Luther, J. M.; Beard, M. C.; Song, Q.; Law, M.; Ellingson, R. J.; Nozik, A. J. *Nano Letters* **2007**, *7*, 1779.

(9) Schaller, R. D.; Sykora, M.; Pietryga, J. M.; Klimov, V. I. *Nano Letters* **2006**, *6*, 424.

(10) Trinh, M. T.; Houtepen, A. J.; Schins, J. M.; Hanrath, T.; Piris, J.; Knulst, W.; Goossens, A. P. L. M.; Siebbeles, L. D. A. *Nano Letters* **2008**, *8*, 1713.

(11) Murphy, J. E.; Beard, M. C.; Norman, A. G.; Ahrenkiel, S. P.; Johnson, J. C.; Yu, P.; Micic, O. I.; Ellingson, R. J.; Nozik, A. J. *Journal of the American Chemical Society* **2006**, *128*, 3241.

(12) Beard, M. C.; Knutsen, K. P.; Yu, P.; Luther, J. M.; Song, Q.; Metzger, W. K.; Ellingson, R. J.; Nozik, A. J. *Nano Letters* **2007**, *7*, 2506.

(13) Sykora, M.; Mangolini, L.; Schaller Richard, D.; Kortshagen, U.; Jurbergs, D.; Klimov Victor, I. *Physical Review Letters* **2008**, *100*, 067401.

(14) Schaller, R. D.; Sykora, M.; Jeong, S.; Klimov, V. I. *Journal of Physical Chemistry B* **2006**, *110*, 25332.

(15) Schaller, R. D.; Petruska, M. A.; Klimov, V. I. *Applied Physics Letters* **2005**, *87*, 253102/1.

(16) Schaller, R. D.; Pietryga, J. M.; Klimov, V. I. *Nano Lett.* **2007**, *7*, 3469.

(17) Pijpers, J. J. H.; Hendry, E.; Milder, M. T. W.; Fanciulli, R.; Savolainen, J.; Herek, J. L.; Vanmaekelbergh, D.; Ruhman, S.; Mocatta, D.; Oron, D.; Aharoni, A.; Banin, U.; Bonn, M. *J. Phys. Chem. C.* **2007**, *111*, 4146.

(18) Gabor, N. M.; Zhong, Z.; Bosnick, K.; Park, J.; McEuen, P. L. *Science* **2009**, *325*, 1367.

(19) Nozik, A. J. *Annual Review of Physical Chemistry* **2001**, *52*, 193.

(20) Klimov, V. I.; Mikhailovsky, A. A.; McBranch, D. W.; Leatherdale, C. A.; Bawendi, M. G. *Science* **2000**, *287*, 1011.

(21) Henglein, A. *Chem. Rev.* **1989**, *89*, 1861.

(22) Kamat, P. V. *Chem. Rev.* **1993**, *93*, 267.

(23) Kamat, P. V. *Progress In Reaction Kinetics* **1994**, *19*, 277.

(24) El-Sayed, M. A. *Accounts of Chemical Research* **2004**, *37*, 326.

(25) Kamat, P. *J. Phys. Chem. C* **2008**, *112*, 18737.

(26) Duonghong, D.; Ramsden, J.; Gratzel, M. *J. Am. Chem. Soc.* **1982**, *104*, 2977.

(27) Ramsden, J. J.; Gratzel, M. *Chem. Phys. Lett.* **1986**, *132*, 269.

(28) Rossetti, R.; Beck, S. M.; Brus, L. E. *J. Am. Chem. Soc.* **1984**, *106*, 980.

(29) Rossetti, R.; Brus, L. E. *J. Phys. Chem.* **1986**, *90*, 558.

(30) Kamat, P. V.; Dimitrijevic, N. M.; Fessenden, R. W. *Journal of Physical Chemistry* **1987**, *91*, 396.

(31) Henglein, A. *Pure & Appl. Chem.* **1984**, *56*, 1215.

(32) Hasselbarth, A.; Eychmuller, A.; Weller, H. *Chemical Physics Letters* **1993**, *203*, 271.

(33) Nosaka, Y.; Miyama, H.; Terauchi, M.; Kobayashi, T. *Journal of Physical Chemistry* **1988**, *92*, 255.

(34) Landes, C. F.; Braun, M.; El-Sayed, M. A. *Journal of Physical Chemistry B* **2001**, *105*, 10554.

(35) Logunov, S.; Green, T.; Marguet, S.; El-Sayed, M. A. *J. Phys. Chem. A* **1998**, *102*, 5652.

(36) Burda, C.; Green, T. C.; Link, S.; El-Sayed, M. A. *J. Phys. Chem. B* **1999**, *103*, 1783.

(37) Sharma, S. N.; Pillai, Z. S.; Kamat, P. V. *Journal of Physical Chemistry B* **2003**, *107*, 10088.

(38) Sykora, M.; Petruska, M. A.; Alstrum-Acevedo, J.; Bezel, I.; Meyer, T. J.; Klimov, V. I. *Journal of the American Chemical Society* **2006**, *128,* 9984.

(39) Boulesbaa, A.; Issac, A.; Stockwell, D.; Huang, Z.; Huang, J.; Guo, J.; Lian, T. *J. Am. Chem, Soc.* **2007**, *129*, 15132.

(40) Huang, J.; Huang, Z.; Jin, S.; Lian, T. *J. Phys. Chem. C* **2008**, *112*, 19734.

(41) Huang, J.; Stockwell, D.; Huang, Z.; Mohler, D. L.; Lian, T. *J. Am. Chem. Soc.* **2008**, *130*, 5632.

(42) Matylitsky, V. V.; Dworak, L.; Breus, V. V.; Basche, T.; Wachtveitl, J. *J Am Chem Soc* **2009**, *131*, 2424.

(43) Hasselbarth, A.; Eychmuller, A.; Eichberger, R.; Giersig, M.; Mews, A.; Weller, H. *Journal of Physical Chemistry* **1993**, *97*, 5333.

(44) Robel, I.; Kuno, M.; Kamat, P. V. *J. Am. Chem. Soc.* **2007**, *129*, 4136.

(45) Robel, I.; Subramanian, V.; Kuno, M.; Kamat, P. V. *J. Am. Chem. Soc.* **2006**, *128*, 2385.

(46) Blackburn, J. L.; Selmarten, D. C.; Ellingson, R. J.; Jones, M.; Micic, O.; Nozik, A. J. *Journal of Physical Chemistry B* **2005**, *109*, 2625.

(47) Klimov, V. I. *J. Phys. Chem. B* **2000**, *104*, 6112.

(48) Klimov, V. I.; Mikhailovsky, A. A.; McBranch, D. W.; Leatherdale, C. A.; Bawendi, M. G. *Phys. Rev. B* **2000**, *61*, R13349.

(49) Burda, C.; Link, S.; Mohamed, M.; El-Sayed, M. *Journal of Physical Chemistry B* **2001**, *105*, 12286.

(50) Landes, C. F.; Burda, C.; Braun, M.; El-Sayed, M. A. *J. Phys. Chem. B.* **2001**, *105*, 2981.

(51) O'Regan, B.; Gratzel, M. *Nature* **1991**, *353*, 737.

(52) Bach, U.; Lupo, D.; Comte, P.; Moser, J. E.; Weissortel, F.; Salbeck, J.; Spreitzer, H.; Gratzel, M. *Nature* **1998**, *395*, 583.

(53) Gratzel, M. *Journal of Photochemistry and Photobiology, C: Photochemistry Reviews* **2003**, *4*, 145.

(54) Miller, R. J. D.; McLendon, G. L.; Nozik, A. J.; Schmickler, W.; Willig, F. *Surface electron transfer processes*; VCH publishers, Inc.: New York, 1995.

(55) Hagfeldt, A.; Gratzel, M. *Chem. Rev.* **1995**, *95*, 49.

(56) Sayama, K.; Sugihara, H.; Arakawa, H. *Chem. Mater.* **1998**, *10*, 3825.

(57) Asbury, J. B.; Hao, E.; Wang, Y.; Ghosh, H. N.; Lian, T. *J. Phys. Chem. B* **2001**, *105*, 4545.

(58) Ellingson, R. J.; Asbury, J. B.; Ferrere, S.; Ghosh, H. N.; Sprague, J. R.; Lian, T.; Nozik, A. J. *J. Phys. Chem. B* **1998**, *102*, 6455.

(59) Tachibana, Y.; Haque, S. A.; Mercer, I. P.; Moser, J. E.; Klug, D. R.; Durrant, J. R. *J. Phys. Chem. B* **2001**, *105*, 7424.

(60) Tachibana, Y.; Moser, J. E.; Graetzel, M.; Klug, D. R.; Durrant, J. R. *J. Phys. Chem.* **1996**, *100*, 20056.

(61) Kuciauskas, D.; Monat, J. E.; Villahermosa, R.; Gray, H. B.; Lewis, N. S.; McCusker, J. K. *J. Phys. Chem. B* **2002**, *106*, 9347.

(62) Hannappel, T.; Burfeindt, B.; Storck, W.; Willig, F. *J. Phys. Chem. B* **1997**, *101*, 6799.

(63) Kallioinen, J.; Benko, G.; Sundstrom, V.; Korppi-Tommola, J. E. I.; Yartsev, A. P. *J. Phys. Chem. B* **2002**, *106*, 4396.

(64) Benko, G.; Kallioinen, J.; Korppi-Tommola, J. E. I.; Yartsev, A. P.; Sundstrom, V. *J. Am. Chem. Soc.* **2002**, *124*, 489.

(65) Heimer, T. A.; Heilweil, E. J.; Bignozzi, C. A.; Meyer, G. J. *J. Phys. Chem. A* **2000**, *104*, 4256.

(66) Haque, S. A.; Tachibana, Y.; Willis, R. L.; Moser, J. E.; Graetzel, M.; Klug, D. R.; Durrant, J. R. *J. Phys. Chem. B* **2000**, *104*, 538.

(67) Asbury, J. B.; Anderson, N. A.; Hao, E.; Lian, T. *J. Phys. Chem. B* **2003**, *107*, 7376.

(68) Asbury, J. B.; Wang, Y. Q.; Hao, E. C.; Ghosh, H. N.; Lian, T. *Res. Chem. Interm.* **2001**, *27*, 393.

(69) Ellingson, R. J.; Asbury, J. B.; Ferrere, S.; Ghosh, H. N.; Sprague, J. R.; Lian, T.; Nozik, A. J. *Z. Phys. Chem. (Muenchen)* **1999**, *212*, 77.

(70) Asbury, J. B.; Wang, Y.; Lian, T. *J. Phys. Chem. B* **1999**, *103*, 6643.

(71) Tachibana, Y.; Nazeeruddin, M. K.; Gratzel, M.; Klug, D. R.; Durrant, J. R. *Chemical Physics* **2002**, *285*, 127.

(72) Durrant, J. R.; Tachibana, Y.; Mercer, I.; Moser, J. E.; Gratzel, M.; Klug, D. R. *Z. Phys. Chem.* **1999**, *212*, 93.

(73) Kallioinen, J.; Benko, G.; Myllyperkio, P.; Khriachtechev, L.; Skarman, B.; Wallenberg, R.; Tuomikoski, M.; Korppi-Tommola, J. E. I.; Sundstrom, V.; Yartsev, A. P. *Journal of Physical Chemistry B* **2004**, *108*, 6365.

(74) Benko, G.; Kallioinen, J.; Myllyperkio, P.; Trif, F.; Korppi-Tommola, J. E. I.; Yartsev, A. P.; Sundstrom, V. *Journal of Physical Chemistry B* **2004**, *108*, 2862.

(75) Benko, G.; Myllyperkio, P.; Pan, J.; Yartsev, A. P.; Sundstrom, V. *J. Am. Chem. Soc* **2003**, *125*, 1118.

(76) Kamat, P. V.; Bedja, I.; Hotchandani, S.; Patterson, L. K. *Journal of Physical Chemistry* **1996**, *100*, 4900.

(77) Palomares, E.; Clifford, J. N.; Haque, S. A.; Lutz, T.; Durrant, J. R. *Journal of the American Chemical Society* **2003**, *125*, 475.

(78) Barzykin, A. V.; Tachiya, M. *J. Phys. Chem. B* **2002**, *106*, 4356.

(79) Barzykin, A. V.; Tachiya, M. *Journal of Physical Chemistry B* **2004**, *108*, 8385.

(80) Hasselmann, G. M.; Meyer, G. J. *J. Phys. Chem. B* **1999**, *103*, 7671.

(81) Nelson, J. *Phys. Rev. B* **1999**, *59*, 15374.

(82) Nelson, J.; Haque, S. A.; Klug, D. R.; Durrant, J. R. *Phys. Rev. B: Condens. Matter Mater. Phys.* **2001**, *63*, 205321.

(83) Hara, K.; Horiguchi, T.; Kinoshita, T.; Sayama, K.; Sugihara, H.; Arakawa, H. *Solar Energy Materials and Solar Cells* **2000**, *64*, 115.

(84) Rensmo, H.; Keis, K.; Lindstrom, H.; Sodergren, S.; Solbrand, A.; Hagfeldt, A.; Lindquist, S. E.; Wang, L. N.; Muhammed, M. *Journal of Physical Chemistry* **1997**, *101*, 2598.

(85) Aegerter, M. A. *Solar Energy Materials and Solar Cells* **2001**, *68*, 401.

(86) Aegerter, M. A.; Schmitt, M.; Guo, Y. *International Journal of Photoenergy* **2002**, *4*, 1.

(87) Barros Filho, D. d. A.; Abreu Filho, P. P.; Werner, U.; Aegerter, M. A. *Journal of Sol-Gel Science and Technology* **1997**, *8*, 735.

(88) Lenzmann, F.; Krueger, J.; Burnside, S.; Brooks, K.; Graetzel, M.; Gal, D.; Ruehle, S.; Cahen, D. *Journal of Physical Chemistry B* **2001**, *105*, 6347.

(89) Bedja, I.; Hotchandani, S.; Kamat, P. V. *J. Phys. Chem.* **1994**, *98*, 4133.

(90) Ferrere, S.; Zaban, A.; Gregg, B. A. *Journal of Physical Chemistry B* **1997**, *101*, 4490.

(91) Asbury, J. B.; Ellingson, R. J.; Ghosh, H. N.; Ferrere, S.; Nozik, A. J.; Lian, T. *J. Phys. Chem. B* **1999**, *103*, 3110.

(92) Stergiopoulos, T.; Arabatzis, I. M.; Cachet, H.; Falaras, P. *Journal of Photochemistry and Photobiology, A: Chemistry* **2003**, *155*, 163.

(93) Guo, J.; Stockwell, D.; Ai, X.; She, C.; Anderson, N. A.; Lian, T. *Journal of Physical Chemistry B* **2006**, *110*, 5238.

(94) Anderson, N. A.; Ai, X.; Lian, T. *J. Phys, Chem. B* **2003**, *107*, 14414.

(95) Ai, X.; Anderson, N. A.; Guo, J.; Lian, T. *Journal of Physical Chemistry B* **2005**, *109*, 7088.

(96) Jacobson, K. I.; Jacobson, R. E. *Imaging Systems*; John Wiley & Sons: New York, 1976.

(97) Nazeeruddin, M. K.; Kay, A.; Rodicio, I.; Humphrybaker, R.; Muller, E.; Liska, P.; Vlachopoulos, N.; Gratzel, M. *J. Am. Chem. Soc.* **1993**, *115*, 6382.

Chapter 2. Experimental Methods

The experimental procedure in this work includes three steps: (1) Synthesis of CdSe quantum dots (QDs) or semiconductor nanocrystalline thin films (ZrO_2, ZnO, SnO_2, In_2O_3); (2) Preparation of QD-adsorbate complex and dye sensitized semiconductor films; and (3) Spectroscopic measurements. The synthesis of quantum dots and semiconductor thin films was based on the published procedures. The latter was slightly modified to produce homogeneous and transparent films. The molecular dyes used in this work are listed as follows: $Re(CO)_3Cl(dcbpy)$ (dcbpy = 4,4'-dicarboxy-2, 2'-bipyridine) (ReC0A) complex, Methylene Blue (MB^+), Flavin mononucleotide (FMN), Phenothiazine (PTZ), Rhodamine B (RhB), Rhodamine 101 (Rh101), and Rhodamine 6G (Rh6G). The semiconductor-molecular dye samples were characterized by static UV-vis absorption spectroscopy and FTIR spectroscopy before the measurement of charge transfer dynamics. Transient visible spectroscopy, transient mid-IR spectroscopy, and time-resolved fluorescence spectroscopy were used to examine the charge transfer dynamics in the interface of semiconductor nanoparticle and adsorbed dye molecules.

2.1. Preparation of QDs and Semiconductor Thin Films.

2.1.1 Preparation of CdSe Quantum Dots.

Trioctylphosphine oxide (TOPO, 99%) capped CdSe nanoparticles were synthesized according to a previously published procedure.[1] Briefly, a mixture of 0.0514 g of CdO, 0.2232 g of n-Tetradecylphonic acid (TDPA, 98%) and 3.7768 g of TOPO in a 25 mL flask was heated to 300-320 °C under N_2 flow. After CdO was dissolved, the temperature of the solution was cooled to 270 °C. Then, a selenium stock solution (0.0411 g of selenium powder dissolved in 2.4 mL of trioctylphosphine (TOP, technical grade 90%)) was quickly injected into this hot solution. The subsequent growth of CdSe nanoparticles was carried out at 250 °C. The reaction was stopped once the desired size of CdSe particles was reached.

Oleic acid (OA)-capped CdSe QDs were synthesized according to an established literature procedure.[2] Briefly, a mixture of CdO (0.0640g), 1-octadecene (ODE, 9.00mL) and OA (0.80mL) in a flask was heated to 320^{o}C under N_2 flow. The amount of OA was adjusted to obtain the desired QDs sizes. After CdO was dissolved, the solution was cooled down to ～ 270 ^{o}C. Another solution containing 102.1 mg of Se in mixed solvents of ODE (2.65 mL) and Tributylphosphine (TBP, 0.35mL) was injected to the hot solution quickly. The reaction mixture was cooled to ~250^{o}C and the temperature was fixed at 250^{o}C for the subsequent growth of CdSe. The reaction was stopped once the desired size of CdSe particles was reached.

The fluorescence quantum yields for the CdSe QDs used in this work range from 6% ～ 10%

2.1.2 Preparation of CdS Quantum Dots.

2.1.3 Preparation of ZrO_2 Nanocrystalline Thin Films.

ZrO_2 thin films were prepared according to the published procedure.[3] ZrO_2 powder was purchased from Degussa Corporation. 2g ZrO_2 powder was ground in a mortar and mixed with 4 mL distilled water. 10 μl acetylacetone and 5 drops of Triton X-100 were then added and the mixture was stirred for at least three days. Several drops of the mixture were spread on the polished sapphire windows. The obtained films were dried in air and baked at 400°C for 1 h in air.

2.1.4 Preparation of SnO_2 Nanocrystalline Thin Films.

SnO_2 colloids for SnO_2 thin films was synthesized according to a published procedure.[4] 250 mL waster in a round bottom flask was vigorously stirred for ～ 30 mins in an ice bath (solution 1). 5 mL $SnCl_4$ was carefully dissolved in 20 mL of HCl (37 wt. %) followed by sonicating for 30 mins (solution 2). The resulting solution 2 was added dropwise into solution 1. The obtained mixture was stirred for another 30 mins, and was then PH adjusted to 3.5 by aqueous ammonia (25%), which led to the precipitation of SnO_2. The precipitate was allowed to sit overnight in the dark, after which was washed at least 3 times with distilled water. The precipitate was then re-suspended in 300 mL of water and the pH value was adjusted to 9.5-10. The solution was stirred overnight, after which it was dialyzed in aqueous ammonia (pH 10) for three days. The resulting transparent SnO_2 colloid was refluxed for 4 h and autoclaved at 150°C for 1 h, then 270°C for 16 h. 100 mL of colloid was concentrated to 30 mL and was mixed with several drops of Triton X-100. The resulting solution was stirred for 1 day and then casted onto polished sapphire windows to prepare the films. The films were air-dried and baked at 400°C for 1h.

2.1.5 Preparation of In_2O_3 Nanocrystalline Thin Films.

In_2O_3 colloids for In_2O_3 thin films were synthesized according to a published procedure.[5,6] Briefly, $InCl_3 \cdot 4H_2O$ (1g) was dissolved in 14 ml of de-ionized H_2Oat 0^oC under vigorous stirring. The solution then was PH adjusted to ~8 by aqueous ammonia (25%), leading to the precipitation of indium hydroxide. The precipitate was collected after centrifuge and dried in vacuum. After that, 4 ml of H_2O, 1 drop of 2,4-pentanedione and 10 drops of Triton X-100 were added to the dried precipitate. The mixture was then stirred vigorously for at least 3 days, and spread onto sapphire windows. The resulting films were air-dried and baked at 400 ^oC for 1 hour.

2.1.6 Preparation of ZnO Nanocrystalline Thin Films.

ZnO nanoparticle colloids for ZnO thin films were prepared similarly to a published procedure.[7] 10 mmol $Zn(Ac)_2$ was added to 5 mL absolute ethanol at 0°C (mixture 1).14 mmol $LiOH \cdot H_2O$ was mixed with 95 mL ethanol, followed by sonicating for 30 mins. The resulting solution was cooled to 0°C (solution 1). Solution 1 was slowly added to the mixture 1 under vigorous stirring (mixture 2). Mixture 2 was washed with the hexane:ethonal (3:1) solution for three times, followed by centrifuge. The ZnO precipitate was then collected and re-suspended in ethanol to make ZnO colloid. To make ZnO films, several drops of the above ZnO colloid was deposited to a polished sapphire window. The resulting film was dried in air and baked at 400°C for 1 hour.

2.2. Preparation of QD-adsorbate Complex and Dye Sensitized Semiconductor Thin Films.

2.2.1. Molecular Adsorbates Used in This Work

ReC0A was synthesized based on published procedures by Debbie Mohler et al. at Emory University.[8] Methylene Blue Chloride, Phenothiazine, Rhodamine B, Rhodamine 101, and Rhodamine 6G were all purchased from Aldrich and used without further purification. Figure 2.1 shows the molecular structures of these dyes.

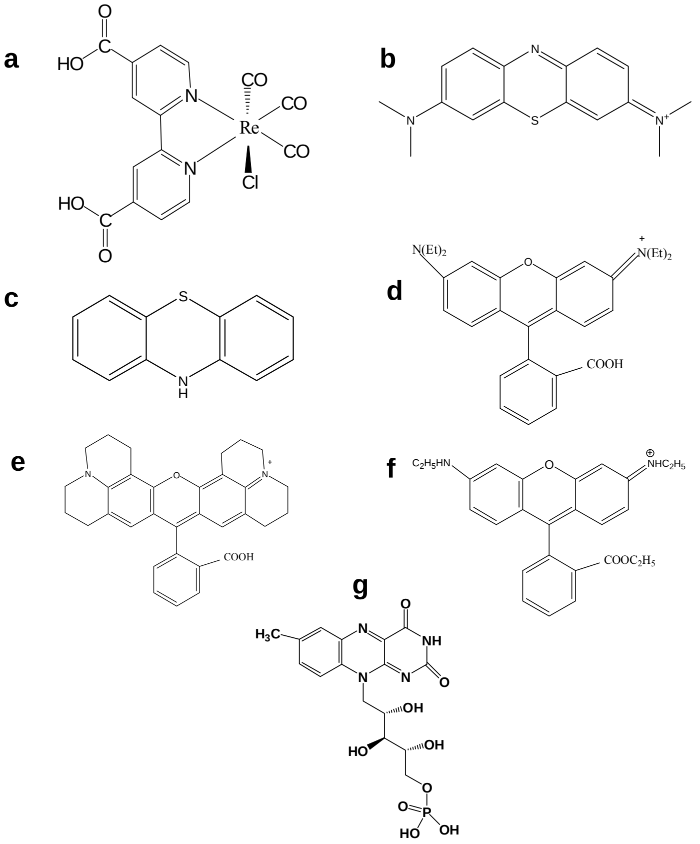

Figure 2.1. Molecular Structures of (a) ReC0A, (b) Methylene Blue, (c) Phenothiazine, (d) Rhodamine B, (e) Rhodamine 101, (f) Rhodamine 6G, and (g) Flavin mononucleotide.

2.2.2. Preparation of QD-Adsorbate Complex and Dye Sensitized Thin Films.

To prepare CdSe-ReC0A complexes and CdSe-MB^+ complexes, ReC0A and MB^+ were first added to CdSe QDs solution in heptane, respectively. The number of adsorbates per QD was controlled by varying the amount of added adsorbates. The mixtures were then sonicated and filtered to remove undissolved adsorbates.

CdSe-PTZ complexes were prepared by adding PTZ to CdSe QDs solution in heptane, followed by sonication. The concentration of PTZ in QD solution was also controlled by varying the amount of added PTZ.

Dye sensitized semiconductor films was prepared by soaking the films in a dye solution.[9] The coverage of dyes on the films was controlled by varying the dye concentration and soaking time. The fresh sensitized film was rinsed with the additional solvent in order to remove physically adsorbed dye molecules, and then dried in air.

2.3. Spectroscopic Measurement.

2.3.1 Transient IR Absorption Measurement.

Ultrafast absorption experiments were conducted by using pump-probe transient absorption scheme.[10] The tunable infrared spectrometer used a regeneratively amplified Ti:Sapphire laser system (Coherent Legend, 800 nm, 150 fs, 2.5 mJ/pulse, 1 KHz repetition rate) and two optical parametric amplifiers (OPAs). The 800 nm pump (1 mJ/pulse) was used to pump an IR-OPA (Coherent OPerA) to produce signal and idler outputs at 1380 nm and 1903 nm, respectively. Tunable mid-IR probe pulses were produced by difference-frequency generation of the signal and idler which were collinearly mixed in an $AgGaS_2$ crystal. The probe pulses have a full width at half-maximum (fwhm) of ～120 cm^{-1} and ~5 μJ energy at 5000 nm. The IR probe pulses were attenuated with a beam splitter and ND filters (to ～10 nJ) and chirp-corrected with Ge windows before the sample.

Pump pulses were generated by a home-built sum frequency setup, in which either the signal or idler outputs (80 and 40 μJ, respectively) of an IR-OPA (Clark-MXR, pumped with 1 mJ of 800nm pulse) were collinearly mixed with the 800 nm beam (~100 μJ) in a BBO crystal to produce tunable pump pulses from 460 nm to 650 nm. The energy of the 532 nm pulse used for the measurement was controlled by a variable neutral density filter wheel. The pump and probe beam diameters at the sample were ～ 250 and 180 μm, respectively. After the sample, the probe (centered at 2000 cm^{-1}) was dispersed in a spectrometer with resolution of 15 nm (5.4 cm^{-1} at 2000 cm^{-1}) and detected with a 32-element mercury cadmium telluride (MCT) array detector. Every other pump pulse was blocked by a synchronized chopper (New Focus 3500) at 500 Hz, and the absorbance change was calculated from sequential pumped vs. unpumped probe pulses.

The instrument response function and zero time delay were determined with a thin Si wafer, which gives an instantaneous mid-IR absorption response after excitation at 532 nm. Typically, the instrument response function was well fit by a Gaussian function with 160 fs fwhm. During the data collection, samples were constantly translated at a speed of 5 mm/min to avoid photodegredation.

2.3.2 Transeint Visible Absorption Measurement

Pump pulses at 532 nm were generated as described in the previous section and focused on the sample with a beam diameter of 300 μm and energy of 25 nJ/pulse. Pump pulses at 400 nm were generated by frequency doubling ~100 μJ of the fundamental in a BBO crystal. The energy of the pump pulses were controlled by a variable neutral-density filter wheel.

The visible probe was generated by attenuating and focusing ~10 μJ of the 800 nm pulse into a rotating CaF_2 window to produce a white light continuum from 370 to 700 nm. The probe was focused on the sample using protected Al parabolic reflectors to a spot size of 150 μm. After the sample, the probe was focused into a fiber-coupled spectrometer (Ocean Optics USB2000, 2048 pixel CCD, ~.25 nm/pixel readout) and detected at a frequency of 10 Hz. The pump pulses were chopped by a synchronized chopper to the same frequency. Samples were constantly translated as described previously to prevent long term photodegredation.

2.3.3 Time-Resolved Fluorescence Spectroscopy

Time–resolved fluorescence measurements were performed in the time-correlated single photon counting (TCSPC) mode under right-angle sample geometry.[11] A mode-locked Ti:Sapphire laser (Tsunami oscillator pumped by a 10 W Millennia Pro, Spectra-Physics) was used to generate femtosecond laser pulses (~100 fs) with a repetition rate of 80 MHz. Pump pulses at 400 nm were produced by doubling the output centered at 800 nm in a BBO crystal. The emission was detected by a micro-channel-plate-photomultiplier tube (Hamamatsu R3809U-51), the output of which was amplified and analyzed by a TCSPC board (Becker & Hickel SPC 600).

References

(1) Peng, Z. A.; Peng, X. *J. Am. Chem. Soc.* **2001**, *123*, 183.

(2) Yu, W. W.; Wang, Y. A.; Peng, X. *Chem. Mater.* **2003**, *15*, 4300.

(3) Nazeeruddin, M. K.; Kay, A.; Rodicio, I.; Humphrybaker, R.; Muller, E.; Liska, P.; Vlachopoulos, N.; Gratzel, M. *J. Am. Chem. Soc.* **1993**, *115*, 6382.

(4) Nutz, T.; Felde, U. Z.; Haase, M. *J. Chem. Phys.* **1999**, *110*, 12142.

(5) Poznyak, S. K.; Golubev, A. N.; Kulak, A. I. *Surf. Sci.* **2000**, *454-456*, 396.

(6) Poznyak, S. K.; Kulak, A. I. *Electr. Acta* **2000**, *45*, 1595.

(7) Meulenkamp, E. *J. Phys. Chem. B* **1998**, *102*, 5566.

(8) Anderson, N. A.; Ai, X.; Chen, D.; Mohler, D. L.; Lian, T. *Journal of Physical Chemistry B* **2003**, *107*, 14231.

(9) Ai, X. Interfacial electron transfer (ET) from sensitizer/dyes to semiconductor nanocrystalline thin films studied by ultrafast infrared spectroscopy. Dissertation, Emory University, 2004.

(10) Huang, J.; Stockwell, D.; Boulesbaa, A.; Guo, J.; Lian, T. *J. Phys. Chem. C* **2008**, *112*, 5203.

(11) Huang, J.; Huang, Z.; Jin, S.; Lian, T. *J. Phys. Chem. C* **2008**, *112*, 19734.

Chapter 3. Exciton Dissociation Dynamics in CdSe Quantum Dots by Electron Transfer to Re-bipyridyl Complexes

3.1. Introduction

Charge separation dynamics in quantum dots (QDs) are currently a subject of intense study because of its potential applications in many electronic devices such as QD based solar cells.[1] A unique attribute of quantum dot based systems in solar cells is the generation of multiple electron-hole pairs (excitons) by absorbing one high energy photon, a process known as multiexciton generation (MEG). The mechanism, efficiency, and generality of MEG are still subjects of intense current debate. If efficient MEG in QDs is proven to be true, it offers en exciting possibility to significantly enhance the efficiency of QD-based solar cells.[2-5] The next major step in achieving this goal following multiple exciton generation is efficient collection of charge carriers, requiring that the electron-hole pairs produced by photoexcitation be separated into free charges before exciton-exciton annihilation process which usually occurs on 10s to 100s time scales.

Ultrafast dissociation of excitons in CdS and CdSe QDs through electron transfer (ET) to molecular acceptors and oxide particles has been reported. For example, Nozik and coworkers observed charge separation in CdS QDs via electron transfer to TiO_2 films with electron injection time scale ～10–50 ps.[6] Kamat et al. bound CdSe QDs to TiO_2 nanoparticles with a thiol linker and observed charge transfer from excited CdSe to TiO_2 by probing the exciton bleach recovery of CdSe.[7] The obtained injection rate was in the range of $0.073–1.95\times10^{11}$ s^{-1}. Most recently, we have separated electron and hole pairs in CdS QDs via electron transfer from CdS to Rhodamine B (RhB) dyes after exciting CdS at 400 nm.[8] The measured separation time varied from 12 ps to 90 ps as the number of RhB molecules on each CdS particle decreased from 4.1 to 1.1.

While some of these studies revealed that excitons in QDs can be dissociated through ultrafast electron transfer pathway to molecular adsorbates with 10s of picoseconds and faster time scales, the factors that control the pathways and rates of charge transfer remain poorly understood. In this chapter, we reported exciton dissociation dynamics in CdSe QDs adsorbed with $Re(CO)_3Cl(dcbpy)$ (dcbpy = 4,4'-dicarboxy-2, 2'-bipyridine) (ReC0A) complex by using both transient absorption spectroscopy and time-resolved fluorescence spectroscopy. ReC0A was chosen for the study because (a) it has appropriate electrochemical potentials with reduction and oxidation potentials of -0.96 and 1.42 V (vs SCE),[9] respectively, enabling it to act as an electron acceptor only, (b) it has three strong CO stretching bands in the mid-IR that can be used as a probe of the acceptor dynamics,[10] and (c) there are a series of this type of complex Re(CO)3(L) with varying numbers of methylene groups (n = 0-5) inserted between the bipyridine ligand and each of the two carboxylate binding groups available in our lab. This enables systematic studies on distance-dependent charge separation between QDs and acceptors in the future.

In current work, we showed that the excitons in CdSe QDs dissociated by ultrafast ET to ReC0A complex:

$$CdSe^*(1S_e,1S_h) + \mathrm{Re}C0A \xrightarrow{k_S} CdSe^+(1S_h) + \mathrm{Re}C0A^- \qquad (3.1)$$

where CdSe* and $CdSe^+$ represent excited and oxidized states of CdSe, respectively, and $ReC0A^-$ represents the oxidized state of ReC0A. Furthermore, it was found that ET rate could be controlled by varying the size of QDs. In CdSe (435nm)-ReC0A complex, exciton dissociation half-time was observed to be ～ 2.3 ps, suggesting the possibility of separating multiple electron-hole pairs generated by the MEG process using QD-based donor-acceptor complexes. In addition, we vary the size of CdSe, and the ratio of donor to acceptor to examine their effects on charge separation rates. The observed separation rates are strongly dependent on both the size of CdSe and the number of ReC0A molecules adsorbed on CdSe QDs. The possible reasons for the observed dependence will be discussed.

3.2 Results

3.2.1. Exciton Dissociation Pathway

3.2.1.1 Static Absorption Measurement. Figure 3.1a shows the UV-vis absorption spectra of CdSe QDs in heptane prepared by established literature procedure.[11] It can be seen that the lowest energy allowed ($1S_{3/2}$(h)-$1S_{1/2}$(e)) exciton transition peaks for these QDs are located at 435 nm, 477 nm, and 505 nm, respectively. Based on the previous reported results by Peng's group, the estimated diameters for CdSe (435nm), CdSe (477nm), and CdSe (505nm) are ～1.8, 2.2 and 2.4 nm, respectively.[12] The fluorescence quantum yields for these QDs are ～ 8 - 12%. Because of the overlap of the absorption of ^{1}MLCT band of ReC0A and the absorption of CdSe QDs, it is difficult to quantitatively determine the number of adsorbed ReC0A per QDs according to UV-vis spectrum. An alternative approach is to use the IR spectrum of ReC0A, in which three CO groups have strong absorption in mid-IR region. Shown in Figure 3.1b are the spectra of ReC0A in CdSe-ReC0A complexes after subtracting the FTIR spectra of CdSe alone. The three bands centered at 1903, 1921 and 2020 cm^{-1} are assigned to CO stretching modes, consistent with our previous reports.[10] Based on the absorbance and known extinction coefficients of CdSe and ReC0A (4078 M^{-1}cm^{-1} for high-frequency CO stretching band), the average number of adsorbed ReC0A molecules per QD particle for CdSe (435nm), CdSe (477nm), and CdSe (505nm) are calculated to be ~ 0.3.[11,13]

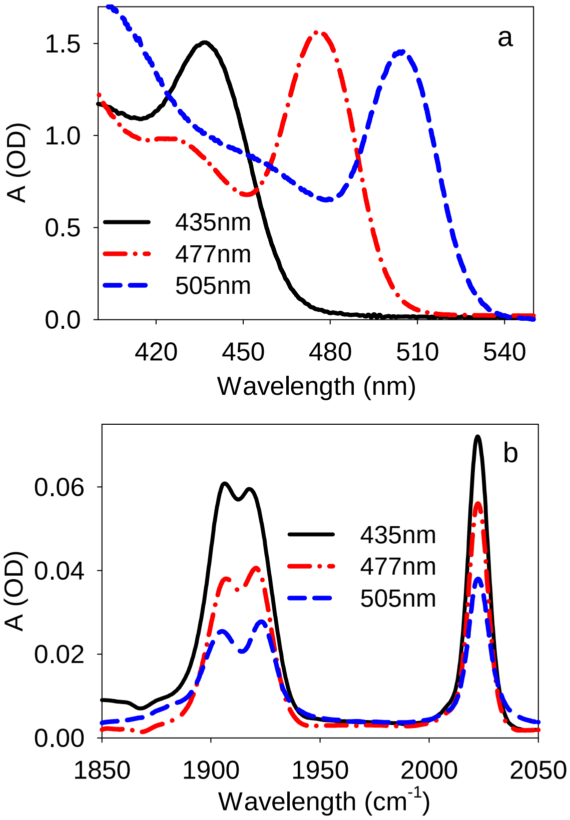

Figure 3.1. (a) UV-vis absorption spectra of CdSe QDs with indicated first exciton peak positions. b) FTIR spectra of ReC0A absorbed on CdSe QDs with indicated first exciton peak positions.

3.2.1.2 Fluorescence Lifetime Measurement. Figure 3.2 shows the fluorescence lifetime decay of CdSe (505nm) QDs adsorbed with different numbers of ReC0A. The fluorescence measurement was recorded at 510 nm after 400 nm excitation. The excitons in free CdSe QDs are long-lived with a lifetime ~ 40 ns. However, in the presence of ReC0A, the exciton lifetime in QDs is reduced, and the quenching rate increased with the number of adsorbed molecules. There are three possible pathways for the quenching of QD excitons by the adsorbate: (1) ET from QD conduction band to the unoccupied molecular orbitals of ReC0A, producing a reduced ReC0A ($ReC0A^-$) and a hole in QDs; (2) hole transfer from valence band of QDs to the occupied molecular orbitals of ReC0A, forming an oxidized ReC0A ($ReC0A^+$) and an electron in the QD conduction band; and (3) energy transfer from QD to ReC0A, producing an excited ReC0A (ReC0A*) and QD in its ground state. Energy transfer is unlikely in this system because of the negligible overlap of the QD emission spectrum with the absorption spectrum of ReC0A. ET and hole transfer processes lead to different products that can be distinguished by transient absorption spectroscopy.

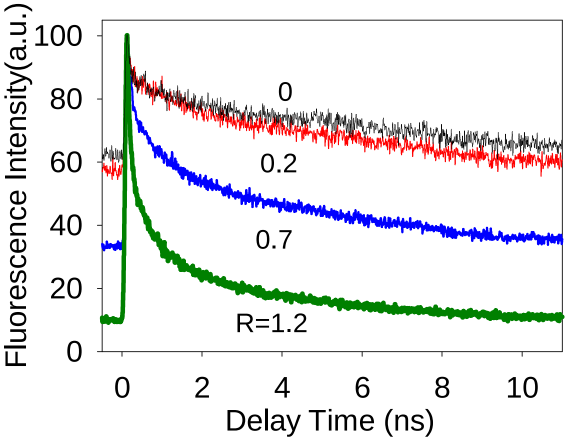

Figure 3.2. Fluorescence decay of CdSe (505nm) with indicated average number (R) of adsorbed ReC0A per QD. Adapted from Ref. 14.

3.2.1.3 Transient IR Absorption Measurement. The transient IR spectra of CdSe(435nm)-ReC0A complex was shown in Figure 3.3. These spectra were obtained after 400 nm excitation with probe wavelength centered at 1900 and 2010 cm^{-1}. The spectra clearly show a bleach of the ground state CO stretches at 1904, 1918 and 2020 cm^{-1}, indicating the depletion of ReC0A molecules in its ground state. In addition to the bleach, two new positive bands are formed at around 1886 and 1998 cm^{-1}, which are red-shifted by ~20 cm^{-1} compared to the low and high frequency CO stretching bands, respectively. These red-shifted bands are similar to those observed at 1883 and 1997 cm^{-1} for the reduced form of $Re(CO)_3(bpy)Cl$ [14] and thus are assigned to the reduced form (anion) of ReC0A molecule. The reduction of the complex ReC0A destabilizes the π^* LUMO of the bipyridine ligand. Because of the mixing between the bipyridine π^* orbital and Re d orbital, the reduction leads to an enhanced charge density at the metal center. This effect increases the $Re \rightarrow CO$ π-back-bonding, weakening the CO bond and thus lowering the stretching frequency.[14] Similar transient IR features were observed in QD-ReC0A complexes of CdSe (477nm) and CdSe (505nm). These results suggest that excitons in CdSe dissociate ET to ReC0A.

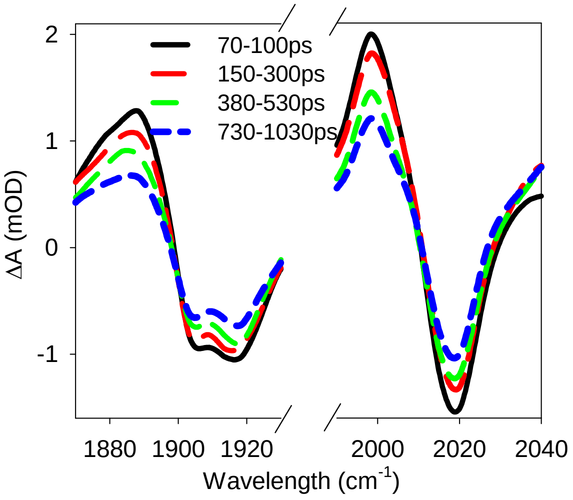

Figure 3.3. (a) Transient IR spectra of CdSe (435nm) -ReC0A complex in the CO stretching mode region at indicated delay times after 400 nm excitation.

The ET process can also be measured by spectral changes in the QDs. As reported by Guyot-Sionnest and coworkers, the presence of 1S electrons in QDs results in a strong 1S(e)-1P(e) intraband transition in the mid-IR region, whose energy and strength are dependent on QD size.[15] At larger sizes, 1S(e)-1P(e) intraband transition has lower resonance frequency and carries more oscillator strength. Therefore, to facilitate the measurement of electron decay kinetics of intraband absorption, larger size CdSe QDs (505 nm) which have an extensive absorption within 1600 – 3300 cm^{-1} spectral range were used to examine exciton dissociation dynamics.

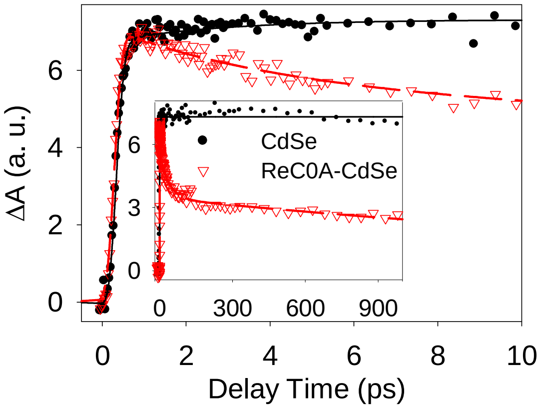

Figure 3.4. Comparison of electron decay kinetics of intraband transition probed in 2070cm^{-1} in CdSe (filled circles) and CdSe-ReC0A (open triangles) after 500 nm excitation. The inset shows the data extended to the longer time scale. Both kinetics have been normalized at the maximum amplitudes for better comparison.

With the loss of electron in the conduction band of CdSe due to ET process in the presence of ReC0A, faster decay kinetics of the intraband absorption are expected in CdSe-ReC0A assemblies as compared to CdSe alone. Shown in Figure 3.4 is the comparison of electron decay kinetics for CdSe and CdSe-ReC0A complex probed at 2070 cm^{-1} with their longer time scale kinetics in the inset. Because there is negligible contribution from the vibrational bands of ReC0A at this frequency, the decay kinetics measured here should directly reflect the intraband electron absorption from CdSe. The electron intraband absorption in CdSe alone (filled circle, Figure 3.4) remains constant with negligible decay within the 1 ns time scale window, suggesting that without an acceptor, the exciton states are long-lived at this wavelength. Additionally, this non-decay feature of electron absorption indicates that this frequency is the resonant frequency of electron intraband transition from 1S(e) to 1P(e) in CdSe. We have recorded the intraband absorption for many sizes of CdSe QDs using different mid-IR spectral regions. The electron signal decay kinetics are sensitive to probe wavelength and only within a small spectral range was the extremely long lifetime observed. When the wavelength was tuned either to lower or higher energy, the absorption signal decayed to a significant extent. This wavelength dependent decay kinetics was clearly observed by comparing the electron decay kinetics of CdSe (505nm) recorded at different wavelengths, which was shown in Figure 3.5. This observation is in satisfactory agreement with the intraband study of electronic relaxation presented by Guyot-Sionnest et al., where the electron in the conduction band of CdSe experiences fast relaxation to its lowest electronic state once the resonant frequency was reached.[15] Therefore, significantly faster decay kinetics of electron in CdSe-ReC0A complex (open triangles in Figure 3.4) directly illustrates electron transfer dynamics from the conduction band of CdSe QDs to ReC0A molecule.

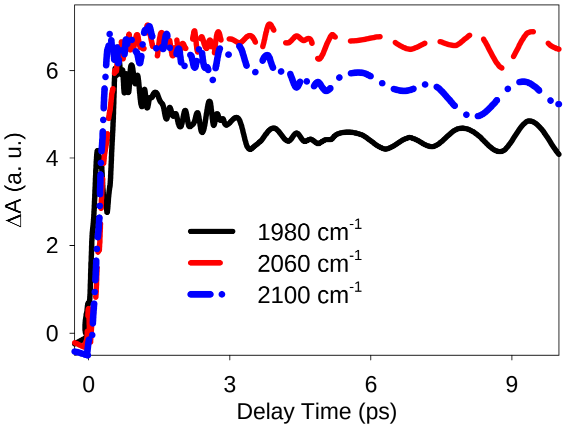

Figure 3.5. Comparison of electron decay kinetics of intraband transition in CdSe probed under different wavelengths after 500 nm excitation.

3.2.1.4 Transient Visible Absorption Measurement. In addition to the intraband absorption, the presence of 1S electron also led to a bleach of the first exciton transition band in the transient visible spectra. This bleach arises from the decrease in occupation of the quantized 1S(e) electronic state, which reduces the oscillator strength of the transition from 1S(h) to this electronic state because of the Pauli exclusion principle.[16] This bleach was observed from both the transient visible spectra of CdSe and CdSe-ReC0A complex as shown Figure 3.6a and b, respectively. After 400 nm excitation, the transient spectra of CdSe and CdSe-ReC0A complex measured at indicated delay times showed bleach of $1S_{3/2}$(h)-$1S_{1/2}$(e) (at 505nm) and $2S_{3/2}$(h)-$1S_{1/2}$(e) (at 450nm) exciton interband transitions. For CdSe alone (Fig. 3.6a), these exciton interband bleaches have negligible recovery on the < 1 ns time window, indicating the long-lived exciton and negligible exciton-exciton annihilation. In contrast, in QD-ReC0A complex (Fig. 3.6b), the bleach of exciton bands recovers by ~60% at 1ns, which is consistent with the dissociation of QD excitons by ET to the adsorbates.

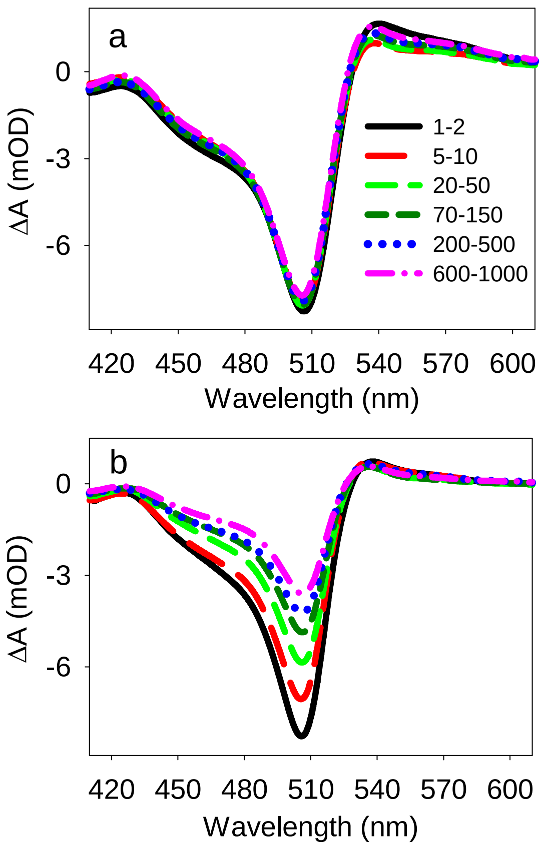

Figure 3.6. Transient visible spectra of CdSe (a), and CdSe (505nm)-ReC0A complex (b), at indicated delay times after 400 nm excitation.

Since intraband electron absorption and exciton bleach of CdSe QDs are both caused by the process of electron filling 1S (e) state after photoexcitation of CdSe, it is instructive to compare the electron transfer kinetics from CdSe to ReC0A as monitored by both transient IR and visible probes. Figure 3.7 shows the comparison of electron decay kinetics of the intraband absorption and exciton bleach recovery of interband absorption monitored by transient IR (filled circles) and visible (open triangles) probes, respectively. The exciton bleach signal was obtained by averaging the transient signal at 500-510 nm and has been inverted and scaled for better comparison. It is clear from the comparison that these kinetic traces are virtually identical, which further confirms that the faster decay kinetics of the intraband transition as well as the fast bleach recovery of the lowest exciton transition in CdSe-ReC0A, compared to those of CdSe alone, arise from the loss of electron from the conduction band of CdSe. This agreement also suggests that both IR absorption decay kinetics and exciton bleach recovery can be used to measure the ET kinetics in these QD-ReC0A complexes.

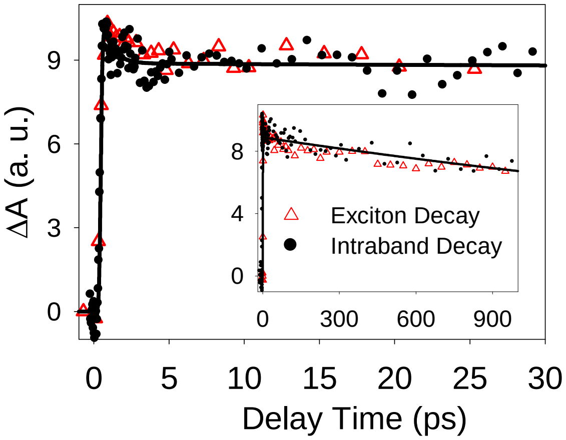

Figure 3.7. Comparison of intraband transition decay kinetics (filled circles) and exciton bleach recovery kinetics (open triangles) for CdSe-ReC0A complex. The exciton bleach signal has been inverted and scaled for better comparison. The insets show the data extended to the longer time scale.

3.2.2. The Effect of the Number of ReC0A per QDs on ET rate.

In the previous section, we have found that exciton quenching rate increases with the concentration of ReC0A, i.e. increasing number of ReC0A per QDs. This concentration dependence feature was also examined by comparing their spectral features in transient absorption spectra. Figure 3.8 shows the FTIR spectra of ReC0A in CdSe(505nm)-ReC0A complexes adsorbed with different numbers of ReC0A. The average numbers of ReC0A per particle in these three complexes were estimated to be 0.2, 0.7 and 1.2, respectively. Figure 3.9a shows the comparison of exciton bleach recovery kinetics of these three samples. These kinetic traces were measured under same conditions. Clearly, Exciton bleach recovery accelerates with the increasing number of ReC0A, indicating an increase of ET rate from CdSe to ReC0A. This trend was also observed in the comparison of the electron decay kinetics for 1S(e)-1P(e) intraband transition, as shown in Figure 3.9b.

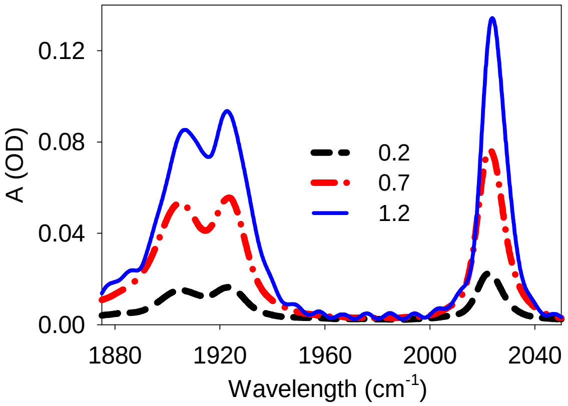

Figure 3.8. FTIR spectra of ReC0A absorbed on CdSe QDs with indicated numbers of ReC0A per particle.

All of these kinetic traces can be well fit with two or three exponential decay functions with one slow component. The fitting parameters for bleach recovery kinetics are listed in Table 3I, in which A_i and τ_i are the amplitude and time constant of the exponential components. Since the signal sizes continue to decay beyond 1 ns, the time constant for the slowest component is not well determined by the fit. As a result, the amplitude-weighted average time constants which depends sensitively on the slow component, is subject to large errors. Instead, we compare the half recovery time $\tau_{1/2}$, the time when signal decays 50%, which are also listed in Table 3I. The obtained half recovery lifetimes are represented by 130 ps, ≈1 ns and > 1 ns for these samples with ratios 1.3, 0.7 and 0.2, respectively. Unfortunately, because of the large amplitudes associated with the longer time constants in the multi-exponential fits, our 1 ns timescale measurements can not provide an accurate representation of the slow dynamics. As a result, it is difficult to compare the charge separation rates quantitatively. A better way for this study might be to use a smaller size CdSe which has much higher oxidation potential in its excited state.

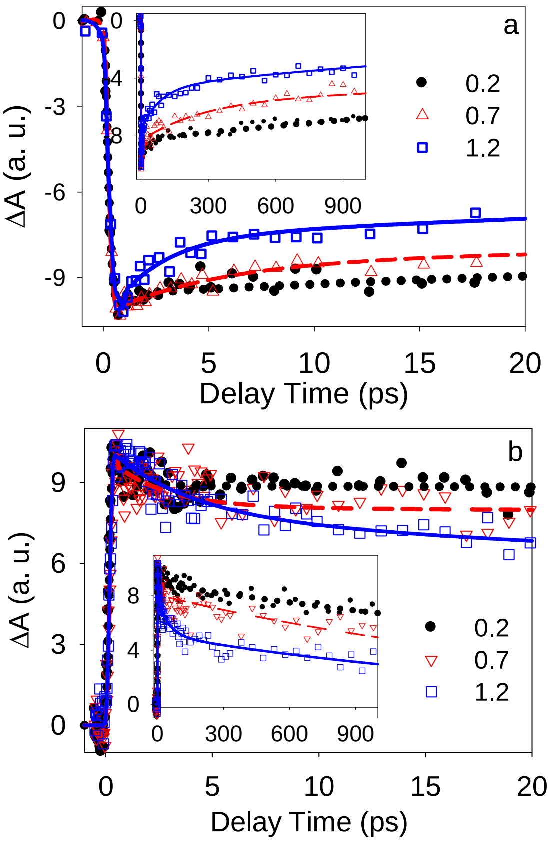

Figure 3.9. (a) Comparison of exciton bleach recovery of CdSe-ReC0A samples after 400 nm excitation. (b) Comparison of decay kinetics of intraband transition of CdSe-ReC0A

samples after 400 nm excitation. The insets show the same data extending to longer time scales.

Table 3I. Fitting parameters for the bleach recovery of CdSe-ReC0A samples with different ratios of ReC0A to CdSe.

Ratio	A_1(%)	τ_1	A_2	τ_2 (ps)	A_3	τ_3 (ps)	$\tau_{1/2}$
0.2	14.6	39.4	85.4	> 1ns			>1ns
0.7	25.3	33.7	74.7	> 1ns			≈1ns
1.2	23.4	2.08	25.3	48.6	51.4	1942	135ps

*A_i and τ_i are fitting parameters for exponential decay fits. $\tau_{1/2}$ is the half recovery time.

3.2.3. The Effect of QD Particle Sizes on ET rate.

Like all quantum dots, the conduction band edge position of CdSe QDs is also dependent on size because of the quantized confinement effect. The decrease of CdSe size shifts its band edge to higher energy as well as increasing the band gap.[17] According to Marcus theory,[18-21] the electron injection rate depends on the driving force, which is the potential energy difference between the donor and acceptor. This is expected to lead to a variation in ET rate with the relative position of CdSe conduction band potential with respect to the LUMO level of ReC0A dye.

Three sizes of CdSe were chosen to investigate the effect of size on charge separation rate. CdSe-ReC0A complexes with different QD sizes have been described in the section of 3.2.1.1. Figure 3.10 shows a comparison of the exciton bleach recovery for these three CdSe-ReC0A complexes. All of these kinetics traces have been normalized at the maximum amplitude for better comparison. It is clear from the comparison that with a decrease in particle size, the bleach recovery is accelerated, indicating an increase in charge separation rates from CdSe QDs to ReC0A dye. The half-recovery time, $\tau_{1/2}$, for CdSe (435nm), CdSe(477nm), and CdSe(505nm) are 2.3 ps, 55.5 ps, and ~ 1 ns, respectively. Based on this comparison, we conclude that the charge separation rates from CdSe QDs to ReC0A molecules are significantly dependent on particle sizes. With the decrease of particle sizes, the charge separation rate increases with orders of magnitude.

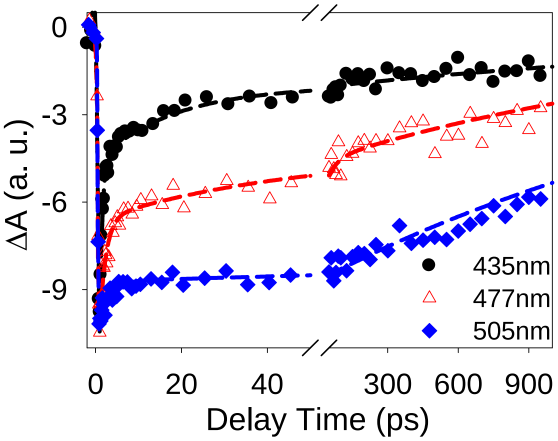

Figure 3.10. Comparison of exciton bleach recovery of CdSe-ReC0A samples for three QD sizes after 400 nm excitation. All kinetic traces have been normalized at the maximum amplitudes for better comparison.

3.3 Discussion

According to Marcus theory, electron transfer rate for a non-adiabatic system is given by:[18]

$$k_{ET}=\frac{2\pi}{h}\frac{|H_0|^2}{\sqrt{4\pi\lambda k_B T}}\exp[-\frac{(\lambda+\Delta G_0)^2}{4\lambda k_B T}] \quad (3.2)$$

where ΔG_0 is the driving force for electron transfer from CdSe (with excited state oxidation potential of V($CdSe^+$/CdSe*) to ReC0A (with reduction potential V($ReC0A^-$

/ReC0A)), H is the electronic coupling strength, and λ is the total reorganization energy. For CdSe-ReC0A systems with varying sizes of CdSe, the values of λ and coupling strength between the donor and acceptor are assumed not to be changing with QD size. Therefore, the observed rate dependence on size can be attributed to the difference in driving force. For the ET process described in quuation 3.1, ΔG is given by:

$$\Delta G_0 = -e[-V(CdSe^+ / CdSe^*) + V(\mathrm{Re}C0A^- / \mathrm{Re}C0A)] \qquad (3.3)$$

where $V(CdSe^+ / CdSe^*)$ is the oxidation potential of exciton in QDs and $V(\mathrm{Re}C0A^- / \mathrm{Re}C0A)]$ is the reduction potential of ReC0A. The oxidation potential of exciton in CdSe QDs can be estimated according to Brus model.[8,22,23] In the model, QD was treated as a spherical well with infinite potential barrier. Then the energy of the lowest exciton state ($E_{\mathrm{CdSe}*}$), a bound pair of 1S electron in the conduction band (CB) and 1S hole in the valence band (VB), is given by[17,22]

$$E_{CdSe*}[1s_e, 1s_h] = E_g + \frac{\hbar^2 \pi^2}{2R^2}[\frac{1}{m_e^*} + \frac{1}{m_h^*}] - \frac{1.8e^2}{4\pi\varepsilon_0 \varepsilon R} \qquad (3.3)$$

where E_g is the bulk band gap, R is the radius of the QD, and m_e* and m_h* are the effective masses of electron and hole, respectively. The second and third terms are the confinement energy of the 1S electron and 1S hole, respectively, and the fourth term results from electron-hole Coulombic attraction. We adopt $m_e* = 1.3m_0$ (m_0 is the free electron rest mass), $m_h* = 4.5m_0$, $\varepsilon = 10$, E_g = 1.7 V for CdSe QDs.[24] Then we can estimate the oxidation potentials of CdSe QDs ($CdSe^*[1s_e, 1s_h] \rightarrow e + CdSe^+[1s_h]$) in the excited state according to the above Brus model. The resulting oxidation potentials for CdSe with the first exciton band at 435 nm, 477 nm, and 505 nm are -1.55 V, -1.37 V, and -1.26 V (SCE), respectively. Taking the reduction potential of ReC0A as -0.96 V, we obtain the ΔG_0 values of -0.59, -0.41 and -0.3 V for the corresponding systems, which increase with decreasing particle sizes. This result indicates that ET reaction in current system is in the Marcus normal region because the observed ET rate increases with the driving force. Unfortunately, due to the unkown value of λ and H as well as the limited time resolution of our measurements with regards to obtaining an accurate fit of kinetics for the largest size of CdSe, we were unable to compare the calculated separation rates with the experimental rates. The possible solution might be to increase the ratio of each sample and thus enhance the charge separation rate as we discussed in previous section.

3.4 Conclusions

Photoinduced charge separation between CdSe quantum dots/adsorbed Re(CO)$_3$Cl(dcbpy) complex (ReC0A) was investigated by using ultrafast infrared and visible time resolved spectroscopy. Optical excitation of the CdSe nanoparticle led to absorbance decrease (bleach) of three CO stretching modes of ReC0A in the ground state and the formation of three red-shifted anion bands. The intraband absorption kinetics (in the mid-IR) of ReC0A-bound CdSe was found to decay faster than those in CdSe, suggesting a quicker loss of electrons from the conduction band of CdSe. Furthermore, a faster bleach recovery of the exciton peak in the visible was observed in CdSe/ReC0A complex than in CdSe. All of these results suggest that excitons in CdSe quantum dots dissociate through electron transfer from the conduction band of CdSe to an unoccupied orbital of ReCOA, forming the anion of ReCOA. The charge separation rates (represented by half decay time) can be controlled intentionally from 2.3 ps to > 1 ns by varying the particle size of CdSe and the number of ReC0A molecules on each CdSe particle. The transfer rate as fast as 2.3 ps was obtained in CdSe QDs with first exciton band at 435 nm. This time is shorter than the lifetime of multi-excitons, which indicates the possibility to separate multiple excitons before the exciton-exciton annihilation process.

References

(1) Huynh, W. U.; Dittmer, J. J.; Alivisatos, A. P. *Science* **2002**, *295*, 2425.

(2) Murphy, J. E.; Beard, M. C.; Norman, A. G.; Ahrenkiel, S. P.; Johnson, J. C.; Yu, P.; Micic, O. I.; Ellingson, R. J.; Nozik, A. J. *Journal of the American Chemical Society* **2006**, *128*, 3241.

(3) Schaller, R. D.; Agranovich, V. M.; Klimov, V. I. *Nature Physics* **2005**, *1*, 189.

(4) Luther, J. M.; Beard, M. C.; Song, Q.; Law, M.; Ellingson, R. J.; Nozik, A. J. *Nano Letters* **2007**, *7*, 1779.

(5) Ellingson, R. J.; Beard, M. C.; Johnson, J. C.; Yu, P.; Micic, O. I.; Nozik, A. J.; Shabaev, A.; Efros, A. L. *Nano Letters* **2005**, *5*, 865.

(6) Blackburn, J. L.; Selmarten, D. C.; Nozik, A. J. *Journal of Physical Chemistry B* **2003**, *107*, 14154.

(7) Robel, I.; Subramanian, V.; Kuno, M.; Kamat, P. V. *Journal of the American Chemical Society* **2006**, *128*, 2385.

(8) Boulesbaa, A.; Issac, A.; Stockwell, D.; Huang, Z.; Huang, J.; Guo, J.; Lian, T. *J. Am. Chem, Soc.* **2007**, *129*, 15132.

(9) Worl, L. A.; Duesing, R.; Chen, P.; Ciana, L. D.; Meyer, T. J. *J. Chem. Soc. Dalton Trans.* **1991**, 849.

(10) Wang, Y.; Asbury, J. B.; Lian, T. *J. Phys. Chem. A* **2000**, *104*, 4291.

(11) Peng, Z. A.; Peng, X. *J. Am. Chem. Soc.* **2001**, *123*, 183.

(12) Yu, W. W.; Qu, L.; Guo, W.; Peng, X. *Chemistry of Materials* **2003**, *15*, 2854.

(13) Yu, W. W.; Qu, L.; Guo, W.; Peng, X. *Chem. Mater.* **2003**, *15*, 2854.

(14) Stor, G. J.; Hartl, F.; van Outersterp, J. W. M.; Stufkens, D. J. *Organometallics* **1995**, *14*, 1115.

(15) Guyot-Sionnest, P.; Hines, M. A. *Applied Physics Letters* **1998**, *72*, 686.

(16) Klimov, V. I. *Annual Review of Physical Chemistry* **2007**, *58*, 635.

(17) Brus, L. E. *Journal of Chemical Physics* **1984**, *80*, 4403.

(18) Marcus, R. A. *J. Chem. Phys.* **1965**, *43*, 679.

(19) Gao, Y. Q.; Georgievskii, Y.; Marcus, R. A. *J. Chem. Phys.* **2000**, *112*, 3358.

(20) Gao, Y. Q.; Marcus, R. A. *J. Chem. Phys.* **2000**, *113*, 6351.

(21) Gosavi, S.; Marcus, R. A. *J. Phys. Chem. B* **2000**, *104*, 2067.

(22) Brus, L. *J. Chem. Phys.* **1983**, *79*, 5566.

(23) Brus, L. E. *J. Chem. Phys.* **1984**, *80*, 4403.

(24) *Semiconductor Electrodes*; Finklea, H., O., Ed.; Elsevier: New York, 1988; Vol. 55.

Chapter 4. Exciton Dissociation in CdS Quantum Dots by Electron Transfer to Flavin

4.1. Introduction

The ability to develop efficient multiple-redox photocatalysts is an increasingly important research problem due to its significant roles in photosynthetic systems as well as in solar energy conversion systems.[1,2] One central issue concerning this development is to fulfill the multi-electron and multi-photon requirements of important multi-electron involved reactions, such as hydrogen and oxygen evolution reactions, with the one-photon/one-electron nature of most molecular photoexcitation.[3] Nature has developed its own set of catalysts proficient at stepwise storage of multiple redox electrons or holes, such as oxygen evolving complex (OEC) in photosystem II[4] and hydrogenases[5]. Unfortunately, only a few molecular photocatalysts have shown the ability to meet the multi-electron stoichiometries of activation reactions.[6-12] For example, poly-nuclear complexes can absorb multiple photons and store charge, and thus have been used to participate in multiple electron transfer reactions.[13] However, among these systems, only one electron can be transferred upon absorbing one photon. A more efficient and different approach is to transfer multiple electrons by absorbing a single photon.

Quantum dot (QD) seems to be ideal alternative to molecular multi-redox photocatalysts due to its capability in generating multiple excitons (electron–hole pairs) by absorbing a single photon, a process known as multiple exciton generation process (MEG). MEG has been reported recently in ultrasmall semiconductor nanocrystals, such as quantum dots[14-19] and carbon nanotubes.[13,20] The mechanism and efficiency of this process are still subjects of intense current debate.[18,21-28] If MEG phenomenon is proven to be true, it may provide a new approach to use QDs as multiple electron/hole photosensitizers in photocatalytic systems.

Since their initial description, QDs have been actively used as photocatalysts in numerous fields, such as synthetic organic chemistry,[29-31] solar fuel,[32] and biocatalytic oxidation and reduction.[33-36] For example, it was shown that ZnS can initiate the addition of allyl radicals to imines or diazo compounds as well as the addition of tertiary amines to electron-deficient alkenes.[29,30] It was also shown that InP/$Fe_2S_2(CO)_6$ assemblies can be used to catalyze proton reduction to produce hydrogen.[32] The authors found that this InP-catalyst can initiate H_2 production reaction at a potential bias significantly positive of the dark equilibrium potential for proton reduction at pH 7 with more than 60% efficiency. Furthermore, semiconductor QDs/biomolecule hybrid systems have been used as photonic initiators for photocurrent generation that probe the biorecognition or biocatalytic transformations. For example, photocurrents were generated by CdS/DNA assemblies associated with electrodes, and the photocurrent direction can be switched by applying the approatiate potential to the electrode. It was also reported that QDs conjugated with enzymes can activate the photocurrent. Pardo-Yissar and co-workers demonstrated the activation of photocurrent by CdS NPs using the hydrolytic biocatalyst acetylcholine esterase.[36] Katz at al. reported on the photocurrent generation by coupling reduced or oxidized cytochrome c (Cyt c) to CdS QDs.[37] They found that the photocurrent direction can be controlled by the redox states of Cyt c. Niemeyer et al. have reported that the conjugation of CdS QDs with the enzyme cytochrome $P450_{BS\beta}$ can catalyze an organic transformation through photo-activation of the QDs.[34] They found that the photogenerated excitons can produce $O_2^{\cdot -}$ and/or $OH^{\cdot}$ radicals, which then activate P450 enzymes to catalyze monooxygeneration of fatty acid substrates.

These reports successfully demonstrated the capability of QDs as attractive photocatalysts in a wide variety of fields, however, to best of our knowledge, QDs as multiple electron/hole photosensitizers have not been reported in photocatalytic systems yet. Towards this goal, it is instructive to investigate the charge separation dynamics in QDs by employing multiple electron acceptors, such as Flavins. In this chapter, we examine the electron transfer dynamics from CdS QDs to Flavin mononucleotide (FMN).

Flavin coenzymes play a central role in biological redox reactions because of their functions as either one-electron or two-electron reactions.[38,39] Additionally, flavins can be photochemically reduced by using simple sacrificial electron donors such as ethylenediaminetetraacetate (EDTA), which opens up a new approach for direct regeneration of reduced flavin cofactors.[40-42] However, the catalytic performance measured according to the reaction rate is one to two orders of magnitude relative to than its conventional setups.[43] This challenge might be overcomed by using MEG in QDs.

In current work, we showed that the excitons in CdS QDs dissociated by ET to FMN by forming the anionic FMN semiquinone form.

4.2 Results and Discussion

4.2.1 Static Absorption Spectra.

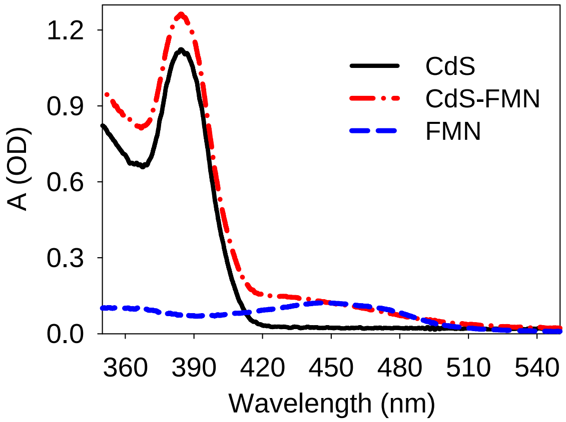

Figure 4.1. UV-visible absorption spectra of CdS (389 nm) in heptane, CdSe (389 nm)-FMN complexes in heptane, and FMN in ethanol.

Figure 4.1 shows the absorption spectra of CdS and CdS-FMN complexes in heptane. The absorption peak of the lowest allowed ($1S_{3/2}$(h)-$1S_{1/2}$(e)) exciton transition is located at 389 nm for these particles. Compared to the spectrum of free QDs (black solid line), CdSe-FMN complexes (red dash-dot line) exhibit an additional absorption band at ~440 nm. This additional absorption peak is consistent with the absorption spectrum of FMN in ethanol, and thus is attributed to the ground state absorption of FMN. The average number of adsorbed FMN per QD is estimated to be ~ 2.7 based on the measured absorbance and extinction coefficients of FMN (11,100 $M^{-1}cm^{-1}$ at 443 nm) and CdSe (2.55 x10^5 $M^{-1}cm^{-1}$).[44]

4.2.2 Transient Absorption Spectra.

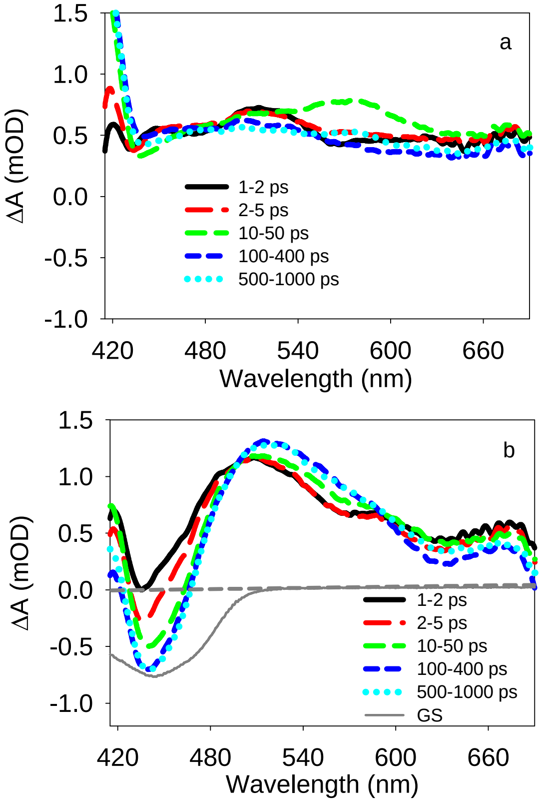

Figure 4.2. (a) Transient spectra of CdS(389nm) at indicated delay times after 400 nm excitation. (b) Transient spectra of CdSe(389nm)-FMN at indicated delay times after 400 nm excitation. The static absorption spectrum of FMN in ethanol is also shown in panel b as gray solid line.

Figure 4.2 shows the transient visible absorption spectra of CdS (389nm) and CdS (389nm)-FMN complexes after 400 nm excitation. These spectra show a broad absorption band in the whole spectrum window and an apparent absorption band at ～ 420 nm at all delay times. The former spectral feature is similar to the broad absorption from 510-700 nm for CdSe QDs reported by our group recently and has been assigned to the hole absorption in visible region.[45] The later one can be assigned to the absorbance of the shifted transition by the carrier-induced Stark effect, which has been attributed to that the presence of an exciton in the QD led to a red-shift of interband exciton absorption peak due to exciton-exciton annihilation. This feature has been observed somewhere else. In QD-FMN complex as shown in Figure 4.2b, in addition to these two features, we observed an well-defined bleach band centered at ～440 nm and an additional absorption band at ～510 nm. In addition, these two species are separated by a clear isosbestic point at 496 nm, indicating the conversion of the species at 440nm to the new absorbing species at 510 nm as a result of QD excitation. The bleach feature at ～440 nm is consistent with the ground state absorption spectrum of FMN (gray solid line in Figure 4.2b), and thus is attributed to the depletion of FMN ground state molecules. The absorption band at 510 nm can be assigned to the anionic FMN semiquinone form which has an intense absorption at 492 nm[46]. The slight difference between this absorption band (510 nm) and the anionic FMN semiquinone form (492 nm) may arise from the spectral overlap of FMN ground state bleach at 440 nm with this semiquinone absorption. This spectral feature can not be attributed to the neutral FMN semiquinone form which has absorption centered at 580 nm. These results indicate that excitons in CdS QDs have been dissociated through transfer one electron to FMN by forming reduced form of ionic FMN.

Due to the small signal sizes of these two species in the transient spectra, it is difficult to analyze their kinetic traces and thus the inability to estimate the ET rate quantitatively according to the transient absorption signals of FMN. However, from the transient spectra of CdS-FMN assemblies, it occurs to us that the formation of FMN semiquinone and the depletion of FMN ground state is not complete until at 1ns time scale. Therefore, ET rate in current system is too slow to compete with exciton-exciton annihilation process in QDs. As we have shown in Chapter 3, ET rate increases with the number of adsorbate per QD, suggesting that ET rate in current CdS-FMN assemblies may be enhanced by loading more FMN on QDs. By employing this approach, we may obtain larger FMN ground state bleach signal size as well as the ionic FMN semiquinone signals. Further studies are required both experimentally and theoretically to have a better understanding of ET dynamics in CdS-FMN assemblies.

4.3 Summary

Photoinduced charge separation in CdS QDs through electron transfer to FMN has been investigated by transient visible spectroscopy. The ET pathway was identified by two spectral features of FMN in CdS-FMN assemblies: ground state bleach at 440 nm and anionic semiquinone absorption at 510 nm. ET rate can not be quantitatively determined in current system due to the small transient signal sizes of these two species. It might be desirable to overcome this problem by increasing the number of FMN per QD and thus the larger signal size. If this goal can be achieved, it is highly desirable that ET rate can be accelerated and thus the possibility to use QD as multiple electron reduction catalysts.

References

(1) Wouters, K. L.; de Tacconi, N. R.; Konduri, R.; Lezna, R. O.; MacDonnell, F. M. *Photosynthesis Research* **2006**, *87*, 41.

(2) Bard, A. J.; Fox, M. A. *Accounts Of Chemical Research* **1995**, *28*, 141.

(3) de Tacconi, N. R.; Lezna, R. O.; Chitakunye, R.; MacDonnell, F. M. *Inorganic Chemistry* **2008**, *47*, 8847.

(4) Manchanda, R.; Brudvig, G. W.; Crabtree, R. H. *Coordination Chemistry Reviews* **1995**, *144*, 1.

(5) Lubitz, W.; Tumas, W. *Chemical Reviews* **2007**, *107*, 3900.

(6) Elvington, M.; Brewer, K. J. *Inorganic Chemistry* **2006**, *45*, 5242.

(7) Molnar, S. M.; Nallas, G.; Bridgewater, J. S.; Brewer, K. J. *Journal of the American Chemical Society* **1994**, *116*, 5206.

(8) Rosenthal, J.; Bachman, J.; Dempsey, J. L.; Esswein, A. J.; Gray, T. G.; Hodgkiss, J. M.; Manke, D. R.; Luckett, T. D.; Pistorio, B. J.; Veige, A. S.; Nocera, D. G. *Coordination Chemistry Reviews* **2005**, *249*, 1316.

(9) Heyduk, A. F.; Nocera, D. G. *Science* **2001**, *293*, 1639.

(10) Esswein, A. J.; Veige, A. S.; Nocera, D. G. *Journal of the American Chemical Society* **2005**, *127*, 16641.

(11) Pfennig, B. W.; Mordas, C. J.; McCloskey, A.; Lockard, J. V.; Salmon, P. M.; Cohen, J. L.; Watson, D. F.; Bocarsly, A. B. *Inorganic Chemistry* **2002**, *41*, 4389.

(12) Konduri, R.; Ye, H. W.; MacDonnell, F. M.; Serroni, S.; Campagna, S.; Rajeshwar, K. *Angewandte Chemie-International Edition* **2002**, *41*, 3185.

(13) Kim, M. J.; Konduri, R.; Ye, H. W.; MacDonnell, F. M.; Puntoriero, F.; Serroni, S.; Campagna, S.; Holder, T.; Kinsel, G.; Rajeshwar, K. *Inorganic Chemistry* **2002**, *41*, 2471.

(14) Schaller, R. D.; Klimov, V. I. *Phys. Rev. Lett.* **2004**, *92*, 186601.

(15) Ellingson, R. J.; Beard, M. C.; Johnson, J. C.; Yu, P.; Micic, O. I.; Nozik, A. J.; Shabaev, A.; Efros, A. L. *Nano Letters* **2005**, *5*, 865.

(16) Luther, J. M.; Beard, M. C.; Song, Q.; Law, M.; Ellingson, R. J.; Nozik, A. J. *Nano Letters* **2007**, *7*, 1779.

(17) Schaller, R. D.; Sykora, M.; Pietryga, J. M.; Klimov, V. I. *Nano Letters* **2006**, *6*, 424.

(18) Trinh, M. T.; Houtepen, A. J.; Schins, J. M.; Hanrath, T.; Piris, J.; Knulst, W.; Goossens, A. P. L. M.; Siebbeles, L. D. A. *Nano Letters* **2008**, *8*, 1713.

(19) Murphy, J. E.; Beard, M. C.; Norman, A. G.; Ahrenkiel, S. P.; Johnson, J. C.; Yu, P.; Micic, O. I.; Ellingson, R. J.; Nozik, A. J. *Journal of the American Chemical Society* **2006**, *128*, 3241.

(20) Gabor, N. M.; Zhong, Z.; Bosnick, K.; Park, J.; McEuen, P. L. *Science* **2009**, *325*, 1367.

(21) Nair, G.; Bawendi, M. G. *Phys Rev Lett* **2007**, *76*, 081304.

(22) Ben-Lulu, M.; Mocatta, D.; Bonn, M.; Banin, U.; Ruhman, S. *Nano Lett.* **2008**, *8*, 1207.

(23) Shabaev, A.; Efros, A. L.; Nozik, A. J. *Nano Letters* **2006**, *6*, 2856.

(24) Rupasov, V. I.; Klimov, V. I. *Phys. Rev. B:* **2007**, *76*, 125321/1.

(25) Schaller, R. D.; Agranovich, V. M.; Klimov, V. I. *Nat. Phys.* **2005**, *1*, 189.

(26) Prezhdo, O. V. *Chem. Phys. Lett.* **2008**, *460*, 1.

(27) Franceschetti, A.; An, J. M.; Zunger, A. *Nano Lett* **2006**, *6*, 2191.

(28) Allan, G.; Delerue, C. *Phys. Rev. B:* **2008**, *77*, 125340.

(29) Marinkovic, S.; Hoffmann, N. *Chemical Communications* **2001**, 1576.

(30) Schindler, W.; Knoch, F.; Kisch, H. *Chemische Berichte* **1996**, *129*, 925.

(31) Kunneth, R.; Feldmer, C.; Knoch, F.; Kisch, H. *Chemistry-a European Journal* **1995**, *1*, 441.

(32) Nann, T.; Ibrahim, S. K.; Woi, P. M.; Xu, S.; Ziegler, J.; Pickett, C. J. *Angewandte Chemie-International Edition* **2010**, *49*, 1574.

(33) Shi, L. X.; Hernandez, B.; Selke, M. *Journal of the American Chemical Society* **2006**, *128*, 6278.

(34) Ipe, B. I.; Niemeyer, C. M. *Angewandte Chemie-International Edition* **2006**, *45*, 504.

(35) Ipe, B. I.; Shukla, A.; Lu, H. C.; Zou, B.; Rehage, H.; Niemeyer, C. M. *Chemphyschem* **2006**, *7*, 1112.

(36) Pardo-Yissar, V.; Bourenko, T.; Wasserman, J.; Willner, I. *Advanced Materials* **2002**, *14*, 670.

(37) Katz, E.; Zayats, M.; Willner, I.; Lisdat, F. *Chemical Communications* **2006**, 1395.

(38) Walsh, C. *Accounts of Chemical Research* **1980**, *13*, 148.

(39) Edmondson, D. E.; Tollin, G. *Topics in Current Chemistry* **1983**, *108*, 109.

(40) Frisell, W. R.; Chung, C. W.; Mackenzie, C. G. *Journal of Biological Chemistry* **1959**, *234*, 1297.

(41) Massey, V.; Stankovich, M.; Hemmerich, P. *Biochemistry* **1978**, *17*, 1.

(42) Hodgson, A. V.; Strobel, H. W. *Analytical Biochemistry* **1996**, *243*, 154.

(43) Hollmann, F.; Taglieber, A.; Schulz, F.; Reetz, M. T. *Angewandte Chemie-International Edition* **2007**, *46*, 2903.

(44) Yu, W. W.; Qu, L.; Guo, W.; Peng, X. *Chem. Mater.* **2003**, *15*, 2854.

(45) Huang, J.; Huang, Z.; Jin, S.; Lian, T. *J. Phys. Chem. C* **2008**, *112*, 19734.

(46) Hanley, S. C.; Ost, T. W. B.; Daff, S. *Biochemical and Biophysical Research Communications* **2004**, *325*, 1418.

Chapter 5. Exciton Dissociation in CdSe Quantum Dots by Hole Transfer to Phenothiazine

5.1. Introduction

In addition to ultrafast electron transfer, dissociation of multiexcitons also requires ultrafast transfer holes to acceptors. However, only few examples have been reported through hole transfer process,[1-4] although exciton dissociation in quantum dots (QDs) through ET pathway have been extensively studied.[5-9] The possible reason might be that direct observation of the hole transfer process by transient absorption techniques is difficult due to the lack of clear spectral signatures of holes in QDs. Several studies reported that the holes in QDs show a featureless and relatively weak broad absorption in the near IR。 [10-12] Klimov et al. have shown that the dynamics in the spectral range up to 2 μm is mainly due to the relaxation hole.[10,11] Burda and co-workers have also investigated the relaxation dynamics of CdSe in the spectral range from 450 nm to 5 μm.[12] They assigned the NIR signal to the hole transition by using a hole quencher to the photoexcited nanoparticles. However, the exact nature of this NIR signal has not been determined.

Most of the current knowledge on hole transfer was based on fluorescence quenching of excited QDs by hole acceptors. For example, fluorescence quenching was observed in QDs capped with amines and thiols, which has been attributed to hole transfer from excited QDs to these functional groups.[2,4,13,14] Recently, El-Sayed et al. reported the studies of the hole transfer process in QDs, which involves the fluorescence of CdSe QD-n-Butylamine system. They observed that fluorescence intensity of CdSe QDs decreases with the addition of butylamine, but their fluorescence lifetime remains unaffected. They proposed that the decrease of CdSe fluorescence is attributed to the eliminating the fluorescence site by binding of the hole acceptor to the hole trapping emitting sites. More recently, Sykora and co-workers reported their studies of charge carrier dynamics in CdSe-Ru polypyridine complexes by using transient PL up-conversion and femtosecond transient absorption experiment.[3] Specifically, they probed the dynamics of exciton bleach recovery to provide the depopulation rate of the electron 1S state, and that of PL quenching to reflect the product of electron and hole population numbers. It was found that the electron dynamics based on transient absorption signal remain almost unchanged, while hole dynamics based on fluorescence signal develop a ～ 5 ps decay component in the CdSe-Ru complex compared to that of CdSe. They attributed this to the hole transfer process.

Although transient absorption measurement can not determine hole transfer process by probing the exciton bleach recovery of QDs, it can distinguish hole transfer from ET or energy transfer by examining the transient spectra of adsorbates. Kamat and co-workers have directly observed the formation of the product of hole transfer from CdSe QDs to p-phenylenediamine, i. e., the adsorbate cation by transient absorption measurements, which directly confirmed the hole transfer process from CdSe QDs to p-phenylenediamine. They reported that the hole transfer time is ～ 10 ns in this system. It was recently noted that in CdS QD-rhodamine complexes, there was negligible hole transfer on the <1 ns time scale despite sufficient driving force for the process.[6] These reported hole transfer processes occurred on very different time scales for reasons that have yet to be understood.

In this chapter, we examine the dynamics of hole transfer from excited CdSe QDs to phenothiazine (PTZ):

$$CdSe^*(1S_e,1S_h) - PTZ \rightarrow CdSe^-(1S_e) - PTZ^{\bullet+} \quad (5.1)$$

where CdSe* and CdSe$^-$ represent excited and reduced states of CdSe, respectively, and PTZ$^{\cdot+}$ represents the oxidized state of PTZ. Phenothiazine is a biologically important molecule and has been used as a probe for studying hole transfer dynamics in DNA because of its ease in chemical oxidation.[15,16] The oxidation potential of PTZ (0.76 V vs SCE)[16,17] is very low such that phenothiazine radical cations can be readily generated by donating one electron. Furthermore, the radical cation (PTZ$^{\cdot+}$) resulting from the hole transfer process exhibits a strong and characteristic absorption at 520 nm[18], well separated from its neural ground-state at 320 nm and thus can be used to monitor the hole transfer dynamics. In this work, we show that excitons in excited CdSe QDs can dissociate by transferring holes to PTZ. The hole transfer rate was measured by following the transient visible absorption of PTZ radical cation and by the fluorescence quenching of CdSe QDs as a function of PTZ concentration. A kinetic model based on a Poisson distribution of the number of adsorbates on each QD was found to adequately describe the adsorbate concentration-dependent fluorescence decay kinetics. According to this model, the hole transfer time was ~2.5 ns in 1:1 CdSe-PTZ complexes and reached ~300 ps in samples with an average of ~6 PTZ per QD.

5.2 Results

5.2.1 Static Absorption Measurement. CdSe QDs used in this experiment was characterized by UV-vis absorption spectroscopy as shown in Figure 5.1a. The absorption peak of the lowest allowed ($1S_{3/2}$(h)-$1S_{1/2}$(e)) exciton transition peak is at 462 nm, and the estimated radius of QDs is 1.8 nm.[19,20] The fluorescence quantum yield of these QDs was ~10%. An extra well-defined absorption peak is observed at 347 nm. This spectral feature is close to the peak at 349 nm for CdSe magic-size cluster reported by Peng et al and has been assigned to a similar CdSe cluster with 17 Cd atoms.[21] Since the magic size clusters can not be excited by 400 nm laser pulse, it was assumed that they did not affect the photoinduced charge transfer processes in this study. Samples 1-4 showed the same QD absorption but increasing amplitudes of the PTZ peak at 280-350 nm. Figure 5.1b shows the the spectra of PTZ, which were obtained by subtracting the absorption of free CdSe from that of CdSe-PTZ solutions. The obtained PTZ absorbance for samples 1, 2, 3, and 4 at 320 nm were 0.15, 0.29, 0.52, and 0.96 OD, respectively. According to the reported values of extinction coefficients of 36000 $M^{-1}\cdot cm^{-1}$ at 462 nm for CdSe QD of this size[5] and 4700 $M^{-1}\cdot cm^{-1}$ for PTZ,[22] we estimated that the concentration of QD particles was 0.4 mM and the concentrations of the PTZ were 0.8, 1.5, 2.7, 5.1 mM, in samples 1, 2, 3, 4, respectively. Since PTZ was slightly soluble in heptane (with a concentration of 0.6 mM in a saturated solution), the free PTZ in heptane solvent also contributes to the absorbance of PTZ in CdSe-PTZ solution. The absorption spectra of these species were similar, leading to the difficulty in quantitatively determining the amount of adsorbed phenothiazine on the surface of each CdSe particle on the basis of UV-visible spectra alone.

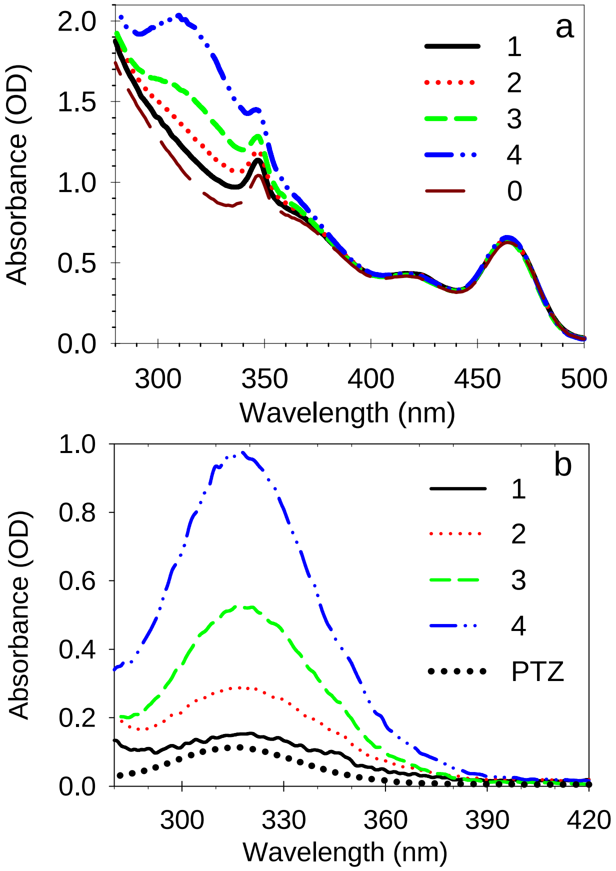

Figure 5.1. (a) UV-visible absorption spectra of CdSe (sample 0) and CdSe-PTZ (samples 1-4) in heptane solution with different concentrations of PTZ. b) Difference spectra between free CdSe (sample 0) and CdSe-PTZ (samples 1-4). The absorption spectrum of PTZ in heptane (dotted line) was also shown.

5.2.2 Fluorescence Lifetime Measurement. Time resolved fluorescence spectroscopy was first used to examine the effect of the presence of PTZ on QD lifetime in CdSe-PTZ complex. Figure 5.2 showed the fluorescence decays of CdSe and CdSe-PTZ solutions with different concentration of PTZ. These kinetics traces were recorded at 470 nm after 400 nm excitation. It is clear that the presence of PTZ reduced the exciton lifetime in the

QDs, and the quenching rate increased with the concentration of PTZ. These results indicate that excitons in QDs were quenched with the addition of PTZ. Energy transfer, electron transfer and hole transfer from QDs to adsorbates can all quench exciton lifetime. Energy transfer was first excluded in this system because of the negligible spectral overlap of QD emission with the absorption of PTZ. Electron and hole transfer processes led to different products that could be distinguished by transient absorption spectroscopy.

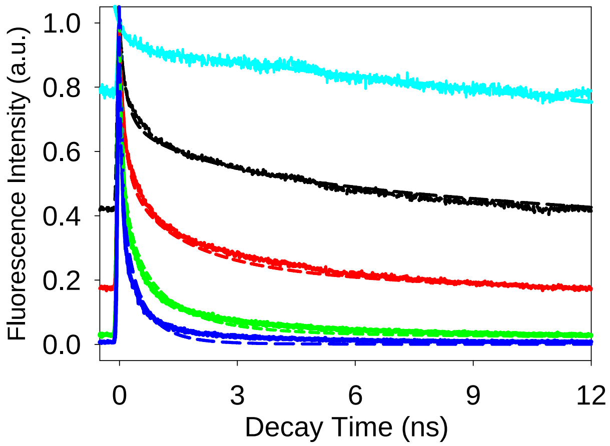

Figure 5.2. QD fluorescence decay (dots) of sample 0 (free QDs) and samples 1-4 (CdSe-PTZ solutions) and their fits (dashed lines) according to the model described in the main text.

5.2.3 Transient Absorption Measurement. Figure 5.3 shows the UV-vis absorption spectra of CdSe and CdSe-PTZ assemblies used for transient absorption measurement. The larger absorption signal for CdSe-PTZ solution compared to that of CdSe in the range of 280-350 nm is attributed to PTZ absorption. The absorbance of CdSe at 462 nm is 0.60 OD and PTZ at 320 nm is 0.88 OD.

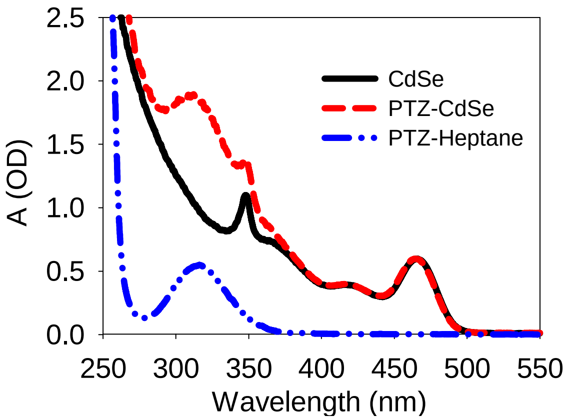

Figure 5.3. UV-visible spectra of CdSe, CdSe-PTZ assemblies and PTZ solution in heptane.

Figure 5.4a shows the transient visible spectra of CdSe-PTZ assembliese measured at indicated delay times after 400 nm excitation. The transient spectra of free CdSe measured under the same conditions are shown in the inset. The spectra for both samples at all delay times show three main features, the bleaches of $1S_{3/2}$(h)-$1S_{1/2}$(e) (at 462 nm) exciton interband transitions, the absorbance of the shifted transition by the carrier-induced Stark effect (at 493 nm), and the broad absorption at 510-600nm. The first two features have been attributed to the presence of an exciton in the QD, which led to a bleach of the iterband exciton transition due to the filling of 1S electron level in the conduction band and a red-shift of interband exciton absorption peak due to exciton-exciton annihilation. Figure 5.4b shows the same spectra of CdSe-PTZ and CdSe as in Figure 4.4a, while we expand the y axis (absorbance change) to smaller scale for clear demonstration of small absorption signals at 510-600 nm. For free CdSe QDs, this broad absorption remains constant on the <1 ns time window. In contrast, in QD-PTZ assemblies, the kinetics of this absorption decays with time as well as a new feature formed at ～520 nm. These two species are separated by a clear isosbestic point at 535 nm, indicating the conversion of the species at 510-600 nm in CdSe QDs to the new absorbing species at 520 nm as a result of QD excitation. The absorption band at 520 nm can be assigned to that of one-electron oxidized PTZ as reported by other researchers.[18] This excludes the possibility of energy transfer or electron transfer processes from CdSe QDs to phenothiazine, the products for which are excited and reduced form of PTZ, respectively. Therefore, in current CdSe-PTZ assemblies, excitons in CdSe have been dissociated through hole transfer to PTZ molecules.

As a result, the broad absorption feature at 510-600 nm, which decays with an identical rate as the formation of cation radical of PTZ, can be attributed to the species associated with the holes in CdSe QDs. As we mentioned in the introduction, charge relaxation dynamics in near IR absorption feature extending from ~0.5 V to 1.1 V has been measured by ultrafast spectroscopy. These authors have attributed these species to holes in CdSe, although the exact nature of the transition has not been determined.[12,23-25] They also observed that the hole trapping process for these NIR absorption features occurs on ~1 ps, which was similar to the rise time of deep trap emission of CdSe observed by fluorescence up-conversion.[26] It remains unclear whether currently observed broad absorption feature in 510-600 nm region are related to near IR absorption species reported by these authors. To best of our knowledge, this is the first observation of hole absorption in visible spectral range. The further experimental and theoretical evidence are required for the assignment of this visible transient.

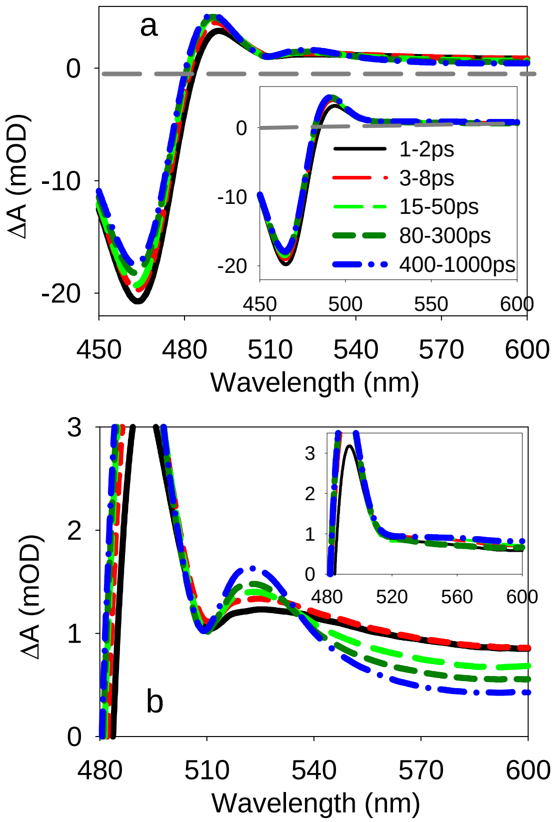

Figure 5.4. (a) Transient spectra of CdSe-PTZ assemblies (main panel) and CdSe (inset) at indicated delay times after 400 nm excitation. (b) Expanded view of the same transient spectra shown in (a).

The pathway of electron transfer or hole transfer can also be distinguished by comparing the kinetics of exciton bleach recovery between CdSe-PTZ assemblies and free CdSe. Figure 5.5 shows the comparison of exciton bleach kinetics of CdSe-PTZ assemblies with that of free CdSe. These kinetic traces were obtained by averaging the kinetics from 460-470 nm. The bleach recovery of CdSe-PTZ assemblies follows the same kinetics as that of free CdSe. We have shown previously that the presence of electron acceptor (ReC0A) in CdSe QDs removes the electron from the conduction band of excited CdSe QDs and accelerates the recovery of exciton interband bleach in CdSe dramatically.[27] Therefore, the similarity of exciton bleach recovery kinetics between CdSe-PTZ and free CdSe ruled out the electron transfer process for CdSe-PTZ system. These results all suggest that excitons in CdSe dissociate by hole transfer from the valence band of CdSe to the occupied orbital of phenothiazine.

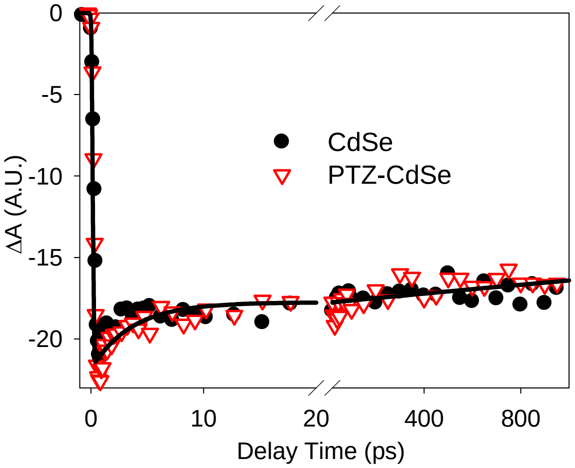

Figure 5.5. Comparison of exciton bleach recovery kinetics at 462 nm for CdSe (filled circles) and CdSe-PTZ assemblies (empty triangles).

The hole transfer dynamics can be probed by carrying out the kinetic studies of the formation of the oxidized state of phenothiazine at 520 nm as shown in Figure 5.6a (filled circles). The kinetic trace can be well fitted by a two exponential rise function with one fast and one slow component. Since the signal size in cation formation kinetic trace continue to rise beyond 1 ns, the time constant for the slow component is not well determined by the fit. As a result, it is difficult to determine the hole transfer rate based on the fitted constants. An alternative method might be to use fluorescence lifetime measurement which has much longer time scale window. Figure 5.6 shows the comparison of cation formation kinetics, the kinetics of fluorescence lifetime decay (solid line) and the dacay kinetics for the broad absorption at 570-650 nm (open squares) within

1 ns time scale. The fluorescence lifetime was measured by exciting the same sample as that in transient measurement at 400 nm and collected at 470 nm. The decay data for the broad absorption was obtained by averaging the transient signals at 570-650 nm. The signal sizes have been normalized to the same maximum amplitude for better comparison. Clearly, all three spectral signatures show the same decay kinetics, which further confirms that hole transfer from CdSe QDs to phenothiazine is the process to quench exciton lifetime. This good agreement also suggests that fluorescence lifetime decay is a sufficient probe of exciton dissociation rate in CdSe QDs. Because of its better signal-to-noise ratio and longer delay time range, the fluorescence decay data was used to quantify the hole transfer rate.

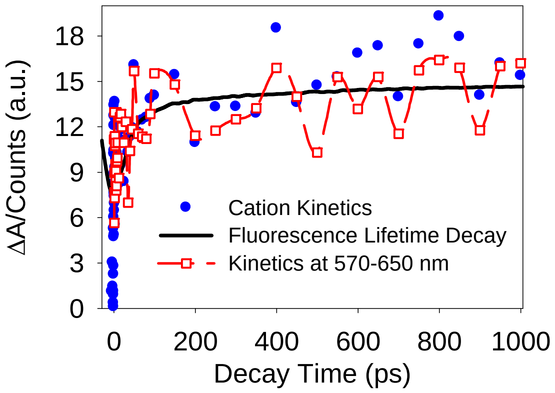

Figure 5.6. Comparison of the formation kinetics of cation absorption at 525 nm (filled circles), broad absorption decay at 570-650 nm (open squares), and fluorescence lifetime decay kinetics (black solid line) for CdSe-PTZ assemblies. The broad absorption signals and fluorescence signals have been normalized to the same initial amplitude as the cation formation signals, and have been inverted for better comparison.

5.3 Discussions

Exponential decay function was used to fit the decay kinetics from fluorescence measurement shown in Figure 5.2. These kinetics traces were non-single exponential and are dependent on the concentration of PTZ, indicating a heterogeneous distribution of hole transfer rates from CdSe to PTZ. The heterogeneity might result from inhomogeneous distribution of the number of adsorbate per QD, the properties (size, trap density) of QDs, and QD-adsorbate interactions.

We assume a Poisson distribution for the number of adsorbates per QD:

$$A_n = f(n,m) = \frac{m^n}{n!}e^{-m} \qquad (5.2)$$

where f_n is the probability of having QDs with n adsorbed molecules and m is the average number of adsorbates per QD. We assume that intrinsic decay rate of exciton is K_0, and the rate of hole transfer in a QD with n adsorbates (k_n) is n times that of a QD with only one adsorbate k_1:

$$k_n = nk_1 \qquad (3.3)$$

With these assumptions, we can then express the fluorescence decay kinetics in terms of the average number of adsorbate on each QD (m) and the transfer rate with n=1 (k_1) by direct applying the formula derived by other groups to our problem:[28,29]

$$[N*(t)] = [N*(0)]e^{-K_0t-m-me^{-k_1t}} \qquad (5.4)$$

where N*(t) and N*(0) are the average concentration of excited QD at delay time t and the initial concentration of excited CdSe QDs, respectively. As mentioned earlier, fluorescence decay kinetic traces for both free CdSe and CdSe-PTZ assemblies are non-single exponential. Therefore, we assume that QD intrinsic lifetime has a static distribution with amplitude B_i and rate constant K_{0i}. We also assume that there is distribution of hole transfer kinetics in 1:1 CdSe-PTZ assemblies, which can be described by a multiexponential function with amplitude and rate constant A_j and k_{nj}. Then equation 4.4 can be modified to[30,31]:

$$[N*(t)] = N*(0)(\sum_j A_j e^{-m+me^{-k_{1j}t}})(\sum_i B_i e^{-K_{0i}t}) \qquad (5.5)$$

In the real TCSPC measurement, the excitation source has a repetition time of 12 ns, leading to none-zero amplitude before t=0 which is resulted from the uncompleted decay of the previous excitation pulse. In this case, the amplitude at t = 0 is sum of N*(0) plus the residual unfinished decay from previous excitation pulse, which can be large for QDs due to its long lifetime (> 12 ns). This problem can be solved by accounting for this non-zero amplitudes before t=0. The measured response with repetition time τ can be expressed as:

$$\frac{S(t)}{C_m N*(0)} = (\sum_j A_j e^{-m+me^{-k_{1j}t}})(\sum_i B_i e^{-K_{i0}t}) + \sum_n (\sum_j A_j e^{-m+me^{-k_{1j}(t+n\tau)}})(\sum_i B_i e^{-K_{i0}(t+n\tau)})$$

(5.6)

where S(t) is the measured signal, τ is 12.048, and C* is a proportional constant depending on the radiative rate and experimental conditions. Assuming that the hole transfer rate is faster than the repetition rate of the excitation pulse, Equation 4.6 can be further simplified to the expression:

$$S(t) = C*[N*(0)]e^{-m}\sum_i B_i e^{-K_{0i}t}[\sum_j A_j e^{-m+me^{-k_{1j}t}} + \frac{1}{1-e^{-k_{0i}T_R}} - 1] \qquad (5.7)$$

By taking m=0, we can determine the intrinsic decay rate K_{0i} by fitting the kinetics of fluorescence decay of free CdSe by using expression 5.7. The decay kinetics of free CdSe (marked as 0 in Figure 5.2) is fitted by a two-exponential function. The fitting parameters are listed in table 5I, in which B_i and τ_i are the amplitude and time constant of the ith exponantial cpmponent. Upon substituting the values of B_1, B_2, τ_1 and τ_2 into expression 5.7, we can fit the decay kinetics of samples 1-4 by using expression 5.7. The decay kinetics of samples 1-4 were fit using the same values of B_1, B_2, τ_1 and τ_2 and varying values of m (to account for different PTZ concentrations). The best fits to this set of decay kinetics are shown in Figure 5.2 and the fitting parameters (A_1, k_{11}, A_2, k_{12}, and four m values for samples 1-4) are listed in Table 5I as well. This model can fit the kinetics at low adsorbate concentration very well, but for the highest adsorbate concentration, the quality of the fit decreased.

Table 5I. Fitting parameters for the fluorescence decay kinetics of CdSe and CdSe-PTZ*

Sample	*m*	*$1/k_{01}$, ns (B_1, %)*	*$1/k_{02}$, ns (B_2, %)*	*$1/k_{11}$, ns (A_1, %)*	*$1/k_{12}$, ns (A_2, %)*	*τ_a (ns)*
0	0	0.23 (31)	59.2 (69)			40.9
1	1.4					25.9
2	2.6			0.77 (68)	6.25 (32)	3.76
3	4.6					0.83
4	6.2					0.30

*A_j, k_{1j}, B_i, k_{0i} (i, j = 1,2) and m are fitting parameters for equation (5.7). τ_a is the amplitude-weighted average lifetimes calculated from multiple exponential fits to the fluorescence decay kinetics.

According to the fitting parameters of A_j, k_{1j} shown in Table 5I, we calculated the amplitude-weighted average hole transfer time. The obtained hole transfer time for the 1:1 CdSe-PTZ complex was 2.5 ns. For samples 1-4 with different average numbers of PTZ per QD, the estimated hole transfer times were 25.9, 3.76, 0.83, and 0.3 ns, respectively. It is instructive to to compare the hole transfer time with exciton-exciton annihilation time. Previous studies have shown that bi-exciton has a lifetime from 22 ps in QDs with radius of 1.7 nm to 363 ps in QDs with radius of 4.1 nm.[32] In current QD/PTZ system, the radius of CdSe QDs was 1.8 nm, which was similar to the reported system (1.7 nm). However, hole transfer rate observed in current CdSe-PTZ system was significantly slower, suggesting that the conditions for hole transfer in this system have to be optimized.

According to Marcus theory,[33] the hole transfer rate in this system is dependent on the driving force and the number of acceptors on the surface. We can use the same approach presented in Chapter 3 and 4 to estimate the driving force for the current hole transfer process. The obtained driving force from the $1S_{3/2}$ level to PTZ was estimated to be ~-0.34 V following published procedure.[19,20] One may increase the driving force for the current system by using acceptors with a lower oxidation potential, and thus the possibility to increase the hole transfer rate. It remains unclear if hole transfer rate is dependent on QD sizes.

5.4 Summary

Photoinduced hole transfer from CdSe QDs (with first exciton peak at 462 nm and estimated radius of 1.8 nm) to phenothiazine (PTZ) was investigated by time-resolved fluorescence and transient absorption spectroscopy. Fluorescence lifetime measurements showed that the presence of PTZ reduced the exciton lifetime of CdSe QDs, and the quenching rate increased with increasing PTZ concentration. Transient absorption spectra of CdSe-PTZ complexes directly revealed the formation of PTZ cation radial. These results suggested that excitons in CdSe QDs dissociated by hole transfer to PTZ and the average hole transfer rate increased at higher adsorbate concentration. A kinetic model based on a Poisson distribution of the number of adsorbates on each QD was found to adequately describe the adsorbate concentration-dependent fluorescence decay kinetics. According to this model, the hole transfer time was ~2.5 ns in 1:1 CdSe-PTZ complexes and reached ~300 ps in a CdSe-PTZ sample in which there were an average of 6.2 adsorbed PTZ molecules per QD.

References

(1) Duonghong, D.; Ramsden, J.; Gratzel, M. *J. Am. Chem. Soc.* **1982**, *104*, 2977.

(2) Sharma, S. N.; Pillai, Z. S.; Kamat, P. V. *Journal of Physical Chemistry B* **2003**, *107*, 10088.

(3) Sykora, M.; Petruska, M. A.; Alstrum-Acevedo, J.; Bezel, I.; Meyer, T. J.; Klimov, V. I. *Journal of the American Chemical Society* **2006**, *128*, 9984.

(4) Landes, C. F.; Burda, C.; Braun, M.; El-Sayed, M. A. *J. Phys. Chem. B.* **2001**, *105*, 2981.

(5) Yu, W. W.; Qu, L.; Guo, W.; Peng, X. *Chem. Mater.* **2003**, *15*, 2854.

(6) Boulesbaa, A.; Issac, A.; Stockwell, D.; Huang, Z.; Huang, J.; Guo, J.; Lian, T. *J. Am. Chem, Soc.* **2007**, *129*, 15132.

(7) Huang, J.; Stockwell, D.; Huang, Z.; Mohler, D. L.; Lian, T. *J. Am. Chem. Soc.* **2008**, *130*, 5632.

(8) Logunov, S.; Green, T.; Marguet, S.; El-Sayed, M. A. *J. Phys. Chem. A* **1998**, *102*, 5652.

(9) Burda, C.; Green, T. C.; Link, S.; El-Sayed, M. A. *J. Phys. Chem. B* **1999**, *103*, 1783.

(10) Klimov, V. I. *J. Phys. Chem. B* **2000**, *104*, 6112.

(11) Klimov, V. I.; Mikhailovsky, A. A.; McBranch, D. W.; Leatherdale, C. A.; Bawendi, M. G. *Phys. Rev. B* **2000**, *61*, R13349.

(12) Burda, C.; Link, S.; Mohamed, M.; El-Sayed, M. *Journal of Physical Chemistry B* **2001**, *105*, 12286.

(13) Guyot-Sionnest, P. *Structure and Bonding (Berlin, Germany)* **2005**, *118*, 59.

(14) Landes, C. F.; Braun, M.; El-Sayed, M. A. *Journal of Physical Chemistry B* **2001**, *105*, 10554.

(15) Takada, T.; Kawai, K.; Fujitsuka, M.; Majima, T. *Proc Natl Acad Sci U S A FIELD Full Journal Title:Proceedings of the National Academy of Sciences of the United States of America* **2004**, *101*, 14002.

(16) Tierney, M. T.; Sykora, M.; Khan, S. I.; Grinstaff, M. W. *Journal of Physical Chemistry B* **2000**, *104*, 7574.

(17) Tierney, M. T.; Grinstaff, M. W. *Journal of Organic Chemistry* **2000**, *65*, 5355.

(18) Ghosh, H. N.; Sapre, A. V.; Palit, D. K.; Mittal, J. P. *Journal of Physical Chemistry B* **1997**, *101*, 2315.

(19) Brus, L. *J. Chem. Phys.* **1983**, *79*, 5566.

(20) Brus, L. E. *J. Chem. Phys.* **1984**, *80*, 4403.

(21) Peng, Z. A.; Peng, X. *Journal of the American Chemical Society* **2002**, *124*, 3343.

(22) Ghosh, H. N.; Sapre, A. V.; Palit, D. K.; Mittal, J. P. *J. Phys. Chem. B* **1997**, *101*, 2315.

(23) Klimov, V. I.; McBranch, D. W.; Leatherdale, C. A.; Bawendi, M. G. *Physical Review B-Condensed Matter* **1999**, *60*, 13740.

(24) Burda, C.; Link, S.; Mohamed, M. B.; El-Sayed, M. *Journal of Chemical Physics* **2002**, *116*, 3828.

(25) Klimov, V. I.; Schwarz, C. J.; McBranch, D. W.; Leatherdale, C. A.; Bawendi, M. G. *Physical Review B-Condensed Matter* **1999**, *60*, R2177.

(26) Underwood, D. F.; Kippeny, T.; Rosenthal, S. J. *J. Phys. Chem. B* **2001**, *105*, 436.

(27) Huang, J.; Stockwell, D.; Huang, Z.; Mohler, D. L.; Lian, T. *Journal of the American Chemical Society* **2008**, *130*, 5632.

(28) Tachiya, M. *Journal of Chemical Physics* **1982**, *76*, 340.

(29) Rogers, M. A. J.; Wheeler, M. F. D. S. E. *Chemical Physics Letters* **1978**, *53*, 165.

(30) Rogers, M. A. J.; Da Silva, M. F.; Wheeler, E. *Chem. Phys. Lett.* **1978**, *53*, 165.

(31) Tachiya, M. *J. Chem. Phys.* **1982**, *76*, 340.

(32) Klimov, V. I.; Mikhailovsky, A. A.; McBranch, D. W.; Leatherdale, C. A.; Bawendi, M. G. *Science* **2000**, *287*, 1011.

(33) Marcus, R. A.; Sutin, N. *Biochem. Biophys. Acta* **1985**, *811*, 265.

Chapter 6. Multiple Exciton Dissociation in CdSe Quantum Dots by Electron Transfer to Methylene Blue

6.1. Introduction

In recent years, the efficient conversion of photon energy to electrical energy has been the key goal of much research in some areas such as solar cells, photocatalysis, and photosynthesis. One of the fundamental limitations to the conversion efficiency of these devices is due to the dissipation of the excess energy above the bandgap of the semiconductor materials used as heat.[1] Under this assumption, the maximum thermodynamic efficiency for the conversion of unconcentrated solar irradiance into electrical free energy in the radiative limit was calculated by Shockley and Queissar in 1961 to be about 31%.[2]

One potential approach to overcome this limit is through multiexciton generation (MEG), a process by which an absorbed photon produces multiple excitons, and hence the quantum efficiency becomes > 100%. MEG phenomenon has been known in bulk semiconductors[3,4] and has been reported recently in ultrasmall semiconductor nanocrystals, such as quantum dots (QDs)[5-10] and carbon nanotubes.[11] However, the mechanism, efficiency and generality of MEG are under intense debates. Some studies reported extremely efficient MEG in PbS, PbSe, PbTe,[5-10] Si,[12,13] CdSe[14,15] and InAs[16,17] QDs, while some reports refuted the claims of efficient MEG in CdSe,[18] InAs[19] and PbS[20] QDs. These reports suggest that MEG efficiencies need to be further improved before its practical applications. Additionally, before the practical application of MEG in devices, multiexcitons have to be dissociated before the ultrafast exciton-exciton annihilation process (10s to 100s ps).[21,22] Ultrafast interfacial charge transfer to the adsorbed molecular adsorbates offers a potential approach to extract multiple excitons in QDs. Such charge transfer processes have been extensively studied since 1980s.[23-39] Some of these studies revealed that the rates of charge transfer to molecular acceptors are on the 10s of picosecond and faster timescale,[24-26,28,33,34,37,39] suggesting the possibility to dissociate multiple excitons by ultrafast charge transfer through molecular adsorbates before the exciton-exciton annihilation process.

This possibility has been successively achieved in CdSe QDs adsorbed with methylviologen (MV^{2+}) reported recently by Matylitsky et al.[40] They demonstrated that up to 4 excitons have been dissociated by ultrafast electron transfer to MV^{2+}. In this study, the number of excitons generated by absorbing multiple photons was calculated according to the photon flux of the pump pulse and the optical density of the sample. However, the quantification of the photon flux J(0), which is determined by the beam focus mode, beam sizes et al., suffers from big errors. Additionally, the numbers of excitons dissociated were determined by the absorption of $MV^{+\cdot}$ at ～ 400 nm which overlapped with the much stronger absorption of QDs in this region. In order to establish an accurate relationship between the average number of excitons per QD generated and excitation powers, as well as the effort to overcome the spectral overlap problems, we investigated the multiple exciton dissociation dynamics in CdSe-MB^{+} complex by examining the exciton bleach amplitude as a function of excitation powers followed by the simulation of these figures.

Methylene blue (MB^+) was chosen as the electron acceptor because of its capability to efficiently scavenge conduction band electrons from semiconductor colloidal particles due to its low reduction potential (-0.23 V vs SCE).[27,41] It was shown that on the > 10 ns time scale, excitation of CdS in the CdS-MB^+ complexes lead to the formation of the one-electron reduced MB^+ (with an absorption band at ~420 nm), and the depletion of MB^+ absorption around 650 nm, suggesting the transfer of electron from CdS to MB^+.[27] Scott's group also reported the investigation of MB^+ reduction by CdS power using light scattering transients. They found a faster decay in the presence of MB^+ for light scattering transients measured at 630 nm and 680 nm and the scattering signals decayed more extensively with increasing dye coverage and attributed that to electron transfer process.[41]

In this chapter, we examine both the single and multiple exciton dissociation dynamics through ET to MB^+. The process can be described in equation (6.1):

$$CdSe*(1S_e,1S_h)-MB^+ \rightarrow CdSe^+(1S_h)-MB^{\cdot} \qquad (6.1)$$

where CdSe* and $CdSe^+$ represent excited and oxidized states of CdSe, respectively, and $MB^{\cdot}$ represent semi-quinone form of the dye (the one electron reduced state of MB^+). MB^+ is a good probe for electron acceptor because the spectral features of $MB^{\cdot}$ (with absorption at 420 nm) is well separated from its ground state at 650nm and oxidized state at 520 nm.[27] In this study, we showed that single exciton in excited CdSe QDs can dissociate in ultrafast time scale by transferring electrons to MB^+. It was noted that the rate of the electron transfer process can reach sub-picosecond in CdSe (510nm)-MB^+ complex by using more than 2 MB^+ molecules per QD.[42] Additionally, because of the capability of larger size QD to adsorb more MB^+ and hence the faster ET rate, CdSe (553nm)-MB^+ complex was chosen to examine multiexciton dissociation dynamics. We show that ET rate in this system is ~2 ps and up to three excitons per QD have been dissociated.

6.2 Results and Discussion

6.2.1 Single Exciton Dissociation Dynamics in CdSe(510nm)-MB^+ Complex

6.2.1.1 ET Pathway in CdSe(510nm)-MB^+ Complex

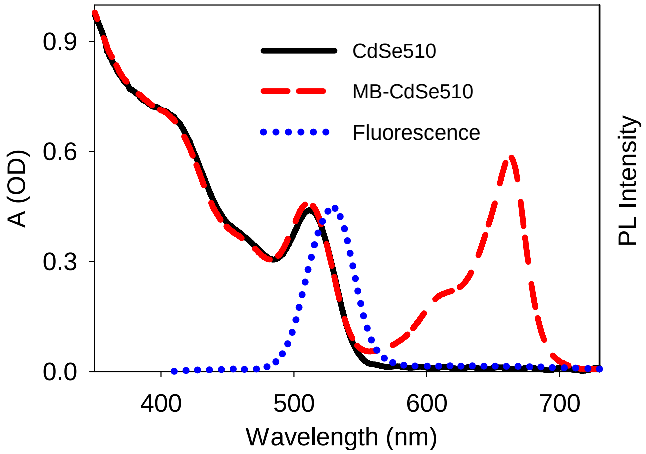

Figure 6.1. UV-visible absorption spectra of CdSe (510 nm) and CdSe (510 nm)-MB^+ complexes in heptane, and fluorescence spectra of CdSe (510 nm) QDs in heptane.

Figure 6.1 shows the absorption spectra of CdSe (510nm) and CdSe(510 nm)-MB^+ complexes in heptane. The absorption peak of the lowest allowed ($1S_{3/2}$(h)-$1S_{1/2}$(e)) exciton transition is located at 510 nm for these particles. Compared to the spectrum of free QDs (black solid line), CdSe(510nm)-MB^+ complexes (red dashed line) exhibit an additional absorption band at 664 nm which has been attributed to the ground state absorption of MB^+ molecule.

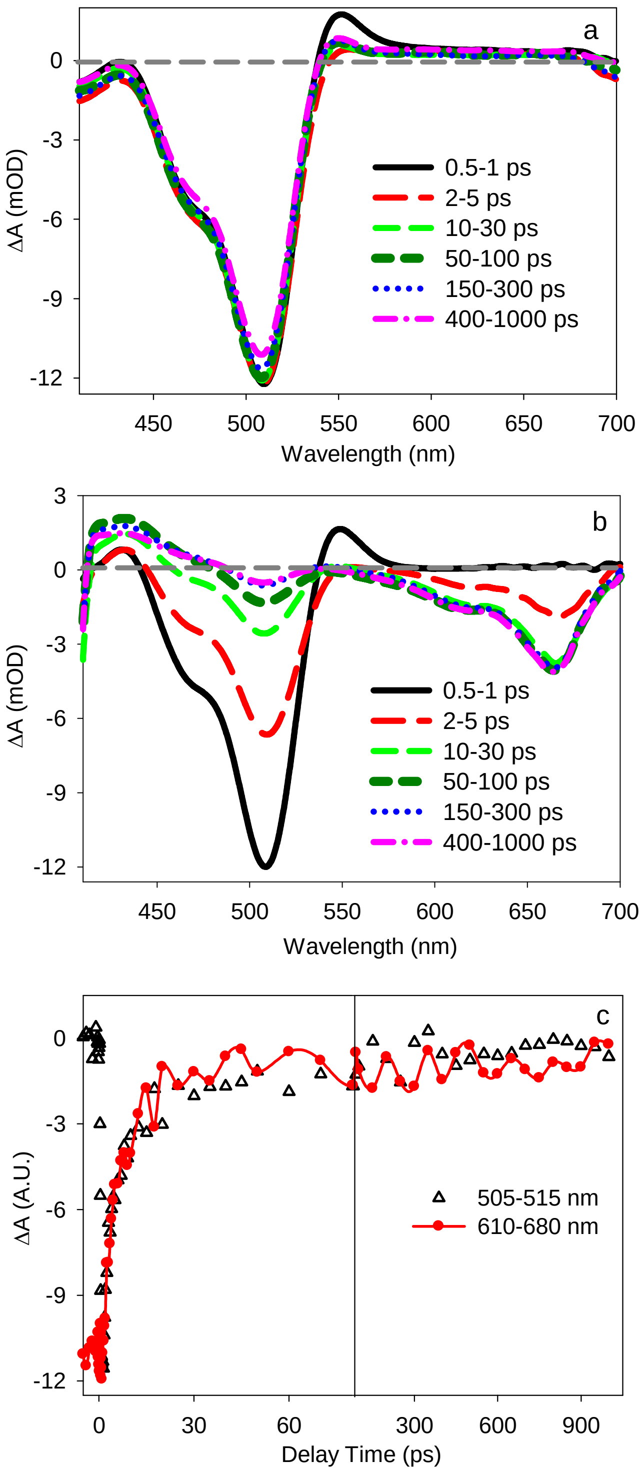

Figure 6.2. (a) Transient spectra of CdSe(510nm) at indicated delay times after 400 nm excitation. (b) Transient spectra of CdSe(510nm)-MB$^+$ at indicated delay times after 400 nm excitation. (c) Comparison of exciton bleach recovery kinetics of CdSe-MB$^+$

assemblies at 505-515 nm (black triangles) and the depletion kinetics of MB^+ in the ground state (red circles). The MB^+ ground state depletion signal has been normalized to the same initial amplitude as the exciton bleach signal and inverted for better comparison.

Figure 6.2 shows the transient visible absorption spectra of CdSe (510nm) and CdSe (510 nm)-MB^+ complexes after 400 nm excitation. These spectra are taken under low excitation energy to ensure negligible populations in multiple exciton states. These spectra show bleaches of $1S_{2/3}$(h)-$1S_{1/2}$(e) (510 nm) and $2S_{2/3}$(h)-$1S_{1/2}$(e) (460 nm) interband exciton transitions at all delay times. In the absence of the adsorbate (Figure 6.2a), these exciton interband bleaches remain constant on the < 1ns time window, indicating long-lived single 1S exciton state and negligible QDs with multiple excitons. In contrast, as shown in Figure 6.2b, in QD-MB^+ complex, the bleach of exciton bands recovers by 95% at 1 ns. It has been shown earlier that 1S exciton bleach (due to state filling of 1S electron level in the conduction band) of QD recovers when the electron is transferred to the adsorbate, while it remain constant when the hole is transferred.[39,43] Therefore, the accelerated recovery of exciton bleach kinetics for CdSe(510nm)-MB^+ compared to that of free CdSe suggested that exciton in CdSe QDs dissociate through electron transfer to MB^+. Further support for electron transfer process can be directly obtained by monitoring the spectral signatures of MB^+ molecule. As shown in Figure 6.2b, the spectra of CdSe(510nm)-MB^+ complex at all delay times exhibit two additional features, a broad bleaching band at 610-680 nm regions, and an apparent absorption band at ~ 430 nm. The spectra of the bleach at 610-680 nm agrees well with UV-visible spectra of MB^+ and can be attributed to the depletion of the ground state of MB^+

molecule. The absorption band at 430 nm can be assigned to the semiquinone form of MB^+ as reported.[27] In addition, the exciton bleach recovery kinetics of CdSe QDs was compared with the depletion kinetics of MB^+ for CdSe(510nm)-MB^+ complex as shown in Figure 6.2c. The kinetic trace of exciton bleach recovery was obtained by averaging the kinetics from 505-515 nm. The depletion kinetics of MB^+ ground state was monitored at ～ 664 nm. The depletion signal has been normalized to the same initial amplitude as the exciton bleach signal and inverted for a better comparison. The QD exciton bleach recovery kinetics agrees well with the growth of the bleach of MB^+ ground state absorption at 664 nm within 1 ns, suggesting that this feature was associated with the loss of electron in the conduction band of CdSe. Similar transient kinetics results (faster exciton bleach recovery, MB^+ ground state bleach, MB^+-semiquinone absorption, et ac.) were also observed in another QD-MB^+ system (with QD the first exciton band of at 470 nm), as shown in Figure 6.3. In addition, the absorption of oxidized state of MB^+, reported to be at 520 nm,[27] was not observed in the transient spectra of CdSe(470nm)-MB^+ complex, which further excludes the possibility of hole transfer process. These results suggest that excitons in CdSe QDs dissociate by transferring electrons to MB^+.

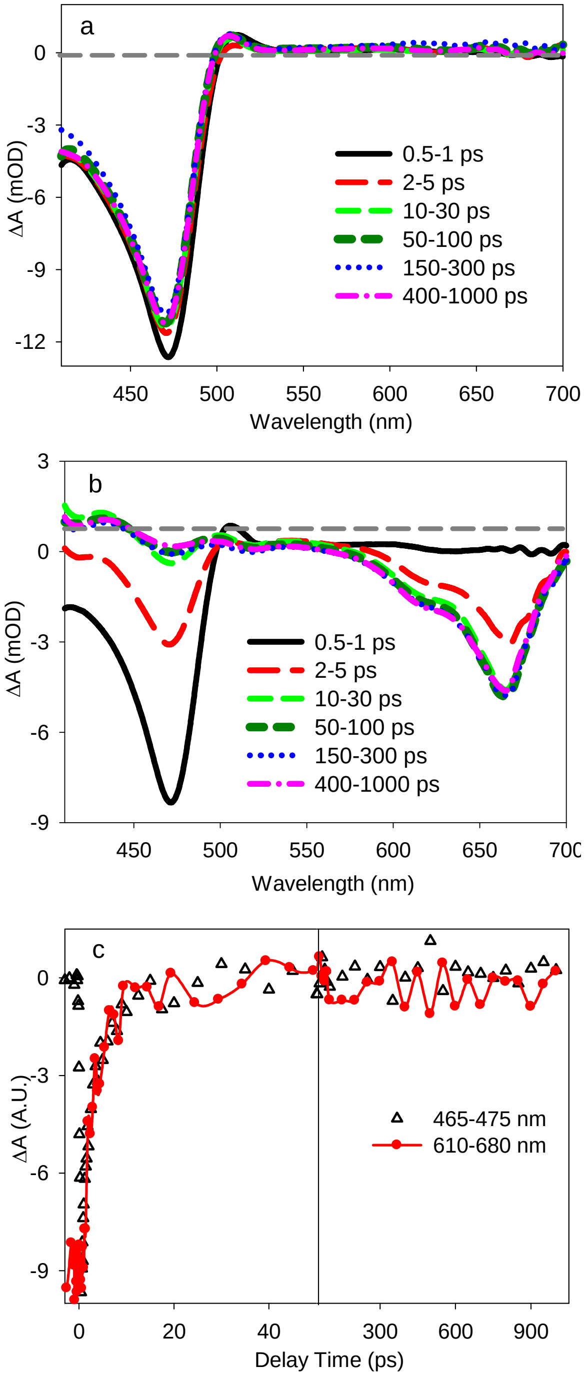

Figure 6.3. (a) Transient spectra of CdSe(470nm) at indicated delay times after 400 nm excitation. (b) Transient spectra of CdSe(470nm)-MB at indicated delay times after 400 nm excitation. (c) Comparison of exciton bleach recovery kinetics of MB-CdSe assemblies at 465-475 nm (black triangles) and the depletion kinetics of MB in the

ground state (red circles). The ground state depletion signal has been normalized to the same initial amplitude as the exciton bleach signal and inverted for better comparison.

6.2.1.2 Energy Transfer Efficiency in CdSe(510nm)-MB$^+$ Complexes

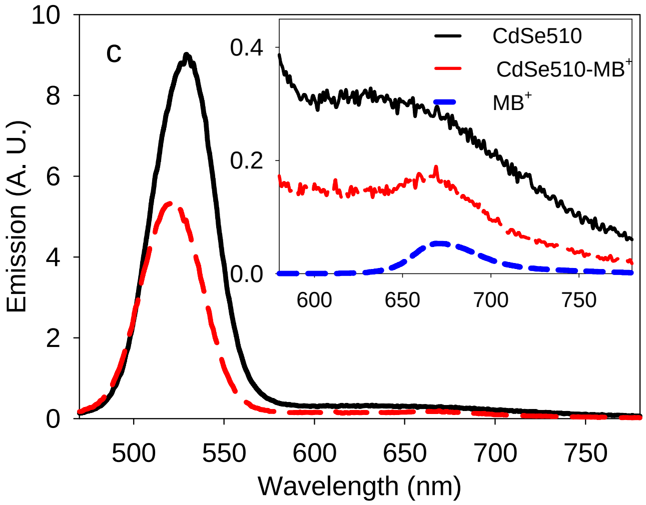

Figure 6.4. Emission spectra of CdSe (510nm) and CdSe(510nm)-MB$^+$ complexes The insets show the expanded view of these spectra as well as MB$^+$ emission spectra obtained according to the approach described in the main text.

Since the emission spectrum of CdSe (510 nm) QDs has a slight overlap with the absorption spectrum of MB$^+$, as shown in Fig. 6.1, energy transfer might be a possible pathway for exciton deactivation in this system. Energy transfer efficiency of CdSe(510nm)-MB$^+$ complexes were analyzed according to the quantum yields of CdSe (in heptane) and MB$^+$ (in methanol) as well as the emission spectra of CdSe(510nm) and CdSe(510nm)-MB$^+$ compelx. The quantum yields of CdSe QD (Φ_{QD}) were measured following 400 nm excitation by using Coumarin 343 (Φ_{C343}, 63 %) as the standard. The obtained quantum yields for CdSe was ～ 8%. The quantum yield of MB^+ in CdSe(510nm)-MB^+ complex (Φ_{QMB}) was measured to be ～ 1% after 660 nm excitation with MB^+ in methanol (Φ_{MB}, 4%) as the standard.

Figure 6.4 shows the emission spectra of CdSe (510 nm) and CdSe (510 nm)-MB^+ complex. The expanded views of these spectra were shown in the insets. Compared to the emission of free CdSe (I_{QD}), the emission of QDs in CdSe(510nm)-MB^+ complex was quenched dramatically. Assuming that the remaining QD emission in CdSe(510nm)-MB^+ complex (I_{fQD}) was due to free CdSe(510nm) in CdSe(510nm)-MB^+ complex solution, we estimated the emission of CdSe(510nm) QDs which was quenched by the presence of MB^+ ($I_{quenched}$):

$$I_{quenched} = I_{QD} - I_{fQD} \qquad (6.2)$$

The emission of MB^+ (I_{MB}) was obtained by subtracting the emission spectrum of CdSe(510nm) from that of CdSe(510nm)-MB^+ complex. The obtained spectra were also shown in the insets of Figure 6.4. With the measured quantum yields and obtained emission for CdSe and MB^+ (in CdSe(510nm)-MB^+ complex), the energy transfer efficiency (η) in CdSe(510nm)-MB^+ complex can be calculated according to:

$$\eta = \frac{I_{MB} / \Phi_{MB}}{I_{quenched} / \Phi_{CdSe}} \qquad (6.3)$$

On the basis of equation 6.3, we estimated the energy transfer efficiency for CdSe(510nm)-MB^+ complex, which was < 5%. Due to this small energy transfer efficiency, we concluded that electron transfer is the dominating pathway for exciton decay in the CdSe(510nm)-MB^+ complexes.

6.2.2 Single Exciton Dissociation Dynamics in CdSe(553nm)-MB$^+$ Complex

6.2.2.1 ET Pathway in CdSe(553nm)-MB$^+$ Complex

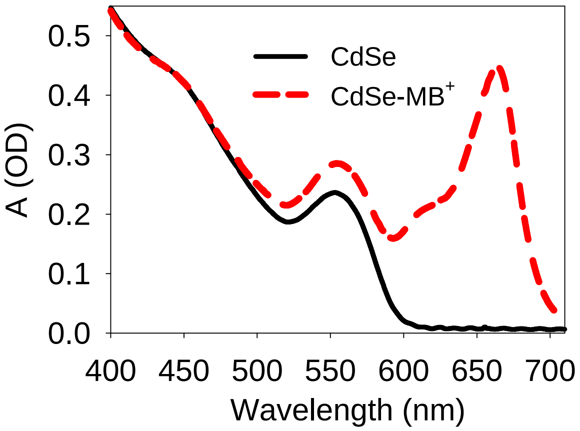

Figure 6.5. UV-visible absorption spectra of CdSe (553 nm) and CdSe (553 nm)-MB$^+$ complex.

Shown in Figure 6.5 is the UV-vis absorption spectra of CdSe(553 nm) and CdSe(553 nm)-MB$^+$ complex in heptane used in this study. The absorption peaks at 553 nm and 460 nm can be assigned to the lowest allowed ($1S_{2/3}$(h)-$1S_{1/2}$(e)) and $1P_{3/2}$(h)-1P(e) exciton transitions, respectively, for these particles. Compared to the spectrum of free QDs (black solid line), CdSe(553 nm)-MB$^+$ complexes (red dashed line) exhibit an additional absorption band at 664 nm which has been attributed to the ground state absorption of MB$^+$ molecule as discussed in the section of 6.2.1. The average number of adsorbed MB$^+$ per QD is estimated to be ~ 3 based on the measured absorbance and known extinction coefficients of MB$^+$ (7.4x10^4 M^{-1}cm^{-1})[44] and CdSe (1.17 x10^5 M^{-1}cm^{-1}).[45]

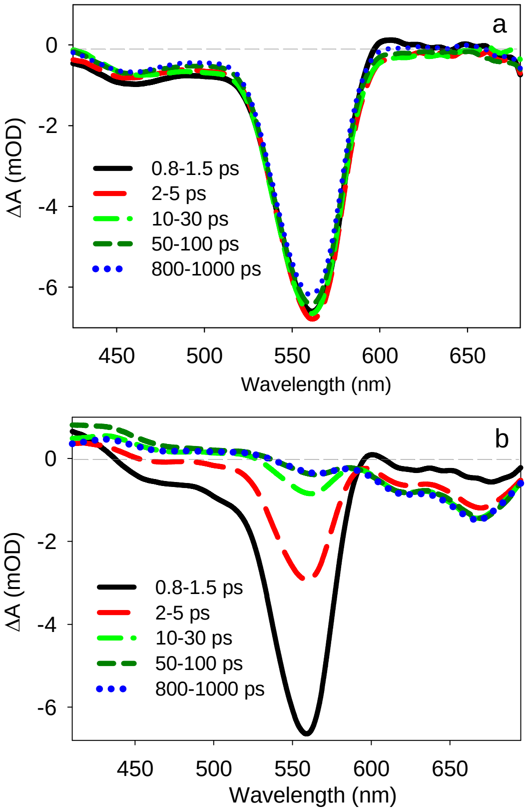

Figure 6.6. (a) Transient visible spectra of CdSe(553nm) at indicated delay times after 400 nm excitation. (b) Transient visible absorption spectra of CdSe(553 nm)-MB^+ complexes at indicated delay times after 400 nm excitation. The spectra were measured with excitation pulse energy of 11 nJ

Figure 6.6a and b show the transient spectra of CdSe(553 nm) and CdSe(553 nm)-MB^+ complex after 400 nm excitation, respectively. These spectra are taken under low excitation energy to ensure negligible populations in multiple exciton states. Compared to the spectra of CdSe alone (Figure 6.6a), we observed three additional features in the CdSe(553 nm)-MB^+ spectra: A faster exciton bleach recovery at 553 nm, an additional bleaching band at 660nm which is consistent with the ground state absorption of MB^+, and a new absorption band observed at 430 nm which can be assigned to the absorption of MB$^{\cdot}$ semiquinone as we reported.[27] These spectra features are consistent with those expected for ET process as we discussed in Section 6.2.1, suggesting that the excitons in CdSe(553 nm) QDs are dissociated through ET to MB$^+$.

Additionally, we compared the exciton bleach recovery of CdSe QDs in CdSe(553 nm)-MB$^+$ complex and MB$^+$ ground state depletion kinetics, as shown in Figure 6.7. The exciton bleach kinetic trace is obtained by averaging the data from 545 nm to 560 nm. The depletion kinetics of MB$^+$ ground state was monitored at ～ 664 nm. The MB$^+$ bleach has been normalized and inverted for a better comparison of its growth with the recovery of QD exciton bleach. It can be seen that these two traces agree well with each other within 1 ns, further supporting the assignment that excitons in CdSe dissociate by transferring electrons to MB$^+$. To quantify the electron transfer rate, we fitted the exciton bleach recovery kinetics with an exponential decay function. The best fit to the recovery kinetics is also shown in Figure 6.7, from which we obtain an amplitude-weighted average ET time of ～ 2.3 ps. This is faster than the exciton-exciton annihilation process, indicating the possibility of dissociating multiexcitons in this system.

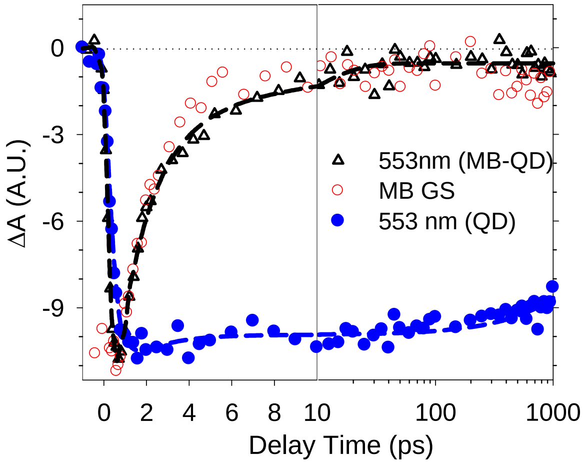

Figure 6.7. Comparison of the recovery kinetics of QD 1S exciton bleach (black open triangles) and the formation kinetics of MB^+ ground state bleach (red open circles) in CdSe(553 nm)-MB^+ complexes. Also shown is the exciton bleach recovery kinetics of QD only (blue filled circles). The MB^+ ground state bleach signal has been normalized and inverted for better comparison. Adapted from Ref. [46]

6.2.2.2 Energy Transfer Efficiency in CdSe(553nm)-MB^+ Complexes

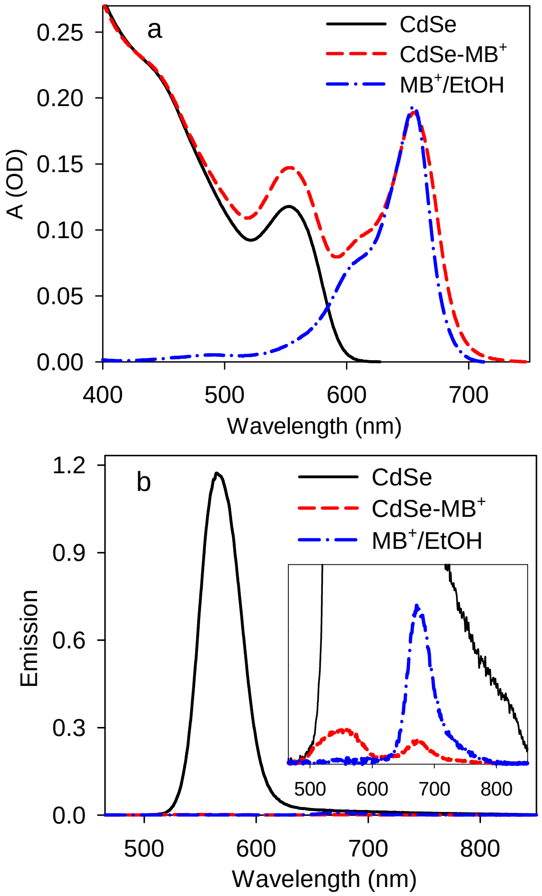

Figure 6.8. a) UV-vis absorption spectra of CdSe(553 nm) in heptane (solid black line), CdSe(553 nm)-MB^+ in heptane (red dashed line) and MB^+ in ethanol (blue dash-dot line). b) Static emission spectra of CdSe(553 nm) in heptane (solid black line), CdSe(553 nm)-

MB^+ in heptane (red dashed line) and MB^+ in ethanol (blue dash-dot line) after 450 nm excitation. Adapted from Ref. [46]

However, in this CdSe(553 nm)-MB^+ complexes, the CdSe emission and MB^+ absorption spectra overlap with each other significantly. Therefore, there is high possibility that energy transfer may contribute to the exciton quenching. To quantify the contribution of energy transfer in exciton quenching, we analyzed the static emission spectra of CdSe(553 nm), CdSe(553 nm)-MB^+ complex, and MB^+ in ethanol according to the approach described in Section 6.2.1.2. According to that approach and using Rhodamine 101 ($\Phi_{Rh101}\approx 100\%$) as standard sample, the quantum yields of CdSe(553 nm) in heptane (Φ_{QD}, 450-nm excitation) was determined to be 5.8%. The quantum yield of MB^+ in CdSe(553 nm)-MB^+ complex (Φ_{QMB}) was found to be ～ 0.13% after 650 nm excitation with MB^+ in ethanol (Φ_{MB}, 4%) as the standard. [47]

The absorption spectrum of the CdSe(553 nm)-MB^+ sample is shown in Figure 6.8a. The ratio of MB^+ to CdSe(553 nm) is similar to that used for the exciton dissociation study shown in Figure 6.5. The static emission spectra of CdSe(553 nm) and CdSe(553 nm)-MB^+ complex are shown in Figure 6.8b. The expanded views of these spectra were shown in the inset. After accounting for the amount of MB^+ emission in CdSe(553 nm)-MB^+ complex due to direct excitation (I_{dMB}), and using the obtained emissions and the measured quantum yields for CdSe(553 nm) and MB^+ (in CdSe(553 nm)-MB^+ complex), we estimated the energy transfer efficiency (η) in CdSe(553 nm)-MB^+ complex according to:

$$\eta = \frac{(I_{QMB} - I_{dMB}) / \Phi_{QMB}}{I_{QD} / \Phi_{QD}} \qquad (6.4)$$

Where I_{QMB} is the emission intensity of MB^+ in CdSe(553 nm)-MB^+ complex and I_{QD} is the exciton emission intensity of CdSe(553 nm) (without MB^+). All emission intensities were obtained by integrating the emission spectra. The η value in this system obtained was estimated to be ～ 6%, indicating that energy transfer does not play a major role in the exciton quenching. Therefore, the exciton dissociation occurs through the ET process with near unity quantity. Additionally, compared to the emission spectra of CdSe(553 nm), > 99% of QD emission is quenched in the presence of MB^+, suggesting that the remaining bleach signal at 553 nm at 100 ps to 1 ns in Figure 6.6b can be attributed to that of MB^+ ground state bleach.

6.2.3. Exciton-Exciton Annihilation

6.2.3.1. Quantifying Exciton-Exciton Annihilation Rate.

As we discussed in the previous sections, single exciton in CdSe QDs dissociates through the ultrafast ET process with near unity quantity to the adsorbed MB^+. In term of its capability to adsorb more MB^+ molecules for large size QD (553nm) as well as the ultrafast ET rate (～2 ps), CdSe(553nm)-MB^+ complex was chosen to examine multiexciton dissociation dynamics.

In order to determine how exciton-exciton annihilation in CdSe(553nm) QDs competes with ET in CdSe(553nm)-MB^+, we first examine exciton-exciton annihilation in CdSe(553nm) under different excitation powers from 11 to 1187 nJ/pulse. Figure 6.9 shows the transient absorption spectra recorded at the selected intermediate pump powers. All of these spectra show bleaches of 1S (553 nm) and 1P (460 nm) exciton transitions at all delay times. However, at low power (11 nJ), the 1S exciton bleach only decays ~ 10%

within 1ns, indicating long exciton lifetime (>> 1 ns). In contrast, at high excitation powers, the 1S exciton bleach recovery in CdSe(553nm) increases with the excitation power. The bleach recovers by ~ 50% within 1ns at excitation powers higher than 376 nJ, indicating the fast exciton-exciton annihilation process in CdSe(553nm) QDs under these conditions. Additionally, the 1P exciton bleach amplitude also increases with the excitation powers, indicating the presence of 1P electrons.

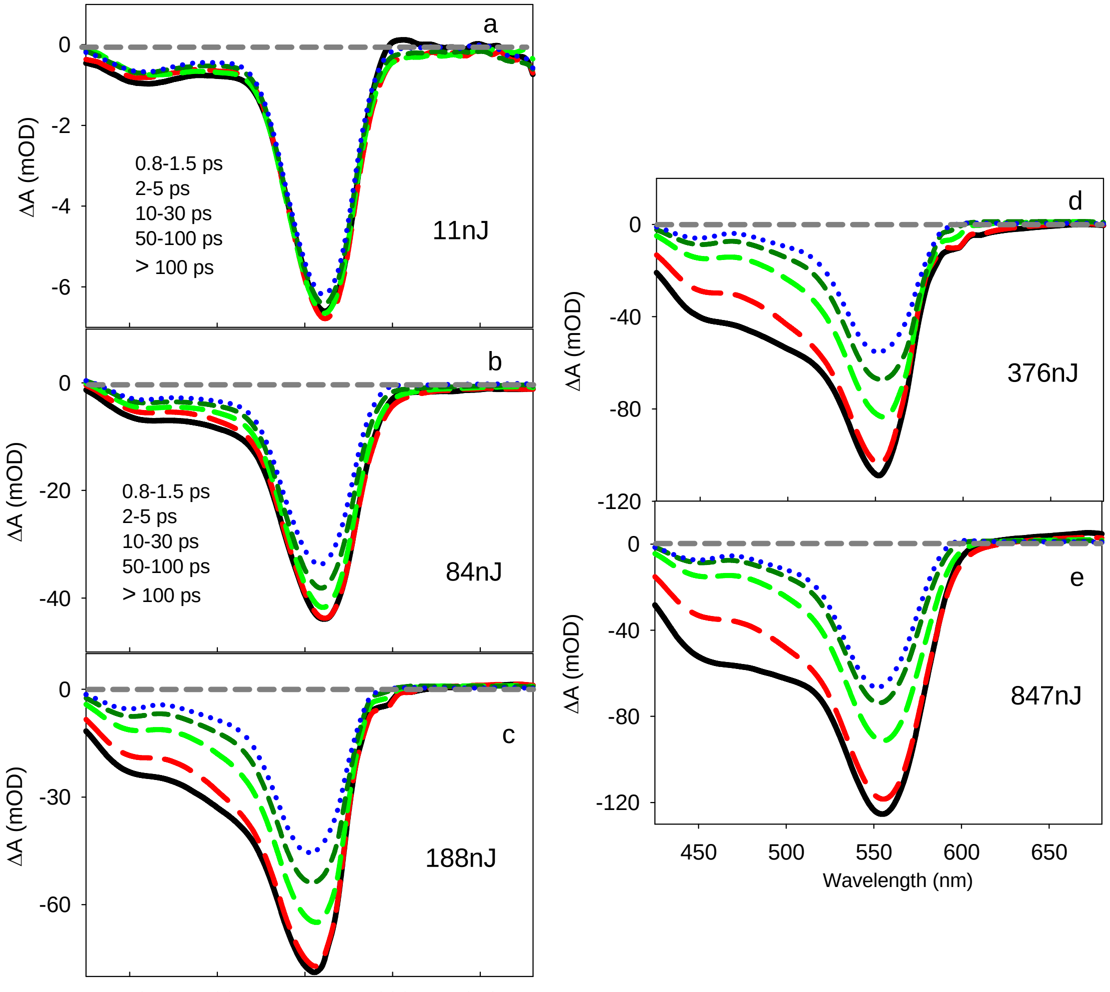

Figure 6.9. **T**ransient visible absorption spectra of CdSe at indicated delay times after 400 nm excitation for various excitation energy (as indicated).

To quantify the exciton-exciton annihilation rate, we analyzed the exaction bleach recovery kinetics for both 1S and 1P transitions under these excitation powers, as shown in Figure 6.10a and b respectively. These kinetic traces have been normalized to unity at 1 ns to account for the different populations of excited QDs under different excitation powers. This normalization can be made because multiple excitons are short-lived (<< 1ns), and single excitons are long lived (>> 1 ns), then at 1 ns all multiple excitons have decayed to single exciton states and single exciton has negligible decay. Therefore, the exciton bleach amplitude at 1 ns directly reflects the population of QDs excited. With this normalization, the larger faster recovery component at high excitation powers (Figure 6.3a) suggests an increasing percentage of QDs with multiple excitons.

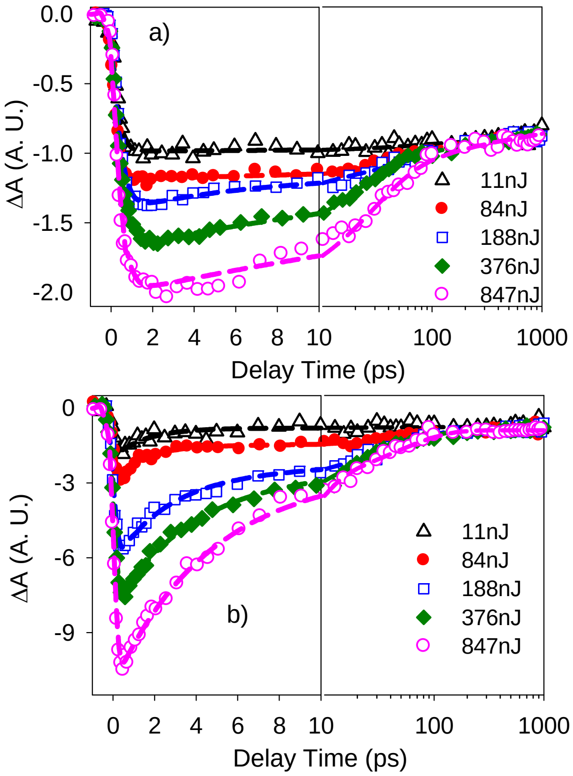

Figure 6.10. Comparison of (a) 1S and b) 1P exciton bleach recovery kinetics of CdSe at indicated excitation energy. Kinetic traces have been normalized to the same value at 1ns.

The left panel shows the data up to 10 ps in linear scale and the right panel displays the data from 10 ps to 1ns in logarithmic scale. Adapted from Ref. [46]

We assume that the number of excitons per QD generated by the excitation pulse obeys a Poisson distribution:

$$P_n(w) = \frac{w^n}{n!} e^{-w} \tag{6.5}$$

where $P_n(w)$ is the probability of having QDs with n excitons and w is the average number of excitons per QD. We further assume that the 1S bleach signal is unaffected by decay between n (>2) to n-1 exciton states, because in QDs 1S exciton absorption is reduced by half with one exciton and completely bleached with two or more excitons due to a 2-fold spin degeneracy in the 1S electron level. That means 1S exciton bleach signal only depends on the decay of bi-exciton (with lifetime of τ_{2X}) and single exciton (with lifetime of τ_{1X}) states. With these two assumptions, we can describe the normalized 1S exciton bleach amplitude at delay time t as follows:

$$\Delta S_{1S}(t) = (1 - P_0 - P_1)e^{-t/\tau_{2X}} + (1 - P_0)e^{-t/\tau_{1X}} \tag{6.6}$$

where $\Delta S_{1S}(t)$ is the normalized absorbance change in the 1S exciton peak at delay time t. The first and second terms in equation 6.6 represent the decay of short-lived bi-exciton state and long-lived single exciton state, respectively. Their amplitudes reflect the probability of finding QDs with two or more excitons and that of the excited QDs with one or more excitons, respectively. For the 1S exciton kinetic traces (Figure 6.10a), all kinetic traces have been normalized to unity at one, indicating that all QDs have been excited ($P_0 = 0$). Equation 6.6 can therefore be modified to:

$$\Delta S_{1S}(t) = (1 - P_1)e^{-t/\tau_{2X}} + e^{-t/\tau_{1X}} \tag{6.7}$$

Equation 6.7 has been used to fit the normalized 1S transient kinetics shown in Figure 6.10a. The best fits to these traces are also shown in Figure 6.10a and the fitting parameters are listed in Table 6I. From these fitting parameters, we obtain an average bi-exciton decay time of 49 (±4) ps and single exciton decay time of >> 1 ns, which are shown in Table 6I as well. Additionally, the best fits reveal a rise time of ~350 fs for the 1S exciton bleach. This rise time is similar to the electron relaxtion rate via Auger process reported for other QDs[48,49] and thus is attributed to the relaxation of electrons from the initially excited 1P level to the 1S level.

Table 6I: Fitting Parameters for the Exciton Bleach Recovery Kinetics of CdSe[a]

	Power	τ_r (100%)	τ_1, ps (A_1,%)		τ_2, ps (A_2,%)	τ_3, ps (A_3,%)
1S	11nJ	～350 fs	>> 1ns	(94)	50.6 (6)	
	84nJ			(78)	52.2 (22)	
	188nJ			(65)	73.0 (20)	5.3 (15)
	376nJ			(55)	21.0 (39)	202.5 (6)
	847nJ			(46)	27.2 (44)	154.0 (10)
	τ_{ave}		>> 1 ns		49±44	
1P	11nJ	< 50 fs	>> 1ns	(39)	48.5 (20)	1.5 (59)
	84nJ			(29)	48.5 (18)	1.2 (53)
	188nJ			(13)	48.5 (31)	2.6 (56)
	376nJ			(11)	48.5 (27)	3.5 (63)
	847nJ			(20)	48.5 (20)	4.5 (72)

[a] The traces (Figure 6.10) are fit with single-exponential rise and multi-exponential decay functions ($\sum_i A_i e^{-t/\tau_i} - e^{-t/\tau_r}$)

In addition to the biexciton lifetime, we can estimate the n (>2) exciton lifetime by examining the 1P exciton bleach recovery kinetics. Shown in Figure 6.10b are the normalized 1P kinetic traces measured under different excitation powers. At low excitation power (11 nJ) when the average number of excitons per QD is smaller than 1, there are a long-lived and a short-lived components. The long-lived component might be due to the effect of the long-lived 1S exciton bleach, although we do not understand the origin of the fast recovery component. The 1P exciton bleach recovery can be fitted with a single-exponential rise and a three-exponential decay using exponential functions. The fitting parameters are listed in Table 6I. The best fits reveal an instantaneous rise component (< 50 fs), which is consistent with the initial excitation of electrons to near the 1P level. Among the three decay components, two components are fixed at >> 1ns and 48.5 ps, in order to account for the effect of 1S bleach on the 1P bleach. The third decay components at high excitation powers (188-847 nJ) are then employed as the lifetime of n (>2) exciton states (τ_{3+X}), which has a time constant of 2.6-4.5 ps.

6.2.3.2. Quantifying the Number of Excitons per QD.

In order to determine the number of excitons per QD, we analyzed the 1S exciton bleach amplitude as a function of excitation power. We consider the amplitude at two time points. One is at time t=0, when no exciton decay has occurred. The other is at time t=1 ns (τ_{2X}<<1ns<< τ_{1X}), when the bi-exciton states have decayed to single exciton states and the single exciton decay is negligible. Figure 6.11a shows the bleach amplitudes at these two time points as a function of excitation powers. It is noted that the amplitude at 1ns (black filled circle) saturates at high excitation power, indicating that all QDs have been excited under high powers. As we mentioned in previous section, at 1 ns all of the excited QDs have decayed to single exciton states; therefore the average number of excitons per QDs at 1 ns at high power is 1. This argument suggests that we can scale the bleach amplitude at 1 ns under high powers to unity and the same scaling factor can be applied to the amplitudes at low powers, so that the normalized 1 ns bleach signal directly shows the average number of excitons per QD under different powers. The amplitude at 1 ps is also scaled by the same normalization factor. The normalized amplitudes (1ps and 1ns) as a function of excitation powers are shown in Figure 6.11b.

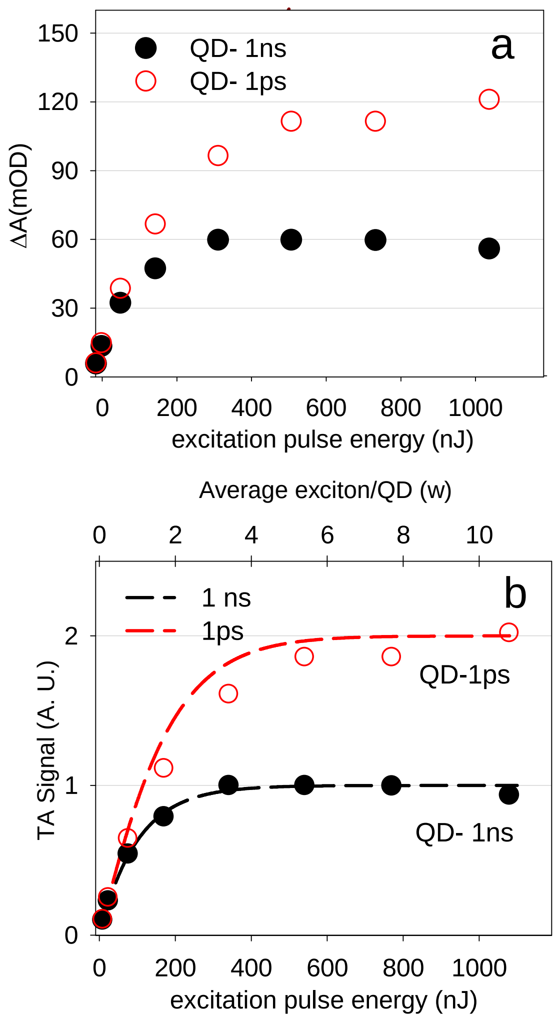

Figure 6.11. (a) Excitation power dependence of the exciton bleach amplitude at t = 1 ps (red open circles) and t = 1 ns (black solid circles) in CdSe(553nm) QDs. (b) Excitation power dependence of the normalized exciton bleach amplitude at t = 1 ps (red open circles) and t = 1 ns (black solid circles) in CdSe(553nm) QDs.

Using the model discussed earlier (section 6.2.3.1), we can fit the normalized exciton bleach signal for different powers at these two time points. The time of 1 ps is taken to represent time 0, when the excitons have not started to decay, and time T ($\tau_{2X} <<$ T<< τ_{1X}) is assumed to be 1 ns. According to equation 6.6 and 6.6, the normalized amplitudes of 1S exciton bleach signals at these two time points are given by:

$$\begin{aligned} \Delta S_{1s}(0) &= 2-(2+w)e^{-w} \\ \Delta S_{1s}(T) &= 1-e^{-w} \end{aligned} \qquad (6.8)$$

These two equations are used to fit the pump power dependent normalized bleach amplitudes at 1ps and 1 ns, respectively. Since w is linearly proportional to the pump power, then the proportionality constant is the only fitting parameters. The dashed lines shown in Figure 6.11b are the fits to the data. From these fits, we obtain an average number of excitons per QD for each excitation energy, which has been plotted as the top horizontal axis of Figure 6.11b. These equations also predict two limiting values. At w<<1, both S(0) and S(T) are equal to w, so the ratio is 1, and at w>>1, their ratio saturates at 2. These ratios are clearly seen in the data, indicating that this model works well for current system.

6.2.4. Multiexciton Dissociation in CdSe(553nm)-MB$^+$ Complex

6.2.4.1. Multiexciton Dissociation Dynamics in CdSe(553nm)-MB$^+$ Complex

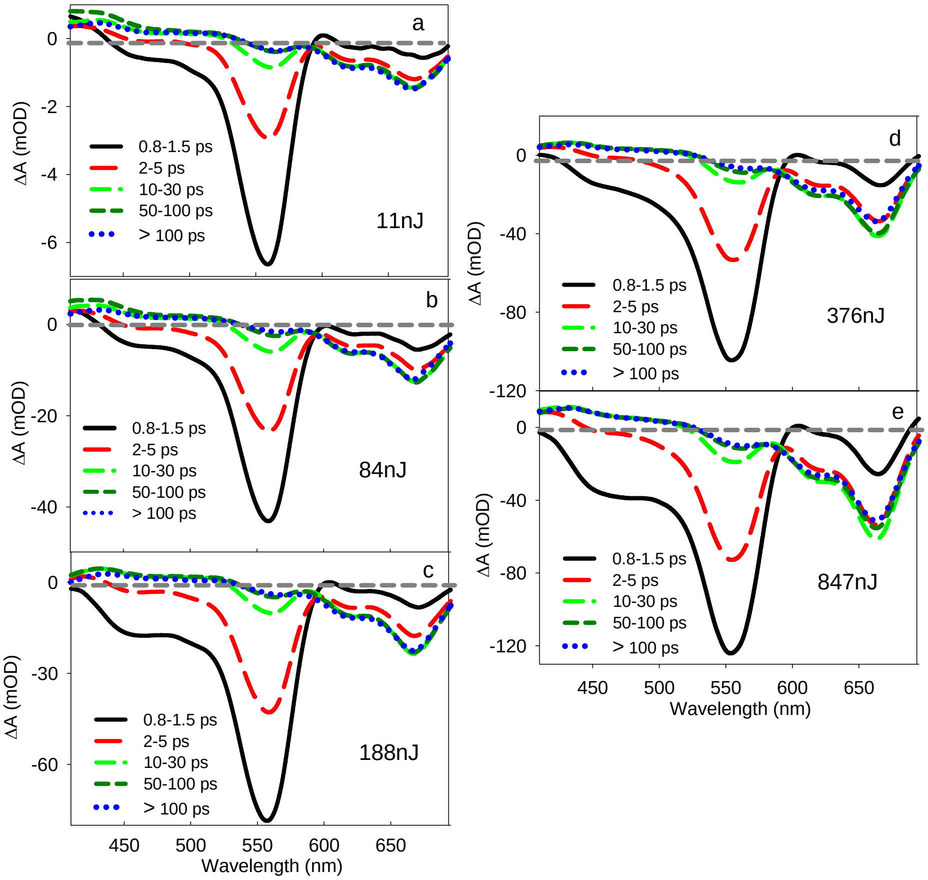

Figure 6.12. Comparison of transient visible absorption spectra of CdSe(553nm)-MB$^+$ complexes at indicated delay times after 400 nm excitation for various excitation energy (as indicated).

To determine how ET competes with exciton-exciton annihilation, we examined the same pump power dependence experiment for the CdSe(553nm)-MB$^+$ complex. Shown in Figure 6.12 the transient spectra of the CdSe(553nm)-MB$^+$ complex measured under different excitation powers. In addition to the power dependence features for 1S and 1P fast bleach recovery, there is a corresponding growth of the bleach of the MB$^+$

ground state as well as a MB$^+$ semiquinone anion absorption with the increase of excitation powers.

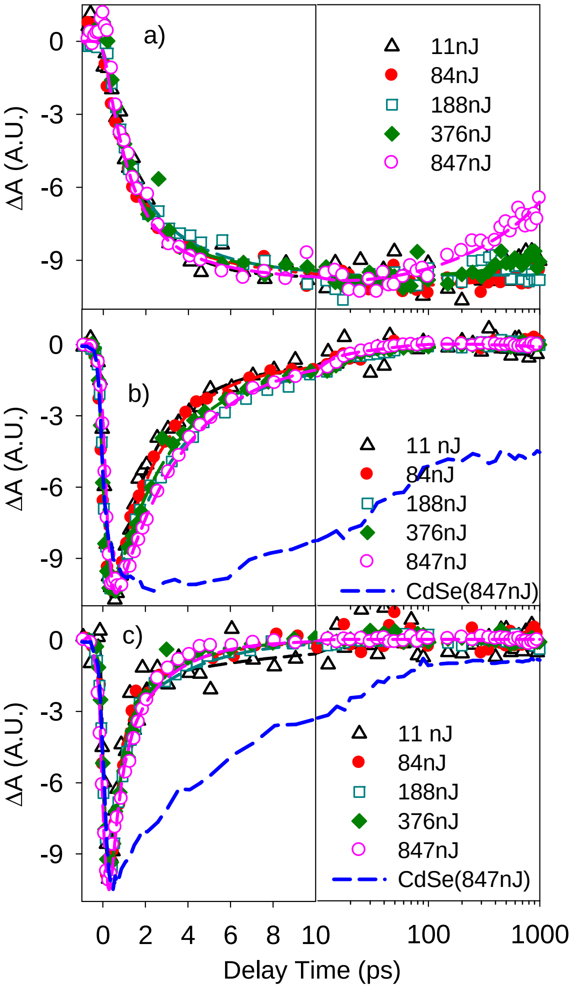

Figure 6.13 Comparison of the kinetics of (a) MB$^+$ bleach formation, b) 1S exciton bleach recovery and c) 1P exciton bleach recovery in CdSe(553nm)-MB$^+$ at indicated excitation energy. Also shown in b) and c) are the 1S and 1P exciton bleach recovery in CdSe only at the highest excitation energy (blue dashed line). All kinetic traces have been normalized to the same maximum amplitude. The left panel shows the data up to 10 ps in linear scale and the right panel displays the data from 10 ps to 1ns in logarithmic scale. Adapted from Ref. [46]

To examine the exciton dissociation rate, we analyzed the MB^+ ground state bleach kinetics, the 1S and 1P exciton bleach recovery kinetics under different excitation powers as shown in Figure 6.13a, b and c, respectively. All of these kinetic traces have been normalized to the same maximum amplitude. As shown in Figure 6.13a, MB^+ ground state bleach growth kinetics is not dependent on the excitation powers. These kinetics can be fit by using a bi-exponential rise function. The obtained fitting parameters are listed in Table 6II, from which we obtained the amplitude weighted average rise times at each excitation power (τ_{ave}, Table 6II). On the basis of τ_{ave}, the averaged rise time of the MB^+ bleach is 2.2 (±0.2) ps. Additionally, a recovery of MB^+ bleach was observed at high excitation power which can be fit with ~ 2 ns component, indicating the recombination of MB• with the holes in QD to reform the ground state of MB^+. In contrast, at low excitation power, the MB^+ bleach shows negligible recovery on the < 1ns time scale, suggesting that the recombination rate decreases with the decrease of excitation powers. This is consistent with the assumption that the recombination rate increases with the concentration of MB• and holes in the QD, suggesting the dissociation of multiple excitons under high excitation power.

Table 6II: Fitting Parameters for MB^+ Ground State Bleach Kinetics in CdSe-MB^{+b}

Power	τ_1, ps (A_1, %)	τ_2, ps (A_2, %)	τ_d (100%)	τ_{ave}, ps
11nJ	1.2 (84)	7.5 (16)	>> 1 ns	2.3
84nJ	1.2 (79)	7.5 (21)	>> 1 ns	2.5
188nJ	1.3 (78)	4.9 (22)	>> 1 ns	2.1
376nJ	1.2 (79)	5.1 (21)	>> 1 ns	2.0
847nJ	1.2 (74)	4.3 (26)	~ 2 ns	2.0
τ_{MB}				2.2 ± 0.2

[b] The traces (Figure 6.13a are fit with single-exponential decay and multi-exponential rise functions ($e^{-t/\tau_d} - \sum_i A_i e^{-t/\tau_i}$). τ_{ave} is the amplitude-weighted average rise time at each excitation powers. τ_{MB} is the average rise time for all excitation powers.

Additionally, we analyzed the 1S exciton bleach recovery kinetics at different excitation power, which are compared in Figure 6.13b. As shown in Figure 6.5 the 1S exciton absorption overlaps with MB^+ ground state absorption. To account for MB^+ ground state bleach signal in the contribution of 1S exciton bleach signal, we subtracted the MB^+ bleach signal from the bleach by scaling the MB^+ bleach signal at 664 nm such that the subtracted exciton bleach amplitude is zero at 1 ns. These kinetics traces can be fit by multi-exponential decay functions with their fitting parameters listed in Table 6III. First, let us compare the 1S exciton bleach recovery time and the MB^+ bleach formation time at different excitation powers. At low power(11 nJ), the 1S exciton bleach recovery time is the same as that of MB^+ bleach formation, while at higher powers, the exciton bleach recovery becomes slower than MB^+ formation. This comparison indicates that the single excitons in CdSe(553nm) QDs decay by electron transfer to MB^+. However, for the multiexciton states generated under high powers, it is possible that not all excitons are dissociated. Some of the excitons may decay by auger recombination with a time constant that is slower than the ET time.

Table 6III: Fitting Parameters for 1S Exciton Bleach Recovery Kinetics of CdSe-MB^{+c}

	Power	τ_1, ps (A_1,%)	τ_2, ps (A_2,%)	τ_{ave}, ps
1S	11nJ	1.2 (85)	9.7 (15)	2.5
	84nJ	1.6 (88)	15.4 (12)	3.2
	188nJ	2.8 (89)	20.3 (11)	4.7

	376nJ	2.2 (88)	18.3 (12)	4.1
	847nJ	2.9 (89)	19.1 (11)	4.7

[c] The traces in Figure 6.13b are fits to a function of single-exponential rise and multi-exponential decay ($\sum_i A_i e^{-t/\tau_i} - e^{-t/\tau_r}$). τ_{ave} is the amplitude-weighted average decay time.

To have an insight of how exciton dissociation from n (>2) exciton states competes with exciton-exciton annihilation, we analyzed the 1P exciton bleach recovery under different excitation powers, as shown in Figure 6.13c. These kinetic traces can be fit by using a multiple-exponential decay function. The obtained fitting parameters are shown in Table 6IV. On the basis of these parameters, we obtained an average time constant 1.2 ps, which is faster than both the 1S exciton bleach recovery and MB^+ bleach formation. This comparison indicates that the exciton dissociation rate in n (>2) exciton states is faster than that in the bi- and single exciton states. Furthermore, the 1S exciton bleach recovery appears to be faster than the biexciton lifetime, and 1P exciton bleach recovery is much faster than n (>2) exciton lifetime, suggesting that ET is a competitive pathway for the dissociation of bi- and multi-exciton states.

Table 6IV: Fitting Parameters for the 1P Exciton Bleach Recovery Kinetics of CdSe-MB^{+d}

	Power	τ_1, ps (A_1,%)	τ_2, ps (A_2,%)	τ_{ave}, ps
1S	11nJ	1.2 (85)	9.7 (15)	2.5
	84nJ	1.6 (88)	15.4 (12)	3.2
	188nJ	2.8 (89)	20.3 (11)	4.7
	376nJ	2.2 (88)	18.3 (12)	4.1
	847nJ	2.9 (89)	19.1 (11)	4.7
1P	11nJ	0.5 (85)	6.3 (15)	1.4
	84nJ	0.7 (78)	3.0 (22)	1.2

	188nJ	0.8 (77)	3.0 (23)	1.3
	376nJ	0.9 (75)	1.9 (25)	1.1
	847nJ	0.9 (75)	2.1 (25)	1.2

---

[d] The traces in Figure 6.13c are fits to a function of single-exponential rise and multi-exponential decay ($\sum_i A_i e^{-t/\tau_i} - e^{-t/\tau_r}$). τ_{ave} is the amplitude-weighted average decay time.

6.2.4.2. Quantifying the Number of Reduced MB$^+$

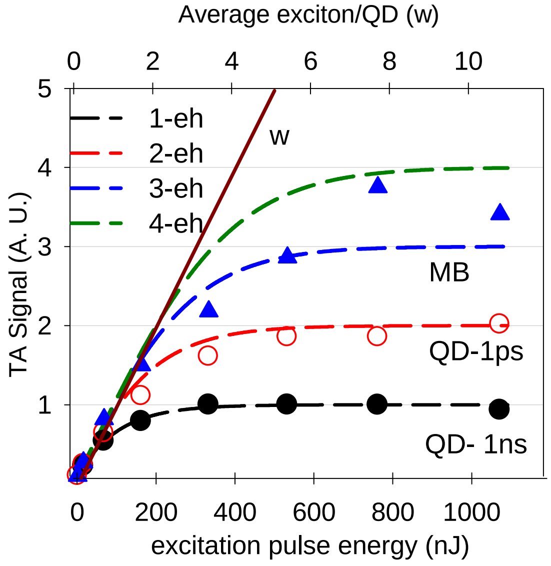

Figure 6.14. Excitation power dependence of the amplitudes of normalized MB$^+$ bleach in QD(553nm)-MB$^+$. The normalized exciton bleach at t = 1ps (red open circles) and t = 1ns (black solid circles) in CdSe(553nm) QDs as a function of excitation power are also shown here. Solid line is the average number of excitons per QD and dashed lines are fits according to equation 6.10. The curves for n_{max}=1 and 2 (equation 9) are the same as those for $\Delta S_{1S}(T)$ and $\Delta S_{1S}(0)$ (equation 6.8), respectively. MB$^+$ bleach signal is normalized such that it equals to the normalized QD 1S exciton bleach signal at the lowest excitation energy. Adapted from Ref. [46]

To determine the number of excitons dissociated, we analyzed the MB^+ bleach amplitude as a function of pump power. At low excitation power, for example at 11 nJ, we have shown that single excitons in CdSe QDs dissociate by ET to MB^+ with near unity efficiency. Under these conditions, each exciton reduces one MB^+, therefore the ratio of reduced MB^+ to exciton per QD is 1:1. On the basis of this result, we thus scaled the maximum MB^+ bleach signal to the normalized 1S exciton bleach at 1 ns in QDs under this low power (11 nJ). The same normalization factor is used to scale the MB^+ bleach signals at high powers. Since the normalized 1S exciton bleach signal at 1 ns in QDs represents the average number of excitons per QD (w), then the normalized MB^+ amplitude directly represents the average number of reduced MB^+ per QD. Figure 6.10 shows the normalized MB^+ bleach signal as a function of excitation power. If all excitons in QDs generated are dissociated by ET to MB^+, then the MB^+ bleach signal should be given by w. However, in this case, the MB^+ bleach signal agrees with w only when $w < 2$. After that, the MB^+ bleach signal becomes smaller than w, indicating that not all excitons are dissociated.

In order to determine the number of exciton dissociated, we modeled the excitation power dependence of the average number of reduced MB^+ shown in Figure 6.14. We assume that there is a maximum number of reduced adsorbates per QD (n_{max}). In a QD where the exciton number $n < n_{max}$, all excitons are dissociated, and each contributes to one reduced adsorbate, therefore, the number of reduced adsorbate is given by n; In contrast, in QD with $n > n_{max}$, the maximum number of reduced adsorbates is limited by n_{max} and hence the number of reduced adsorbates is given by n_{max}. With this assumption, the average number of reduced MB^+ as a function of excitation power can be given by:

$$N_{A^-} = \sum_{n=0}^{n_{\max}-1} P_n(w) \times n + \sum_{n=n_{\max}}^{\infty} P_n(w) \times n_{\max} \qquad (6.9)$$

Where N_{A^-} is the average number of reduced MB^+. The predicted N_{A^-} values as a function of the excitation energy for n_{max} from 1-4 are shown as the dashed lines in Figure 6.14. It has been shown that the predicted curves at n_{max} =1 or 2 follow closely to the normalized 1S bleach amplitude at 1ns and 1 ps, respectively, which is consistent with the above maximum number (n_{max}) assumption. Additionally, the curve for n_{max}=3 is in good agreement with the experimental data, indicating that up to 3 excitons have been dissociated by ET to MB^+. It was also noted that the average number of MB^+ per QD in CdSe(553nm)-MB^+ complex is ～3, which is same as the number of excitons dissociated in current system. This similarity may suggest that the number of excitons can be dissociated in QD-adsorbate system is limited by the number of adsorbate per QD, which implies that we may dissociate more excitons in current CdSe(553nm)-MB^+ complex by increasing the number of adsorbed MB^+ per QD. Ongoing experimental studies are investigating the effect of the number of adsorbed MB^+ per QD on the number of excitons dissociated.

6.3 Summary

We have investigated charge separation dynamics between CdSe QDs and methylene blue by transient visible absorption. The electron transfer process in CdSe-MB^+ complexes was identified by transient absorption study, in which both the accelerated bleach recovery and the formation of MB^+ radical anion were observed. It was shown that in CdSe(553nm)-MB^+ complex, single exciton in CdSe(553nm) QDs can dissociate by ultrafast electron transfer (ET) to MB^+ with an average time constant of ～ 2 ps and with unity efficiency when ～ 3 MB^+ were adsorbed to QDs. This implies the potential to separate multiexcitons before exciton-exciton annihilation process in this system.

Multi-exciton dissociation dynamics in CdSe(553nm) QDs adsorbed with methylene blue (MB^+) molecules were then investigated by transient visible absorption spectroscopy. Comparison of ET time in QD(553nm)-MB^+ complexes with the exciton decay dynamics in QDs shows that ultrafast ET process competes effectively with exciton-exciton annihilation. It was also noted that 1P exciton bleach recovery is faster than 1S exciton bleach recovey, suggesting that exciton dissociation in the n(>2)-exciton states is faster than those in single or bi-exciton states. Under current conditions, up to three excitons per QD have been dissociated by ultrafast ET to MB^+. The number of exciton dissociated appears similar to the average number of adsorbed MB^+ per QD, indicating that all of the MB^+ in current system has been reduced by ET.

References

(1) Nozik, A. J. *Physica E: Low-Dimensional Systems & Nanostructures (Amsterdam, Netherlands)* **2002**, *14*, 115.

(2) Shockley, W.; Queisser, H. J. *Journal of Applied Physics* **1961**, *32*, 510.

(3) Wolf, M.; Brendel, R.; Werner, J. H.; Queisser, H. J. *J. Appl. Phys.* **1998**, *83*, 4213.

(4) Kolodinski, S.; Werner, J. H.; Wittchen, T.; Queissera, H. J. *Appl. Phys. Lett.* **1993**, *63*, 2405.

(5) Schaller, R. D.; Klimov, V. I. *Phys. Rev. Lett.* **2004**, *92*, 186601.

(6) Ellingson, R. J.; Beard, M. C.; Johnson, J. C.; Yu, P.; Micic, O. I.; Nozik, A. J.; Shabaev, A.; Efros, A. L. *Nano Letters* **2005**, *5*, 865.

(7) Luther, J. M.; Beard, M. C.; Song, Q.; Law, M.; Ellingson, R. J.; Nozik, A. J. *Nano Letters* **2007**, *7*, 1779.

(8) Schaller, R. D.; Sykora, M.; Pietryga, J. M.; Klimov, V. I. *Nano Letters* **2006**, *6*, 424.

(9) Trinh, M. T.; Houtepen, A. J.; Schins, J. M.; Hanrath, T.; Piris, J.; Knulst, W.; Goossens, A. P. L. M.; Siebbeles, L. D. A. *Nano Letters* **2008**, *8*, 1713.

(10) Murphy, J. E.; Beard, M. C.; Norman, A. G.; Ahrenkiel, S. P.; Johnson, J. C.; Yu, P.; Micic, O. I.; Ellingson, R. J.; Nozik, A. J. *Journal of the American Chemical Society* **2006**, *128*, 3241.

(11) Gabor, N. M.; Zhong, Z.; Bosnick, K.; Park, J.; McEuen, P. L. *Science* **2009**, *325*, 1367.

(12) Beard, M. C.; Knutsen, K. P.; Yu, P.; Luther, J. M.; Song, Q.; Metzger, W. K.; Ellingson, R. J.; Nozik, A. J. *Nano Letters* **2007**, *7*, 2506.

(13) Sykora, M.; Mangolini, L.; Schaller, R. D.; Kortshagen, U.; Jurbergs, D.; Klimov, V. I. *Phys. Rev. Lett.* **2008**, *100*, 067401/1.

(14) Schaller, R. D.; Sykora, M.; Jeong, S.; Klimov, V. I. *Journal of Physical Chemistry B* **2006**, *110*, 25332.

(15) Schaller, R. D.; Petruska, M. A.; Klimov, V. I. *Applied Physics Letters* **2005**, *87*, 253102/1.

(16) Schaller, R. D.; Pietryga, J. M.; Klimov, V. I. *Nano Lett.* **2007**, *7*, 3469.

(17) Pijpers, J. J. H.; Hendry, E.; Milder, M. T. W.; Fanciulli, R.; Savolainen, J.; Herek, J. L.; Vanmaekelbergh, D.; Ruhman, S.; Mocatta, D.; Oron, D.; Aharoni, A.; Banin, U.; Bonn, M. *J. Phys. Chem. C.* **2007**, *111*, 4146.

(18) Nair, G.; Bawendi, M. G. *Phys Rev Lett* **2007**, *76*, 081304.

(19) Ben-Lulu, M.; Mocatta, D.; Bonn, M.; Banin, U.; Ruhman, S. *Nano Lett.* **2008**, *8*, 1207.

(20) Pijpers, J. J. H.; Ulbricht, R.; Tielrooij, K. J.; Osherov, A.; Golan, Y.; Delerue, C.; Allan, G.; Monn, M. *Nature Physics* **2009**, *5*, 811.

(21) Klimov, V. I. *Annual Review of Physical Chemistry* **2007**, *58*, 635.

(22) Nozik, A. J. *Annual Review of Physical Chemistry* **2001**, *52,* 193.

(23) Duonghong, D.; Ramsden, J.; Gratzel, M. *J. Am. Chem. Soc.* **1982**, *104*, 2977.

(24) Ramsden, J. J.; Gratzel, M. *Chem. Phys. Lett.* **1986**, *132*, 269.

(25) Rossetti, R.; Beck, S. M.; Brus, L. E. *J. Am. Chem. Soc.* **1984**, *106*, 980.

(26) Rossetti, R.; Brus, L. E. *J. Phys. Chem.* **1986**, *90*, 558.

(27) Kamat, P. V.; Dimitrijevic, N. M.; Fessenden, R. W. *Journal of Physical Chemistry* **1987**, *91*, 396.

(28) Henglein, A. *Pure & Appl. Chem.* **1984**, *56*, 1215.

(29) Hasselbarth, A.; Eychmuller, A.; Weller, H. *Chemical Physics Letters* **1993**, *203*, 271.

(30) Nosaka, Y.; Miyama, H.; Terauchi, M.; Kobayashi, T. *Journal of Physical Chemistry* **1988**, *92*, 255.

(31) Kamat, P. V. *Chem. Rev.* **1993**, *93*, 267.

(32) Landes, C. F.; Braun, M.; El-Sayed, M. A. *Journal of Physical Chemistry B* **2001**, *105*, 10554.

(33) Logunov, S.; Green, T.; Marguet, S.; El-Sayed, M. A. *J. Phys. Chem. A* **1998**, *102*, 5652.

(34) Burda, C.; Green, T. C.; Link, S.; El-Sayed, M. A. *J. Phys. Chem. B* **1999**, *103*, 1783.

(35) Sharma, S. N.; Pillai, Z. S.; Kamat, P. V. *Journal of Physical Chemistry B* **2003**, *107*, 10088.

(36) Sykora, M.; Petruska, M. A.; Alstrum-Acevedo, J.; Bezel, I.; Meyer, T. J.; Klimov, V. I. *Journal of the American Chemical Society* **2006**, *128*, 9984.

(37) Boulesbaa, A.; Issac, A.; Stockwell, D.; Huang, Z.; Huang, J.; Guo, J.; Lian, T. *J. Am. Chem, Soc.* **2007**, *129*, 15132.

(38) Huang, J.; Huang, Z.; Jin, S.; Lian, T. *J. Phys. Chem. C* **2008**, *112*, 19734.

(39) Huang, J.; Stockwell, D.; Huang, Z.; Mohler, D. L.; Lian, T. *J. Am. Chem. Soc.* **2008**, *130*, 5632.

(40) Matylitsky, V. V.; Dworak, L.; Breus, V. V.; Basche, T.; Wachtveitl, J. *J Am Chem Soc* **2009**, *131*, 2424.

(41) Quitevis, E. L.; Martorell, J.; Chang, Y.; Scott, T. W. *Chemical Physics Letters* **2000**, *319*, 138.

(42) Huang, J.; Huang, Z.; Yang, Y.; Lian, T. *J. Phys. Chem. C, in preparation* **2009**.

(43) Huang, J.; Huang, Z.; Jin, S.; Lian, T. *Journal of Physical Chemistry*, ACS ASAP.

(44) Narband, N.; Uppal, M.; Dunnill, C. W.; Hyett , G.; Wilson, M.; Parkin, I. P. *Phys. Chem. Chem. Phys.* **2009**, *11*, 10513.

(45) Yu, W. W.; Qu, L.; Guo, W.; Peng, X. *Chem. Mater.* **2003**, *15*, 2854.

(46) Huang, J.; Huang, Z. Q.; Yang, Y.; Zhu, H. M.; Lian, T. Q. *Journal of the American Chemical Society* **2010**, *132*, 4858.

(47) Olmsted, J., III. *Journal of Physical Chemistry* **1979**, *83*, 2581.

(48) Cooney, R. R.; Sewall, S. L.; Dias, E. A.; Sagar, D. M.; Anderson, K. E. H.; Kambhampati, P. *Phys. Rev. B* **2007**, *75*, 245311/1.

(49) Klimov, V. I.; Mikhailovsky, A. A.; McBranch, D. W.; Leatherdale, C. A.; Bawendi, M. G. *Phys. Rev. B* **2000**, *61*, R13349.

Chapter 7. Interfacial Electron Transfer from Organic Dyes to Semiconductor Nanocrystalline Thin Films

7.1. Introduction

Interfacial electron transfer (ET) dynamics between dye sensitizer and semiconductor nanoparticles has specific interest from both fundamental and applied viewpoints because of its role in improving the efficiency of dye sensitized solar cell (DSSC).[1-3] The ET dynamics in different combinations of sensitizer and semiconductors have been reported in the past decade. Among them, ET dynamics in $Ru(dcbpy)_2(NCS)_2$ [dcbpy=(4,4'-dicarboxy-2,2'-bipyridine)](RuN3) sensitized semiconductors has been the most extensively studied systems due to their high light-to-electric energy conversion efficiency in DSSC.[4-14] The highest efficiency in DSSCs was achieved in RuN3 sensitized TiO_2 nanocrystalline thin films. The solar to electric power conversion efficiencies of the cell based on RuN3 sensitized TiO_2 films was reported to be ～10% with an incident-photon-to-current conversion efficiency (IPCE) near unity at peak absorption wavelengths.[15,16] This high IPCE has been attributed to ultrafast electron injection from the RuN3 excited states to TiO_2,[5-12,17-25] and a much slower charge recombination from TiO_2 to the oxidized dye molecules and redox electrolytes.[13,14,26-32] On the contrary, the cells based on other semiconductors, such as SnO_2, ZnO, Nb_2O_5, WO_3, Ta_2O_5 and In_2O_3 et al. show lower efficiency,[4,33-40] the reasons for which remain unclear. In order to have an insight of how to improve the efficiencies of these cells, it is necessary to have a better understanding of the impact of the properties of semiconductor and sensitizers on ET dynamics.

The ET dynamics from RuN3 dyes to several different semiconductor films, such as TiO_2, SnO_2, ZnO and In_2O_3, has been investigated and compared by many groups.[4,6-14,19,41-45] It has been shown that ET dynamics in these films consists of a < 100 fs ultrafast component and one or more slower components on the picosecond or longer time scales.[43-45] However, injection dynamics to TiO_2 are dominated by ultrafast injection, while those to SnO_2, In_2O_3 and ZnO are dominated by slower components. In the comparison of the fast component which reflects the injection rates from ^{1}MLCT of RuN3 among these semiconductors, it was found that ET rate follows the order of $TiO_2 > SnO_2 \approx In_2O_3 >$ ZnO. This observation has been attributed to the difference of their electron accepting density of states.

On the other hand, one can also test the injection dependence on density of states by comparing the electron injection kinetics to the same semiconductor from adsorbates with varying excited state potentials. Electron injection from RuN3, Ru505, and Ru470 to TiO_2,[15] SnO_2,[46] In_2O_3,[43] and Nb_2O_5[16] have been reported and compared. It was found that the injection rates from these dyes to each above semiconductor follow the order of RuN3 > Ru505 > Ru470, decreasing with the lowering excited state oxidation potentials, which is consistent with the reduction of semiconductor accepting states. These comparisons of injection rates among different semiconductors as well as different sensitizers suggest the dependence of ET dynamics on the electron accepting state density in the semiconductor.

Unfortunately, the above comparisons involve distinct injection processes which result from unthermalized and thermalized excited states of Ru dyes. In the Ru dye sensitized semiconductor films, optical excitation promotes the electrons from their ground state to its ^{1}MLCT state, which is higher above the conduction band edge. The molecules in the unthermalized state can either inject electrons into semiconductors or undergo relaxation to triplet excited states within the tens of fs to ps time scale. The relaxed molecule will then inject electron into the semiconductor at a much slower rate.[11,12] In principle, the dependence of ET on the nature of semiconductors can be examined by either the fast injection rate from unthermalized states or the slow injection from relaxed states. However, the energetics of the triplet state in Ru dyes is usually near the conduction band edge of semiconductors. The injection rate from triplet state is hence sensitive to the density of trap/surface states, which is usually quite different from the bulk qualities of semiconductors. Therefore, it is necessary to use a sensitizer with a redox potential higher above the conduction band edge of the semiconductors as well as that its injection kinetics is not complicated by biphasic injection kinetics.

An alternative sensitizer to investigate the injection dependence on semiconductors and adsorbates is to use Rhodamine (Rh) dyes, such as Rhodamine B (RhB), Rhodamine 101 (Rh101), and Rhodamine 6G (Rh6G) with their molecular structures shown in Chapter 2. As organic chromophores, Rh dyes do not undergo significant relaxation to triplet states, removing the complexity of biphasic injection kinetics. Additionally, the higher excited state oxidation potentials of Rh dyes (RhB, -0.94 V; Rh101, -0.89 V; Rh 6G, -0.88 V vs SCE) compared to the conduction band edge of the semiconductors ensures that the density of accepting states of the semiconductors are less sensitive to trap/surface states.[47-49]

In this chapter, we report a comparison of the ET dynamics from RhB to In_2O_3, SnO_2 and ZnO nanocrystalline thin films. The process of interest can be represented in the following scheme:

$$RhB^* + nano \xrightarrow{k_{CS}} RhB^+ + nano^- \xrightarrow{k_{CR}} RhB + nano \qquad (6.1)$$

where RhB, RhB* and RhB^+ represent RhB molecules in the ground, excited, and oxidized states, respectively, and k_{CS} and k_{CR} are charge separation (injection) and recombination rates. The dynamics of the injected electron in the semiconductor were monitored by ultrafast IR spectroscopy, and the dynamics of dye in the ground, excited and cation states were probed by transient visible spectroscopy. Since RhB easily forms aggregates under high concentrations as reported previously by Alig and coworkers,[50] the dependence of the injection dynamics on dye coverage and excitation power density were examined first on each film, followed by the investigation of the dependence of the injection rates on the properties of these semiconductors.

Additionally, we also compared the electron injection kinetics from different Rh dyes to In_2O_3 and SnO_2 films by transient IR spectroscopy in order to test the effect of dye energetics on ET dynamics. We found the same trend of change in injection dynamics by lowering the dye excited state oxidation potential. Possible origins of the observed semiconductor dependence as well as sensitizer dependence were discussed.

7.2 Results

7.2.1 Effects of Semiconductors on the Injection Rate.

7.2.1.1 Non-ET Dynamics in RhB Sensitized ZrO_2 Films

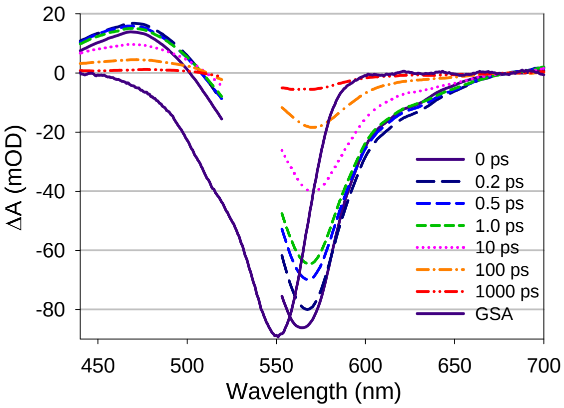

Figure 7.1. Transient visible absorption spectra of RhB/ZrO_2 at indicated delay times after excitation at 532 nm. Also plotted along the negative vertical axis is the ground state absorption (GSA) of RhB/ZrO_2 (thick solid line) recorded by a static UV-vis absorption spectrometer. The transient spectra consist of the bleach of ground state absorption at 550 nm, stimulated emission (560-670nm, red shifted from GSA), and absorption of RhB excited state at 470 nm. All features are formed instantaneously and decay with identical kinetics. Adapted from Ref. [51]

As discussed in the section 7.1, the dynamics of ET process can be measured by monitoring the spectral features of the injected electrons in the semiconductor nanoparticles as well as the sensitizer.[5,52] The former has strong IR absorption, which can be probed by using transient IR spectroscopy. The latter includes the signals from RhB molecules in the ground, excited and oxidized states, which can be distinguished by using transient visible spectroscopy. Comparison of injected electrons in the IR and the sensitizer kinetics in the visible allows unambiguous assignment of the injection and recombination processes.

The transient absorption spectra of RhB sensitized ZrO_2 nanocrystalline thin films were first examined in order to facilitate the assignment of these species. The band edge of ZrO_2 lies at ~-1.5 V (SCE) at pH 0,[3] more negative than that of the excited oxidation potential of RhB (-0.94V SCE).[53,54] Therefore, it acts as a substrate on which we can examine the noninjecting behavior of the adsorbate and thus the only spectral features associated with RhB ground and excited states should be present. It was shown that RhB/ZrO_2 sample exhibited negligible signal (data not shown) in transient IR absorption measurements, which is consistent with the lack of injected electrons in ZrO_2. Figure 7.1 shows the transient visible absorption spectra of RhB on ZrO_2 after 532 nm excitation. The transient spectra consist of two features: the bleach band at 500-600 nm and a new absorption band centered at ~470nm which are separated by an isosbestic point at 509 nm. These features form instantaneously and decay with the same kinetics. The broad bleach band can be attributed to the depletion of the ground state molecule and the stimulated emission of the excited molecules. The bleach of the ground state absorption band can be distinguished from the stimulated emission by comparing the bleach band with the static UV-vis absorption spectrum of RhB on ZrO_2, which is also plotted in Figure 7.1. It can be seen that in addition to the ground state bleach, there is also negative absorbance change red-shifted from the absorption peak. This feature can be assigned to the stimulated emission (SE) from the excited state. The absorption feature with a maximum at 470 nm is consistent with the absorption of RhB excited state and thus assigned to the RhB excited state.[55] These spectral features are similar to that of RhB in solution except for different peak positions and shortened lifetime. The lifetime of the excited state is multiexponential, with a short-lived component of ~100 ps, and a long-lived component on the order of a few nanoseconds. The short lived component is attributed to quenching between RhB molecules, and their effect on injection kinetics should be carefully examined. The long lived component matches well with the emission lifetime of free RhB molecules in solution.

7.2.1.2. ET Dynamics in RhB Sensitized In_2O_3 Films

7.2.1.2.1. Coverage Dependence Measured by Transient IR Spectroscopy.

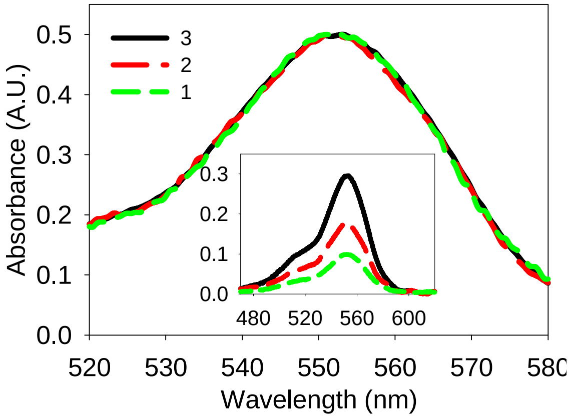

Figure 7.2. UV-visible spectra of RhB/In_2O_3 films at three different coverage levels, 1 (0.1 OD), 2 (0.18 OD), and 3 (0.3 OD). All spectra were normalized to the same peak height for better comparison of peak shift. The original spectra are shown in the inset.

It is well known that organic dyes with large π ring systems can form aggregates readily at high dye coverage.[50,56,57] In order to examine the effect of aggregates on ET dynamics, we first examined the dependence of ET dynamics to In_2O_3 films on RhB coverage levels. Figure 7.2 shows the normalized UV-vis spectra of RhB on In_2O_3 films with absorbance at 553 nm of 0.1, 0.18, and 0.3 OD, (named as sample 1, 2, and 3) respectively. The UV-vis spectra before normalization are shown in the inset of Figure

7.2 and the absorption of unsensitized In_2O_3 film has been subtracted from these samples. For these different coverage levels, the band width and peak shift are almost the same, which indicates that between the absorbance ranges of 0.1 OD to 0.3 OD, the aggregation effect of RhB on In_2O_3 films is negligible.

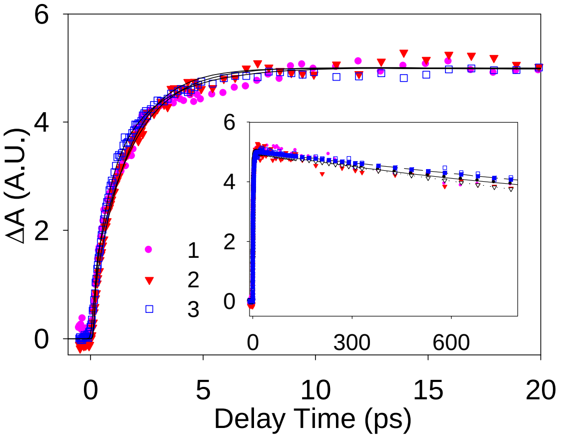

Figure 7.3. IR transient absorption kinetic traces of RhB/In_2O_3 films 1-3 after 532 nm excitation. The inset shows the data extended to longer time scale. The signal sizes, which have been scaled by the number of absorbed excitation photons, reflect relative injection yields.

As shown in scheme (7.1), the injection dynamics can be followed by directly probing injected electrons in the semiconductor. The kinetic traces of RhB on In_2O_3 films 1-3 are shown in figure 7.3. The data extended to the longer time delay scale is shown in the inset. These kinetics traces were recoded at probe wavelength ~5000 nm, where the adsorbate has negligible absorption. Therefore, the signal can be attributed to injected electrons in the nanoparticles.[5,52] All of these traces have been normalized to correspond to the same number of absorbed photons for better comparison of injection yield. The kinetic traces of RhB/In_2O_3 films at three different coverage are virtually identical, confirming negligible effect of aggregate formation on ET dynamics at the examined coverage level (<0.3 OD).

7.2.1.2.2. Excitation Power Dependence Measured by Transient IR Spectroscopy.

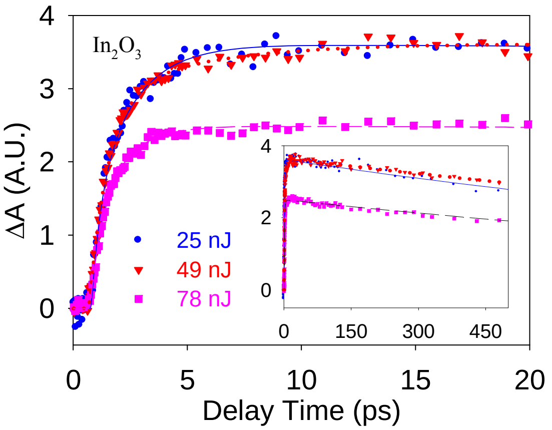

Figure 7.4. Transient IR kinetic traces of RhB/In_2O_3 film measured at excitation energy densities of 51, 100 and 159 μJ/cm^2 (shown as 25, 49, 78 nJ respectively). The signal sizes have been scaled by the corresponding pump powers to reflect the relative injection yield. The inset shows the data at longer time scale.

We have shown that excited molecules can be quenched by each other when the adsorbed dye molecules on the nanoparticle surface are adjacent, as shown in Figure 7.1. The quenching rate of this process increases with the increasing number of excited molecules, which is dependent on the photon flux of the excitation pulse. As a result, the electron transfer kinetics may be affected by the excitation density even in samples with no noticeable aggregate formation, as shown for RuN3 sensitized SnO_2.[45] To examine the effect of excitation density on injection dynamics, the ET dynamics of RhB on In_2O_3 film with the lowest loading level of RhB were examined by using three different 532 nm excitation densities, 51, 100 and 159 μJ/cm^2 (or pulse energy of 25, 49, 78 nJ/pulse respectively). Figure 7.4 showed the comparison of IR absorption signals of injected electrons (at ~5 μm) under these three different excitation powers. These kinetics traces have been normalized by the corresponding pump powers so that the signal sizes reflect the relative injection yields under these conditions. The injection yield at the highest pump power (78 nJ) is significantly lower than those at lower pump powers. Since at this coverage level there is negligible aggregate formation, the reduced injection yield at high excitation density can be attributed to quenching between excited molecules. The kinetics and injection yields at the two lower pump powers are nearly identical, suggesting that at these excitation powers and adsorbate coverage level, the injection kinetics are not influenced by quenching between dye molecules. The origin of this pump power dependence will be discussed later.

7.2.1.2.3. Transient Visible Spectra of RhB/In_2O_3.

Transient visible spectroscopy is also used to examine interfacial ET dynamics by monitoring spectral signatures of RhB. Figure 7.5a and 5b show the transient visible spectra of RhB/In_2O_3 (sample OD=0.3 at 553 nm) measured under the excitation pulse of 25 nJ/pulse at 532 nm. As shown in Figure 7.5a, at the early time (~0.2 ps), the transient spectrum consists of a ground state bleach, stimulated emission and excited state absorption (~460 nm), which is similar to that of RhB on ZrO_2. Within the first few picoseconds (<5ps), a new species forms at 490 nm and the excited state (the stimulated emission at 550-650 nm and absorption at 460nm) decays. The former can be assigned to the formation of cation radical of RhB.[54] These result indicates the excited state of RhB is quenched to form RhB cation through ET to In_2O_3. Additionally, at later time, for example, after 10 ps (Figure 7.5b), the spectra consist of only two species: ground state bleach and cation absorption band at 490nm, which are separated by an isosbestic point at 513 nm. The former bleach feature is consistent with the ground state absorption of RhB, indicating negligible contribution of stimulated emission of excited molecules. These results indicate that electron injection is complete by 10 ps. Furthermore, at later time, the cation absorption decays, which correlates with the recovery of the ground state bleach, isuggesting the recombination process of RhB cation with an electron to reform RhB ground state.

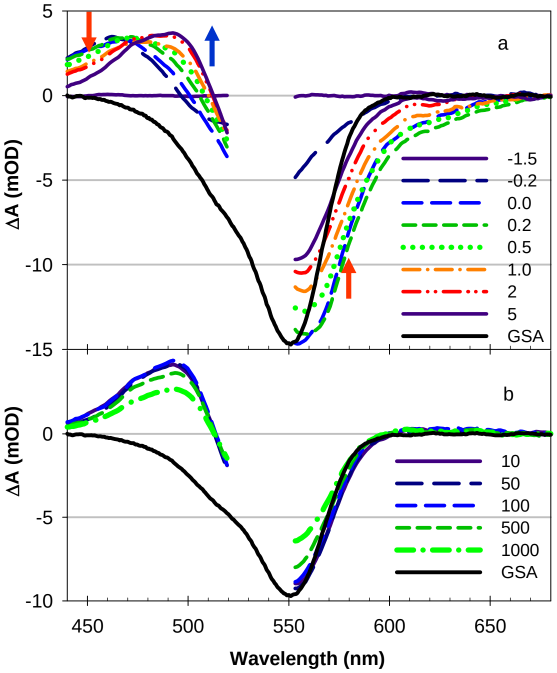

Figure 7.5. Transient visible absorption spectra of RhB/In_2O_3 at delay times (a) -1.5 to 5 ps and (b) 10 ps to 1 ns after 532 nm excitation. The static absorption spectrum of RhB ground state (GSA, black solid curve) has been inverted and scaled for better comparison with the bleach. The legends indicate delay time in units of picoseconds. In early time delays (figure a), the spectra show the decay of excited state absorption at ~460 nm and

stimulated emission at 600-650 nm (the red arrows) and the corresponding growth of the oxidized RhB at ~490 nm (the blue arrow), indicating the formation of RhB cation by electron transfer from the excited RhB to In_2O_3. After 10 ps (figure b), the spectra show the decay of oxidized RhB and the corresponding recovery of ground state bleach, which can be attributed to the recombination of oxidized RhB with injected electrons to regenerate RhB molecules in the ground state. Adapted from Ref. [51]

7.2.1.2.4. Comparison of Visible and IR Spectral Signatures.

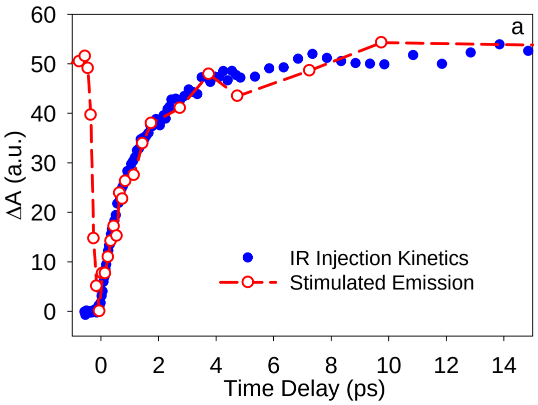

Figure 7.6. Comparison of the growth of the IR absorption of injected electrons (filled circles) and decay of the stimulated emission (SE, open circles) of excited RhB molecules in RhB/In_2O_3. The SE signal has been displaced vertically and normalized for better comparison. The good agreement confirms the process of electron injection from RhB excited state to In_2O_3.

Figure 7.6 compares the kinetics of stimulated emission and injected electron formation (IR absorption). The stimulated emission kinetics were obtained by averaging the transient signal at 600-650 nm, which, as shown in Figure 7.4, contains only the contribution of stimulated emission of excited molecules. The kinetics traces were identical at these wavelengths and were averaged to improve the signal-to-noise ratio. The IR kinetics of injected electrons were obtained by averaging multiple measurements obtained with low dye coverage and excitation power density (~0.1 OD at 553nm and <49 nJ). For better comparison, the stimulated emission signal has been displaced vertically and scaled such that its decay can be compared with the formation of IR signal. Clearly, the excited state (stimulated emission) decay agrees with the formation of IR absorption signal of injected electrons. This agreement suggests that the excited RhB molecules deplete due to electron transfer to In_2O_3, forming injected electrons in the semiconductor and RhB cations. Since there is negligible effect of aggregate formation and quenching between the excited RhBs, the measured injection rate reflects the ET process of isolated RhB on In_2O_3 and can be used for comparison with the injection rate from RhB to other semiconductors under similar conditions. Similar comparison of IR signal with the decay of excited state absorption (at 460 nm) and formation of cation absorption (at 490 nm) has not been carried out because the latter two bands have considerable spectral overlap with each other and the ground state bleach.

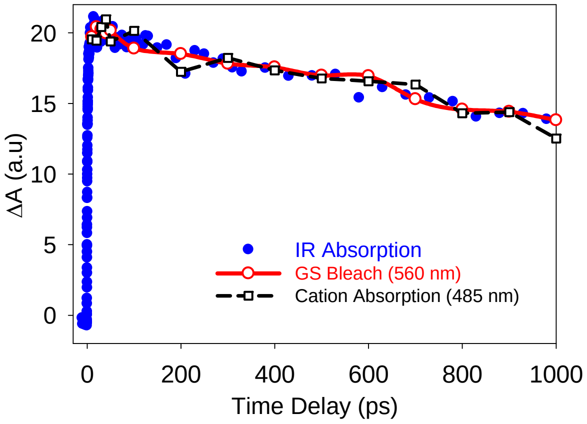

Figure 7.7. Comparison of the recovery of RhB ground state bleach (red open circles) with the decay of cation absorption (black squares) and the IR absorption of injected electrons (blue filled circles). The ground state bleach signal has been inverted for better comparison. These species show identical kinetics, which demonstrates that the injected electrons and RhB cations recombine to reform the RhB molecules in the ground state.

Figure 7.7 compares the RhB cation absorption decay, the ground state bleach recovery (inverted), and IR absorption decay kinetics of injected electrons. Clearly, all three spectral signatures are identical, confirming that the cation and injected electrons recombine to regenerate RhB molecules in the ground state. The good agreement also suggests that the IR absorption is a sufficient probe of injected electron population in the semiconductor.

7.2.1.3. ET Dynamics in RhB Sensitized SnO_2 Films

7.2.1.3.1. Coverage Dependence Measured by Transient IR Spectroscopy.

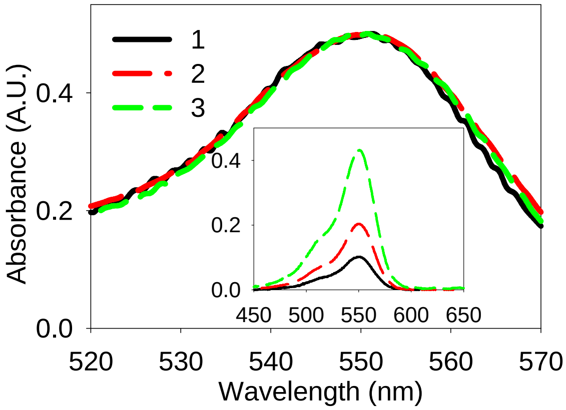

Figure 7.8. UV-vis spectra of RhB/SnO_2 films at three different coverage levels (OD = 0.1, 0.2 and 0.43 at 551 nm for samples 1, 2, 3, respectively). All spectra were

normalized to the same peak height for better comparison. The inset shows their original spectra.

Figure 7.8 shows the UV-vis spectra of RhB on SnO_2 films with different coverage levels. The peak absorbances of RhB were 0.1, 0.2 and 0.43 OD at 551 nm for samples 1, 2 and 3 respectively. Negligible peak shift was observed among these samples, indicating little to no aggregation of RhB molecules. Figure 7.9 compares the transient IR kinetics in these samples after 532 nm excitation (~100 μJ/cm^2). The kinetics traces were measured with probe wavelength at ~5000 nm and their amplitudes have been scaled by the number of absorbed photons so that the signal sizes reflect relative injection yield. At low adsorbate coverage (sample 1 and 2), the injection kinetics and signal amplitudes are independent of the coverage. However, the signal amplitude at high coverage (sample 3 in Figure 7.9) is ~20% lower than those at lower coverage, indicating a lower injection yield at higher dye coverage. Because of the lack of absorption peak shift that typically accompanies dye aggregation on the substrate surface, the lower injection yield is attributed to quenching among excited RhB molecules.

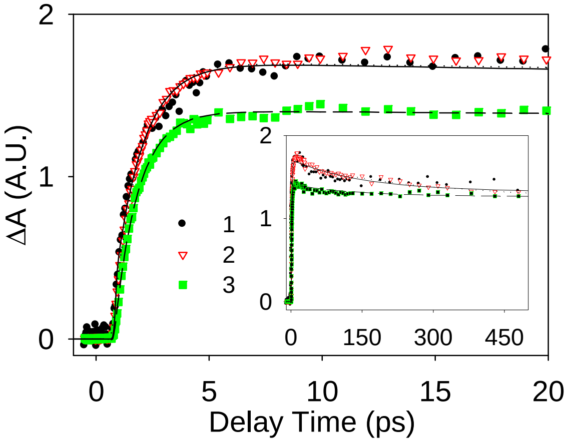

Figure 7.9. Transient IR absorption kinetic traces of RhB/SnO_2 films 1-3. The inset shows the data at longer time scale. The signal sizes have been normalized to correspond to the same number of absorbed excitation photons.

7.2.1.3.2. Excitation Power Dependence Measured by Transient IR Spectroscopy.

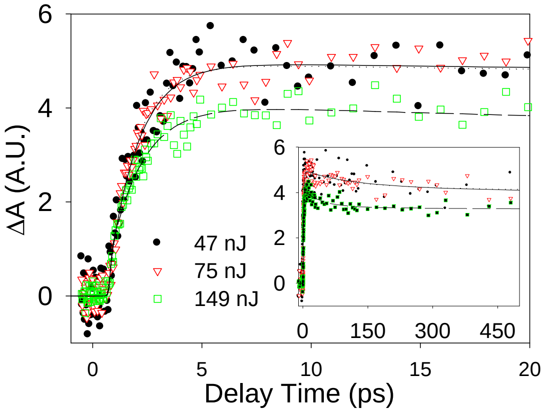

Figure 7.10. Kinetic traces of RhB/SnO_2 films measured at excitation energy density of 96, 153 and 304 μJ/cm^2 (shown as 47, 75 and 149 nJ, respectively). The signal sizes have been scaled by the corresponding pump power. The inset shows the same transient data up to 500 ps.

The pump power dependence of the ET kinetics for RhB/SnO_2 film (0.12 OD at 551 nm) is shown in Figure 7.10. The kinetics and injection yields for the lowest two pump intensities (47 and 75 nJ per pulse) were almost identical, but the injection yield at the highest pump power (149 nJ per pulse) is ~25% lower. The reduced injection yield at high pump power is attributed to quenching between excited molecules. The result also indicates that at low pump power (< 75 nJ or 153 μJ/cm^2), the electron injection kinetics are not affected by excited state quenching processes.

7.2.1.3.3. Transient Visible Spectra of RhB/SnO_2

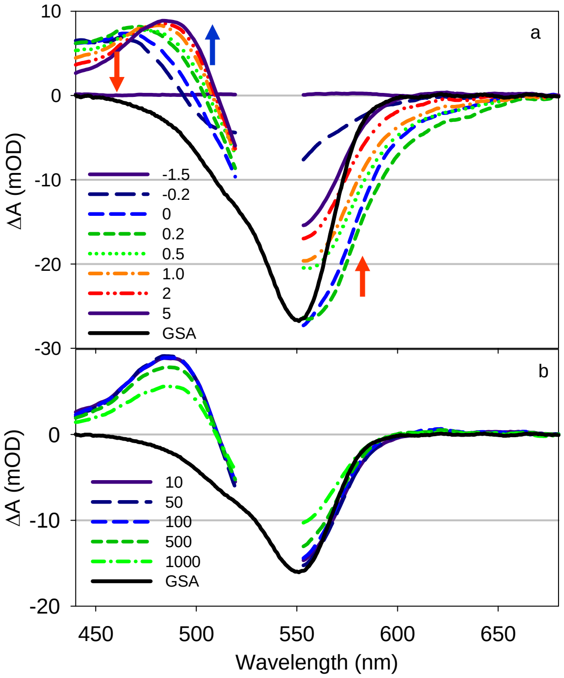

Figure 7.11. Transient visible absorption spectra of RhB/SnO_2 at indicated delay times (a) -1.5 to 5 ps and (b) 10 ps to 1 ns after 532 nm excitation. The static absorption spectrum of RhB ground state (GSA, black solid curve) has been inverted and scaled for better comparison with the bleach. At early time delay (figure a), the spectra show the decay of excited state absorption at ~460 nm and stimulated emission at 600-650 nm (the red arrows) and the corresponding growth of the oxidized RhB at ~490 nm (the blue arrow). After 10 ps (figure b), the spectra show the decay of oxidized RhB and the corresponding recovery of ground state bleach.

Transient visible spectra of RhB/SnO_2 (sample OD~0.2 at 551 nm and excitation pulse of 25 nJ/pulse at 532 nm) are shown in Figure 7.11. These spectra exhibit nearly identical features as RhB/In_2O_3 (Figure 7.5 a & b). In the first few picoseconds, the spectra evolution shows the decay of the excited RhB (absorption at ~460 nm and stimulated emission at 570-650 nm) and the formation of the cation (~490 nm), indicating electron transfer from the RhB excited state to SnO_2. The ET process is completed by 5 ps, after which there is no change in peak positions, as shown by the isosbestic point (at 510 nm) present in Figure 7.11b. In the 10 ps to 1 ns delay time window, the amplitudes of the cation absorption and ground state bleach decrease due to the recombination of cation with injected electrons to reform RhB molecules in the ground state.

7.2.1.3.4. Comparison of IR and Visible Spectral Signatures

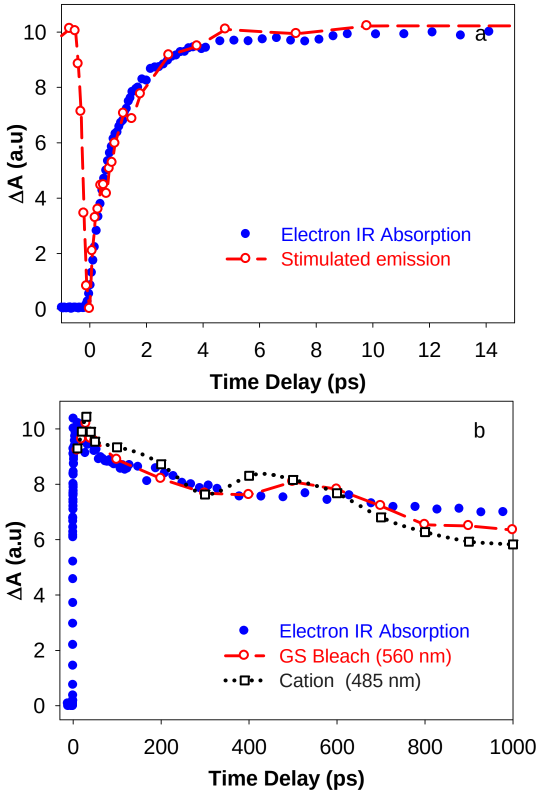

Figure 7.12. (a) Comparison of the formation kinetics of the IR absorption of injected electron in SnO_2 (filled circles) with decay kinetics of the stimulated emission of RhB excited state in 600-650 nm region (open circles) in RhB/SnO_2. The SE signal has been displaced vertically for better comparison. (b) Comparison of the decay of RhB ground

state bleach (inverted, open circles), RhB cation absorption (squares) and the injected electron IR absorption (filled circles) observed at later time delays.

A direct comparison of the visible RhB SE decay kinetics with IR absorption (injected electron in SnO_2) is presented in Figure 7.12a. The SE kinetics were obtained by averaging the transient signals in the stimulated emission region (600-650 nm) shown in Figure 7.11. The IR kinetics of injected electrons were obtained by averaging multiple measurements obtained with low dye coverage and excitation power density (<0.2 OD and 49 nJ). The excited state (stimulated emission) decay follows the same kinetics as the growth of the injected electrons (IR absorption). This agreement suggests that under these experimental conditions, all excited RhB molecules undergo electron transfer to SnO_2 and there are no other quenching pathways.

The decay of the injected electrons (IR absorption), RhB cation (absorbance change at 485 nm) and recovery of the ground state bleach are compared in figure 7.12b for delay times from 10 ps to 1 ns. It is evident that all signals decrease with the same kinetics, suggesting that the decay is due to the recombination of electrons in SnO_2 with RhB cations to reform the ground state RhB molecules. The good agreement of visible and IR signatures also suggests that, similar to those on In_2O_3, the transient IR signal amplitude in RhB/SnO_2 reflects the concentration of injected electrons and that there is negligible decrease of electron absorption cross section due to relaxation processes within the semiconductor nanoparticles.

7.2.1.4. ET Dynamics in RhB Sensitized ZnO Films

7.2.1.4.1. Coverage Dependence Measured by Transient IR Spectroscopy.

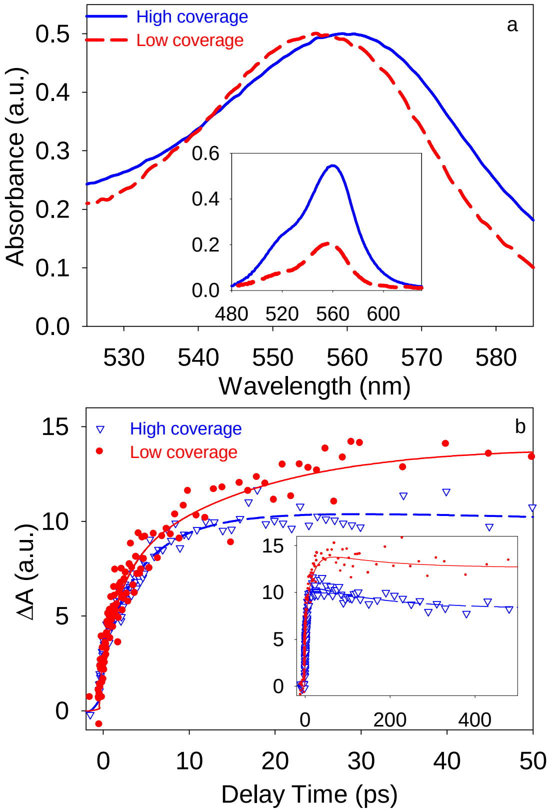

Figure 7.13. (a) UV-vis spectra of RhB/ZnO films at two different coverage levels: low coverage (0.2 OD) and high coverage (0.58 OD). The spectra were normalized to the same peak height for better comparison. The inset shows the original spectra. (b) Transient IR absorption kinetic traces of RhB/ZnO films at low and high coverage. The inset extends the data to 500 ps. The signal sizes have been scaled to correspond to the same number of absorbed excitation photons.

The normalized absorption spectra for RhB/ZnO with low (0.2 OD at 556 nm) and high (0.58 OD at 561nm) coverage are shown in Figure 7.13a. A peak shift of 5 nm to the red occurs in the sample at higher dye adsorption. It is believed that this shift is a result of J-aggregate formation on the surface of ZnO.[58-60]

The transient kinetics traces for these samples are compared in Figure 7.13b. These kinetics traces were measured with excitation at 532 nm (~110 nJ/pulse) and probed at 5000 nm. Their signal sizes have been scaled by the number of absorbed photons and their amplitudes reflect the relative injection yield. The sample with higher coverage shows smaller signal amplitude at ~1ns. The growth kinetics in these samples appear to be similar within the first 7 ps, but a slower rise component observed in the low coverage sample is absent in the higher coverage sample. We attribute this to the intermolecular quenching of excited dye molecules, which reduce the lifetime of RhB excited state. This process suppresses electron injection components that are slower than the intermolecular excited state quenching and has negligible effect on molecules that undergo faster injection. Due to signal-to-noise considerations, we were unable to study samples with lower coverage utilizing our transient IR probe.

7.2.1.4.2. Excitation Power Dependence Measured by Transient IR Spectroscopy.

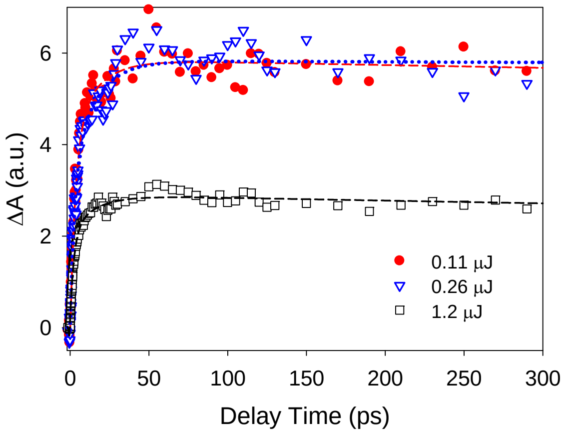

Figure 7.14. Transient IR kinetic traces of RhB/ZnO films measured at excitation energy densities of 225, 531 and 2450 μJ/cm^2 (shown as 0.11, 0.26 and 1.2 μJ, respectively). The signal sizes have been scaled by the pump power to reflect the relative injection yield.

Shown in Figure 7.14 is a comparison of transient IR injection kinetics of RhB/ZnO (with peak absorbance of 0.2) under excitation densities of 225, 531 and 2450 μJ/cm^2 (0.11, 0.26 and 1.2 μJ, respectively) at 532 nm. These traces have been normalized by the excitation power to reflect relative injection yields. At the two lowest pump powers, the scaled signal amplitudes of injected electrons are the same and injection kinetics are nearly identical, suggesting a negligible effect from quenching of excited molecules at this excitation density and coverage level. The kinetics trace of RhB/ZnO at high pump power is noticeably different, where injection yield is ~50% lower due to intermolecular quenching processes. Significantly higher pump power is used for the ZnO films because the IR absorption cross-section of injected electrons in this material is much lower than those in SnO_2 and In_2O_3. The pump powers at which the intermolecular quenching process is negligible are different in ZnO, SnO_2 and In_2O_3 films. This variation is most likely due to the different effective surface areas in these nanocrystalline thin films.

7.2.1.4.3. Transient Visible Spectra of RhB/ZnO

The transient visible absorption spectra of RhB/ZnO (0.2 OD at 556 nm and excitation pump power of 25 nJ at 532 nm) are shown in Figure 7.15. At early delay time (~200 fs), the spectrum consists of a bleach of RhB ground state (peak 556 nm), and the absorption (460 nm) and stimulated emission (570- 650 nm) of the excited RhB. With the increase of delay time, the excited state features (absorption at 460 nm and stimulated emission from 600-650 nm) decay to form the cation absorption at 490 nm. After 50 ps (see Figure 7.15b), the spectra consist only of a bleach of RhB ground state and the absorption of RhB cation. There is no remaining stimulated emission of the excited molecules, as indicated by the correlation of the bleach spectrum with the ground state absorption of RhB. Furthermore, a clear isosbestic point between the ground state bleach and cation absorption is formed at 513 nm. These results suggest that the excited state decay and the cation formation are completed by 50 ps. From 50 ps to 1 ns, there is negligible change of the amplitudes of cation absorption and the ground state bleach, suggesting the lack of recombination of RhB cation with injected electrons in the <1 ns time scale.

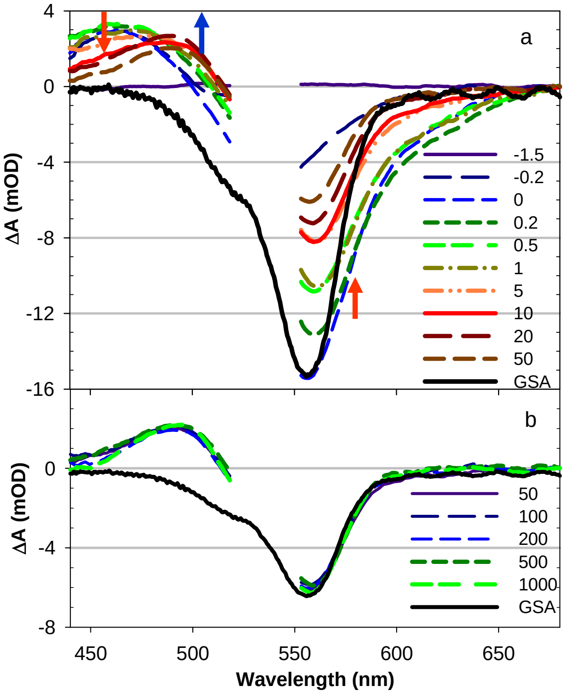

Figure 7.15. Transient visible absorption spectra of RhB/ZnO at indicated delay times (in units of ps) after 532 nm excitation, (a) -1.5 to 50 ps, and (b) 50 ps to 1 ns. The static absorption spectrum of RhB ground state (GSA, black solid curve) has been inverted and scaled for better comparison with the bleach. In early time delay (figure a), the spectra show the decay of excited state absorption at ~450 nm and stimulated emission from 600-

650 nm (the red arrows) and the corresponding growth of the oxidized RhB at ~490 nm (the blue arrow). After 50 ps (figure b), the spectra consist of cation absorption and ground state bleach, both of which show negligible decay up to 1 ns.

7.2.1.4.4. Comparison of IR and visible spectral signatures

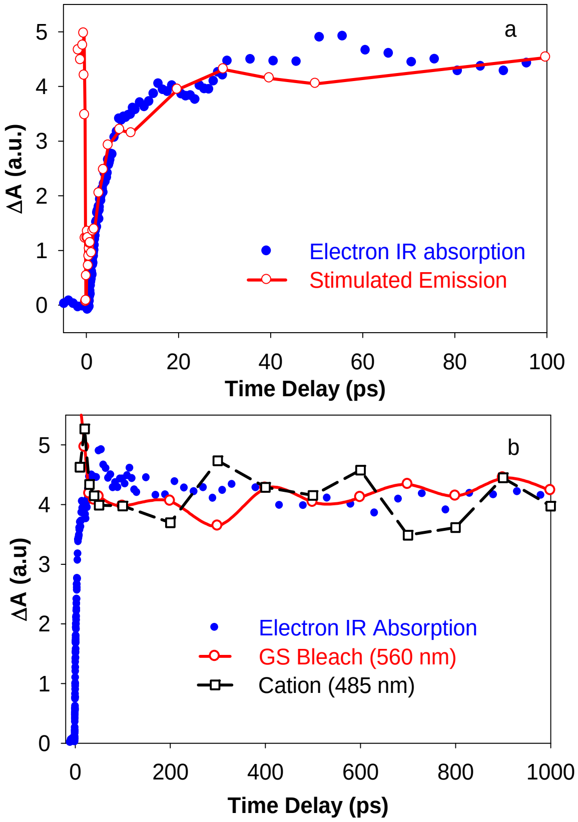

Figure 7.16. (a) Comparison of the IR absorption of injected electrons (filled circles) and the decay of stimulated emission of RhB at 600-650 nm (open circles) in RhB/ZnO. The good agreement suggests that excited RhB depletes through electron transfer to ZnO, and other decay pathways are negligible. (b) Comparison of the RhB ground state bleach (open circles) and RhB cation absorption (squares) with the IR absorption (filled circles) of injected electrons at later time delays. The bleach signal has been inverted and scaled for better comparison.

The decay kinetics of RhB stimulated emission and the IR absorption kinetics of the injected electrons in RhB/ZnO samples are compared in Figure 7.16a. The stimulated emission kinetics were obtained by averaging the transient signals at 600-650 nm. The IR kinetics of injected electrons were obtained by averaging multiple measurements with low dye coverage and excitation power density (~0.2 OD and <260 nJ). Within the signal-to-noise ratio of the measurements, these kinetics traces are identical, suggesting that the excited RhB depletes through electron transfer to ZnO. The agreement also indicates that under these conditions, there is negligible effect of intermolecular quenching of excited RhB molecules, consistent with the pump power dependence study shown in Figure 7.14. The decays of injected electron IR absorption, RhB cation absorption, and the recovery of the RhB ground state bleach in the 50 ps-1 ns time window are compared in Figure 7.16b. These traces agree with each other within the experimental error of the measurements and show negligible electron recombination on the < 1ns time scale.

7.2.1.5. Comparison of Electron Injection dynamics from RhB to In_2O_3, SnO_2 and ZnO Films

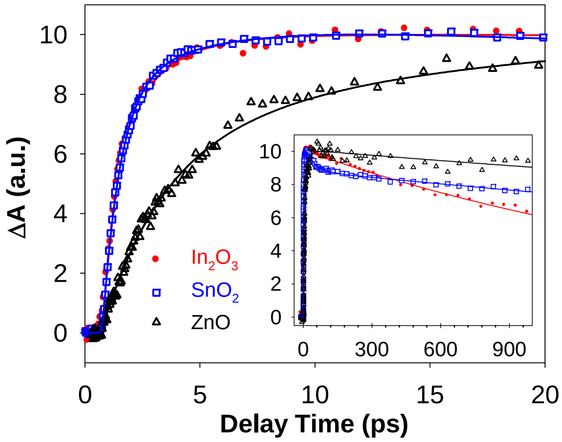

Figure 7.17. IR absorption kinetic traces of RhB on In_2O_3, SnO_2 and ZnO films averaged over multiple trials. All kinetic traces have been normalized at the maximum amplitudes for better comparison. The inset shows the data up to 1ns.

On the basis of the discussion of the previous sections, ET dynamics measured under low dye coverage and low excitation power are not influenced by intermolecular quenching processes and electron transfer is the dominating excited state quenching pathway. Therefore, the ET kinetics obtained under these conditions are used to examine the effect of semiconductor nature on electron injection rate. Figure 7.17 shows the comparison of the transient IR absorption kinetic traces of RhB dyes on In_2O_3, SnO_2 and ZnO films. These traces are obtained after averaging multiple measurements obtained with low dye coverage and excitation power density and have been normalized to the same maximum amplitude for better comparison. Clearly, the injection rates from RhB to In_2O_3 and SnO_2 are similar, but to ZnO is much slower.

The exponential function is used to fit these kinetic traces in order to quantify the injection rates. The kinetics traces of RhB/SnO_2 and RhB/In_2O_3 can be fit by a single exponential rise, and RhB/ZnO can be fit with two exponential rises. The best fits to these traces are also shown in Figure 7.17 and the fitting parameters are listed in Table 7I. From the fitting parameters, the amplitude weighted average time constants τ_{ave} are obtained for each semiconductor, which are listed in Table 7I as well. The electron injection times for RhB to In_2O_3 and SnO_2 films are 1.20±0.03 and 1.19±0.04, respectively, which are much shorter than that of ZnO (7.0 ±0.8 ps). The error bars indicate standard deviation of multiple measurements. As discussed earlier, the decay of the IR signal can be attributed to the recombination of injected electron with RhB cation. The recombination processes are different in these samples, but they are all much slower than 1 ns and cannot be well determined in this study.

Table 7I: Fitting Parameters of the injection kinetics in RhB/semiconductor films

	A_1	τ_1 (ps)	A_2	τ_2(ps)	τ_{ave} (ps)*
In_2O_3	1.0	1.20			1.20±0. 03
SnO_2	1.0	1.19			1.19±0. 04
ZnO	0.62	2.6	0.38	14.2	7.0±0. 8

* error bar indicates the standard deviation of multiple measurements.

7.2.2 Effects of Dye Energetics on the Injection Rate.

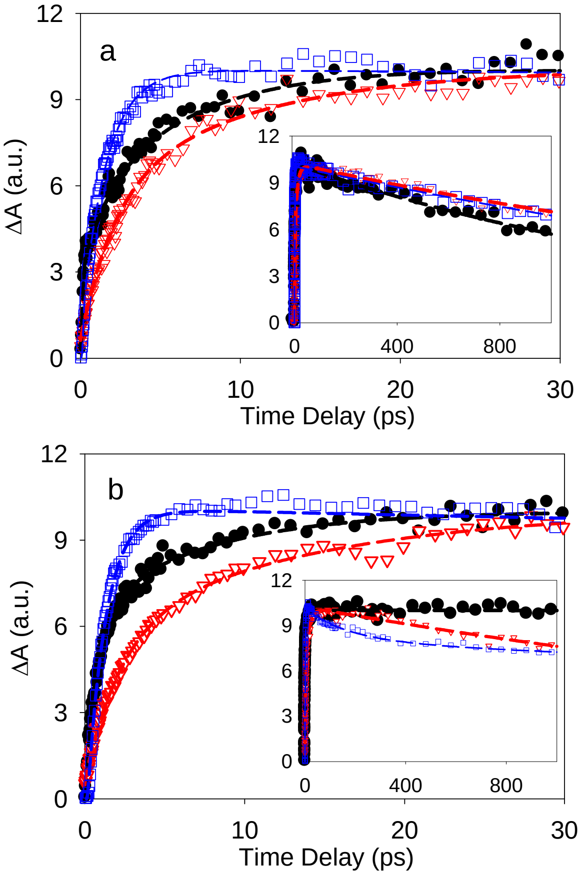

Figure 7.18. (a) Comparison of electron injection kinetics from Rh101, Rh6G, and RhB to In_2O_3, and (b) Comparison of electron injection kinetics from Rh101, Rh6G, and RhB to SnO_2. All kinetic traces have been normalized at the maximum amplitudes for better comparison. The inset shows the data up to 1ns.

In order to investigate the effect of dye energetics on ET rate, we examined the ET dynamics from different Rh dyes to the same semiconductor films by monitoring the injected electrons in semiconductor. Shown in Figure 7.18 a and b are the comparisons of ET kinetics for Rh dyes (RhB, Rh101 and Rh6G) to $In_2O_3$and SnO_2 films, respectively. The insets show the data extended to the longer time delay scale. All data were measured with 532 nm excitation under low excitation energy in order to have negligible quenching between excited molecules, and all traces have been normalized at maximum amplitude for better comparison. It is clear from the comparison that the injection rates from these three dyes to both In_2O_3 and SnO_2 films follow the order of RhB > Rh101 >Rh6G, decreasing with the lowering of the excited state oxidation potential of Rh dyes.

To quantify the electron injection rates, these kinetic traces were fitted by exponential rise functions. All of the traces can be adequately fitted by two-exponential components. The best fits for these traces were also shown in Figure 7.18 and the obtained injection rates are summarized in Table 7II. Also shown in Table 7II are the rates for RhB to these semiconductor films. As shown in Table 7II, the injection rates of Rh dyes on both In_2O_3 and SnO_2 films decrease from RhB to Rh101 and Rh6G. It is interesting to note that electron injection rates from the same Rh dye to In_2O_3 and SnO_2

appears to be similar for each different Rh dye, which is consistent with the trend observed in the study for RuN3 and RhB.

Table 7II: The amplitude weighted lifetime of the injection kinetics in Rh dyes/semiconductor films

	RhB	Rh101	Rh6G
In_2O_3	1.20	3.49	7.48
SnO_2	1.19	3.07	7.93

7.3. Discussion.

7.3.1. Effects of Semiconductors on the Injection Rate

As shown in Figure 7.17 and Table 7I, the injection rates from RhB to In_2O_3 is similar to that of SnO_2, but is much faster than ZnO. This is consistent with the trend observed in recent series of experiments that compared electron injection dynamics from RuN3 to different semiconductors. Adopting an approach similar to Marcus and co-workers, in the nonadiabatic limit, the total ET rate is given by:[61,62]

$$k_{ET} = \frac{2\pi}{\hbar} \int_{-\infty}^{\infty} d\varepsilon \rho_0(\varepsilon) |H_0|^2 \frac{1}{\sqrt{4\pi\lambda k_B T}} \exp[-\frac{(\lambda + \Delta G_0 + \varepsilon)^2}{4\lambda k_B T}] \quad (7.2)$$

where ε is the energy relative to the band edge, $\rho_0(\varepsilon)$ is the density of states per unit energy within the effective volume per metal center, V_0 (defined as unit cell volume/number of metal centers per cell); ΔG_0 is the driving force for electron transfer from adsorbate (with excited state oxidation potential of $V(S^+/S^*)$ to the conduction band edge (V_{CB}); and λ is the total reorganization energy.

According to equation 7.2, the electron injection rate depends on the total available accepting states in the semiconductor as well as electronic coupling and reorganization energy. The conduction band density of states can be estimated from its electron effective mass, which is given by:

$$\rho_{0C}(\varepsilon)d\varepsilon = V_0 \frac{(2m^*)^{3/2}}{2\pi^2\hbar^3}\sqrt{\varepsilon}d\varepsilon \qquad (7.3)$$

where m* is the effective mass of electrons in conduction band. The effective mass m* and V_0 in equation (7.3) for In_2O_3,[63,64] SnO_2,[64,65] and ZnO,[63,66] has been reported to be similar for these three semiconductor films. The conduction band edge positions for In_2O_3, SnO_2 and ZnO films were estimated to be -0.423, -0.343, and -0.813 V (vs SCE), which were obtained according to the Nerstian equation: $V_{fb} = V_{fb}^0 - pH * 0.059V$ by assuming PH 7 for the current system. Considering similar conduction band positions and electron effective mass in In_2O_3 and SnO_2, one would expect similar injection rates if the electronic coupling strengths with RhB are similar. Therefore, the observed similar injection rates for In_2O_3 and SnO_2 films implies the dominating role of density of conduction state on ET rates as well as the comparable electronic coupling strength for RhB to these two films. In the case of ZnO, the electron injection rate is much slower than that of In_2O_3 and SnO_2, which might be attributed to its higher conduction band edge position and thus smaller density of accepting states.

7.3.2. Effects of Dye Energetics on the Injection Rate

As discussed in section 7.3.1, the electron injection rate depends on the total available accepting states in the semiconductor as well as electronic coupling and reorganization energy. The density of accepting states in the conduction band of semiconductor is dependent on the relative position of the adsorbate potential with respect to the conduction band edge. We estimated the driving force values for RhB, Rh101 and Rh6G on In_2O_3, which are -0.517, -0.467, and -0.457, respectively, decreasing from RhB to Rh101 and Rh6G. Assuming that the strength of electronic coupling to these semiconductors are similar in these dye sensitized semiconductors, the electron injection rates of Rh dyes on In_2O_3 films are expected to become slower from RhB to Rh101 and Rh6G due to the decreasing driving force. The expected trend was observed for these Rh dyes on both films. The same trend is also observed in Rh dye sensitized SnO_2 films.

As shown in Table 7II, electron injection rates to In_2O_3 and SnO_2 are similar for each Rh dye, which is consistent with the trend observed in the study for RuN3 and RhB. This observation further implies that the electronic coupling strengths for Rh dyes to In_2O_3 and SnO_2 are comparable.

7.4. Summary

Interfacial electron transfer dynamics from excited RhB to In_2O_3, SnO_2 and ZnO films were investigated by monitoring both the broad mid-IR absorption signal of injected electrons and the visible absorption signals of RhB in the ground, excited and cation states. The effects of dye aggregation and excited-state quenching on the injection dynamics were also examined and were shown to be negligible under low dye coverage and excitation power density. The electron injection rates from RhB to these three different semiconductors were found to be similar (1.2ps) in In_2O_3 and SnO_2, but they were ~6 times faster than that to ZnO. These trends of ET rates follow qualitatively that of the conduction band density of states.

The injection kinetics from different Rh dyes to In_2O_3 and SnO_2 were also examined by transient IR spectroscopy to understand their dependence on the dye energetics. The injection rates were found to be decrease in the order of RhB > Rh101 > Rh6G, following the lowering of excited state potentials in these dyes. Additionally, the injection kinetics on In_2O_3 was similar to that on SnO_2 for all Rh dyes. These results may suggest a dominating role of conduction band density of states in determining the ET rates, although a better understanding requires more experimental and theoretical studies.

References

(1) Miller, R. J. D.; McLendon, G. L.; Nozik, A. J.; Schmickler, W.; Willig, F. *Surface electron transfer processes*; VCH publishers, Inc.: New York, 1995.

(2) Kamat, P. V. *Chem. Rev.* **1993**, *93*, 267.

(3) Hagfeldt, A.; Gratzel, M. *Chem. Rev.* **1995**, *95*, 49.

(4) Sayama, K.; Sugihara, H.; Arakawa, H. *Chem. Mater.* **1998**, *10*, 3825.

(5) Asbury, J. B.; Hao, E.; Wang, Y.; Ghosh, H. N.; Lian, T. *J. Phys. Chem. B* **2001**, *105*, 4545.

(6) Ellingson, R. J.; Asbury, J. B.; Ferrere, S.; Ghosh, H. N.; Sprague, J. R.; Lian, T.; Nozik, A. J. *J. Phys. Chem. B* **1998**, *102*, 6455.

(7) Tachibana, Y.; Haque, S. A.; Mercer, I. P.; Moser, J. E.; Klug, D. R.; Durrant, J. R. *J. Phys. Chem. B* **2001**, *105*, 7424.

(8) Tachibana, Y.; Moser, J. E.; Graetzel, M.; Klug, D. R.; Durrant, J. R. *J. Phys. Chem.* **1996**, *100*, 20056.

(9) Kuciauskas, D.; Monat, J. E.; Villahermosa, R.; Gray, H. B.; Lewis, N. S.; McCusker, J. K. *J. Phys. Chem. B* **2002**, *106*, 9347.

(10) Hannappel, T.; Burfeindt, B.; Storck, W.; Willig, F. *J. Phys. Chem. B* **1997**, *101*, 6799.

(11) Kallioinen, J.; Benko, G.; Sundstrom, V.; Korppi-Tommola, J. E. I.; Yartsev, A. P. *J. Phys. Chem. B* **2002**, *106*, 4396.

(12) Benko, G.; Kallioinen, J.; Korppi-Tommola, J. E. I.; Yartsev, A. P.; Sundstrom, V. *J. Am. Chem. Soc.* **2002**, *124*, 489.

(13) Heimer, T. A.; Heilweil, E. J.; Bignozzi, C. A.; Meyer, G. J. *J. Phys. Chem. A* **2000**, *104*, 4256.

(14) Haque, S. A.; Tachibana, Y.; Willis, R. L.; Moser, J. E.; Graetzel, M.; Klug, D. R.; Durrant, J. R. *J. Phys. Chem. B* **2000**, *104*, 538.

(15) O'Regan, B.; Gratzel, M. *Nature* **1991**, *353*, 737.

(16) Nazeeruddin, M. K.; Kay, A.; Rodicio, I.; Humphrybaker, R.; Muller, E.; Liska, P.; Vlachopoulos, N.; Gratzel, M. *J. Am. Chem. Soc.* **1993**, *115*, 6382.

(17) Asbury, J. B.; Anderson, N. A.; Hao, E.; Lian, T. *J. Phys. Chem. B* **2003**, *107*, 7376.

(18) Asbury, J. B.; Wang, Y. Q.; Hao, E. C.; Ghosh, H. N.; Lian, T. *Res. Chem. Interm.* **2001**, *27*, 393.

(19) Ellingson, R. J.; Asbury, J. B.; Ferrere, S.; Ghosh, H. N.; Sprague, J. R.; Lian, T.; Nozik, A. J. *Z. Phys. Chem. (Muenchen)* **1999**, *212*, 77.

(20) Asbury, J. B.; Wang, Y.; Lian, T. *J. Phys. Chem. B* **1999**, *103*, 6643.

(21) Tachibana, Y.; Nazeeruddin, M. K.; Gratzel, M.; Klug, D. R.; Durrant, J. R. *Chemical Physics* **2002**, *285*, 127.

(22) Durrant, J. R.; Tachibana, Y.; Mercer, I.; Moser, J. E.; Gratzel, M.; Klug, D. R. *Z. Phys. Chem.* **1999**, *212*, 93.

(23) Kallioinen, J.; Benko, G.; Myllyperkio, P.; Khriachtechev, L.; Skarman, B.; Wallenberg, R.; Tuomikoski, M.; Korppi-Tommola, J. E. I.; Sundstrom, V.; Yartsev, A. P. *Journal of Physical Chemistry B* **2004**, *108*, 6365.

(24) Benko, G.; Kallioinen, J.; Myllyperkio, P.; Trif, F.; Korppi-Tommola, J. E. I.; Yartsev, A. P.; Sundstrom, V. *Journal of Physical Chemistry B* **2004**, *108*, 2862.

(25) Benko, G.; Myllyperkio, P.; Pan, J.; Yartsev, A. P.; Sundstrom, V. *J. Am. Chem. Soc* **2003**, *125*, 1118.

(26) Kamat, P. V.; Bedja, I.; Hotchandani, S.; Patterson, L. K. *Journal of Physical Chemistry* **1996**, *100*, 4900.

(27) Palomares, E.; Clifford, J. N.; Haque, S. A.; Lutz, T.; Durrant, J. R. *Journal of the American Chemical Society* **2003**, *125*, 475.

(28) Barzykin, A. V.; Tachiya, M. *J. Phys. Chem. B* **2002**, *106*, 4356.

(29) Barzykin, A. V.; Tachiya, M. *Journal of Physical Chemistry B* **2004**, *108*, 8385.

(30) Hasselmann, G. M.; Meyer, G. J. *J. Phys. Chem. B* **1999**, *103*, 7671.

(31) Nelson, J. *Phys. Rev. B* **1999**, *59*, 15374.

(32) Nelson, J.; Haque, S. A.; Klug, D. R.; Durrant, J. R. *Phys. Rev. B: Condens. Matter Mater. Phys.* **2001**, *63*, 205321.

(33) Hara, K.; Horiguchi, T.; Kinoshita, T.; Sayama, K.; Sugihara, H.; Arakawa, H. *Solar Energy Materials and Solar Cells* **2000**, *64*, 115.

(34) Rensmo, H.; Keis, K.; Lindstrom, H.; Sodergren, S.; Solbrand, A.; Hagfeldt, A.; Lindquist, S. E.; Wang, L. N.; Muhammed, M. *Journal of Physical Chemistry* **1997**, *101*, 2598.

(35) Aegerter, M. A. *Solar Energy Materials and Solar Cells* **2001**, *68*, 401.

(36) Aegerter, M. A.; Schmitt, M.; Guo, Y. *International Journal of Photoenergy* **2002**, *4*, 1.

(37) Barros Filho, D. d. A.; Abreu Filho, P. P.; Werner, U.; Aegerter, M. A. *Journal of Sol-Gel Science and Technology* **1997**, *8*, 735.

(38) Lenzmann, F.; Krueger, J.; Burnside, S.; Brooks, K.; Graetzel, M.; Gal, D.; Ruehle, S.; Cahen, D. *Journal of Physical Chemistry B* **2001**, *105*, 6347.

(39) Bedja, I.; Hotchandani, S.; Kamat, P. V. *J. Phys. Chem.* **1994**, *98*, 4133.

(40) Ferrere, S.; Zaban, A.; Gregg, B. A. *Journal of Physical Chemistry B* **1997**, *101*, 4490.

(41) Asbury, J. B.; Ellingson, R. J.; Ghosh, H. N.; Ferrere, S.; Nozik, A. J.; Lian, T. *J. Phys. Chem. B* **1999**, *103*, 3110.

(42) Stergiopoulos, T.; Arabatzis, I. M.; Cachet, H.; Falaras, P. *Journal of Photochemistry and Photobiology, A: Chemistry* **2003**, *155*, 163.

(43) Guo, J.; Stockwell, D.; Ai, X.; She, C.; Anderson, N. A.; Lian, T. *Journal of Physical Chemistry B* **2006**, *110*, 5238.

(44) Anderson, N. A.; Ai, X.; Lian, T. *J. Phys, Chem. B* **2003**, *107*, 14414.

(45) Ai, X.; Anderson, N. A.; Guo, J.; Lian, T. *Journal of Physical Chemistry B* **2005**, *109*, 7088.

(46) Jacobson, K. I.; Jacobson, R. E. *Imaging Systems*; John Wiley & Sons: New York, 1976.

(47) Fischer, A. B.; Bronstein-Bonte, I. *Journal of Photochemistry* **1985**, *30*, 475.

(48) Frank, A. J. O., J. W.; Calvin, M. *The Journal of Physical Chemistry* **1979**, *83*, 716.

(49) Heinlein, T.; Knemeyer, J.-P.; Piestert, O.; Sauer, M. *Journal of Physical Chemistry B* **2003**, *107*, 7957.

(50) Alig Anna, R. G.; Gourdon, D.; Israelachvili, J. *J Phys Chem B FIELD Full Journal Title:The journal of physical chemistry. B* **2007**, *111*, 95.

(51) Huang, J.; Stockwell, D.; Boulesbaa, A.; Guo, J.; Lian, T. *J. Phys. Chem. C* **2008**, *112*, 5203.

(52) Anderson, N. A.; Lian, T. *Annual Review of Physical Chemistry* **2005**, *56*, 491.

(53) Fisher, A. B.; Bronstein-Bonte, I. *J. Photochem.* **1985**, *30*, 475.

(54) Beaumont, P. C.; Johnson, D. G.; Parsons, B. J. *J. Photochem. and Photobio. A* **1997**, *107*, 175.

(55) Beaumont, P. C.; Johnson, D. G.; Parsons, B. J. *Journal of Photochemistry and Photobiology, A: Chemistry* **1997**, *107*, 175.

(56) Nishikiori, H.; Fujii, T. *Journal of Physical Chemistry B* **1997**, *101*, 3680.

(57) Liu, D.; Fessenden, R. W.; Hug, G. L.; Kamat, P. V. *J. Phys. Chem. B* **1997**, *101*, 2583.

(58) Del Monte, F.; Levy, D. *Journal of Physical Chemistry B* **1998**, *102*, 8036.

(59) Martinez, V. M.; Arbeloa, F. L.; Prieto, J. B.; Lopez, T. A.; Arbeloa, I. L. *Journal of Physical Chemistry B* **2004**, *108*, 20030.

(60) Yao, H.; Omizo, M.; Kitamura, N. *Chemical Communications (Cambridge)* **2000**, 739.

(61) She, C.; Anderson, N. A.; Guo, J.; Liu, F.; Goh, W.; Chen, D.-T.; Mohler, D. L.; Tian, Z.-Q.; Hupp, J.; Lian, T. *J. Phys. Chem. B.* **2005**, *109*, 19345.

(62) Sakata, T.; Hashimoto, K.; Hiramoto, M. *J. Phys. Chem.* **1990**, *94*, 3040.

(63) Fujiwara, H.; Kondo, M. *Physical Review B: Condensed Matter and Materials Physics* **2005**, *71*, 075109/1.

(64) *Semiconductor Electrodes*; Finklea, H., O., Ed.; Elsevier: New York, 1988; Vol. 55.

(65) Button, K. J.; Fonstad, C. G.; Dreybrodt, W. *Phys. Rev. B* **1971**, *4*, 4539.

(66) Henrich, V.; Cox, P. *The Surface Science of Metal Oxides*; Cambridge University Press: Cambridge, 1996.